QUANTUM COHERENCE EFFECTS IN NOVEL QUANTUM OPTICAL SYSTEMS

A Dissertation

by

EYOB ALEBACHEW SETE

Submitted to the Office of Graduate Studies of
Texas A&M University
in partial fulfillment of the requirements for the degree of

DOCTOR OF PHILOSOPHY

August 2012

Major Subject: Physics

QUANTUM COHERENCE EFFECTS IN NOVEL QUANTUM OPTICAL SYSTEMS

A Dissertation

by

EYOB ALEBACHEW SETE

Submitted to the Office of Graduate Studies of
Texas A&M University
in partial fulfillment of the requirements for the degree of

DOCTOR OF PHILOSOPHY

Approved by:

Chair of Committee,	Marlan O. Scully
Committee Members,	M. Suhail Zubairy
	Olga Kocharovskaya
	Goong Chen
Head of Department,	George Welch

August 2012

Major Subject: Physics

ABSTRACT

Quantum Coherence Effects in Novel Quantum Optical Systems. (August 2012)

Eyob Alebachew Sete, B. S., Addis Ababa University;

M. S., Addis Ababa University

Chair of Advisory Committee: Dr. Marlan O. Scully

Optical response of an active medium can substantially be modified when coherent superpositions of states are excited, that is, when systems display quantum coherence and interference. This has led to fascinating applications in atomic and molecular systems. Examples include coherent population trapping, lasing without inversion, electromagnetically induced transparency, cooperative spontaneous emission, and quantum entanglement.

We study quantum coherence effects in several quantum optical systems and find interesting applications. We show that quantum coherence can lead to transient Raman lasing and lasing without inversion in short wavelength spectral regions–extreme ultraviolet and x-ray–without the requirement of incoherent pumping. For example, we demonstrate transient Raman lasing at 58.4 nm in Helium atom and transient lasing without inversion at 6.1 nm in Helium-like Boron (triply-ionized Boron). We also investigate dynamical properties of a collective superradiant state prepared by absorption of a single photon when the size of the sample is larger than the radiation wavelength. We show that for large number of atoms such a state, to a good approximation, decays exponentially with a rate proportional to the number of atoms. We also find that the collective frequency shift resulting from repeated emission and reabsorption of short-lived virtual photons is proportional to the number of species in the sample. Furthermore, we examine how a position-dependent excitation phase

affects the evolution of entanglement between two dipole-coupled qubits. It turns out that the coherence induced by position-dependent excitation phase slows down the otherwise fast decay of the two-qubit entanglement. We also show that it is possible to entangle two spatially separated and uncoupled qubits via interaction with correlated photons in a cavity quantum electrodynamics setup. Finally, we analyze how quantum coherence can be used to generate continuous-variable entanglement in quantum-beat lasers in steady state and propose possible implementation in quantum lithography.

To My Wife Senait Amdework Amare

ACKNOWLEDGMENTS

I would like to express my deepest gratitude to my advisor Dr. Marlan O. Scully for his invaluable guidance and advice during my PhD studies. His insightful approach to scientific problems has taught me how to deal with difficult problems. His vastness in knowledge has provided me the opportunity to learn various topics in physics. I also thank him for giving me the opportunity to meet many collaborators. Thanks to my committee members Dr. M. Suhail Zubairy, Dr. Olga Kacharovskaya, Dr. Goong Chen, and Dr. Robert D. Nevels (substitute) for useful discussions.

I would also like to thank my colleagues Dr. Yuri Rostovtsev, Dr. Jonathan P. Dowling, Dr. Hichem Eleuch, Dr. Sumanta Das, Dr. Konstantin Dorfman, and Dr. Anatoly Svidzinsky for fruitful collaborations on various topics over the years. It has been a great pleasure to discuss and learn physics from them. I also thank Dr. Arinbold Gomachov, Dr. Moochan Kim, Dr. Chris O'Brien, Dr. Dong Sun, Dr. Qingqing Sun, Dr. Sabine Woelk, Adrew Traverso, Luqi Yuan, Shuai Yang, Zeyang Liao, and many more for stimulating discussions and for their friendship.

Many thanks to Ms. Kimberly Chapin for invaluable advice she has given me during my studies. I am also grateful to Mr. Clayton Holle for taking care of financial issues and travel arrangements. Mrs. Sandi Smith, thank you for taking care of paper works especially for my final examination. Thanks to my friends Dr. Solomon F. Duki, Dr. Abay Gadisa, Bekele Homa, Melaku Bogale, and Wondimu Teka for their friendship and encouragement. Thanks also to all my friends in College Station, Houston, and Austin who made my stay in Aggieland memorable and enjoyable.

I am grateful to the Welch Foundation and the Herman F. Heep and Minnie Belle Heep Texas A&M University Endowed Fund for financial support.

My sincere gratitude goes to my mother Shewaye Woldesemayat, my father Ale-

bachew Sete, and my siblings Tigist, Ayelech, Gezahegn, Teguada, Fikadu and Dawit for their moral support and encouragement. Last but not least, I would like to thank my beloved wife Senait Amdework Amare for her care, patience, and love during my studies. She has been a source of strength and inspiration even during difficult times.

TABLE OF CONTENTS

CHAPTER Page

CHAPTER Page

LIST OF TABLES

LIST OF FIGURES

FIGURE Page

FIGURE Page

FIGURE Page

FIGURE Page

FIGURE Page

FIGURE Page

CHAPTER I

INTRODUCTION

Quantum coherence is one of the most intriguing applications of quantum mechanics. When coherent superposition of states of atoms or molecules are excited, that is, when the system display quantum coherence or interference the optical response of a medium gets modified substantially. This has led to interesting phenomena and uncommon results. Examples of applications of quantum coherence include coherent population trapping [1, 2, 3], lasing without inversion (LWI) [4, 5, 6], cooperative spontaneous emission (superradiance) [7], and quantum entanglement [8, 9, 10] among others.

The key idea is that when atoms are prepared in coherent superposition states, the addition of probability amplitudes corresponding to different pathways leading to the same end point may give rise to destructive interference. For example, in lasing without population inversion, different absorption processes interfere destructively, resulting in reduction or even cancelation of stimulated absorption under certain conditions. At the same time, the stimulated emission process remain intact, leading to the possibility of gain even though only a fraction of the population is in the excited state. This implies that lasing is possible even if most of the population is in the ground state.

Another interesting application of quantum coherence is the phenomenon of cooperative spontaneous emission or superradiance. First coined by Dicke [7], superradiance involves a large number of two-level atoms prepared in a collective state where half of the atoms are in the excited state and the other half in the ground state. This

---

The journal model is Physical Review A.

state exhibits coherence and the radiation emitted by such a system is anomalous– the intensity of the emitted radiation is proportional to the square of the number of atoms. In recent years, other initial states has been considered to explore the physics of superradiance. For example, single-photon state–a state in which one atom excited and the rest in the ground state, gives insight into the physics of cooperative emission and has been the subject of intense investigation [11, 12, 13, 14, 15]. Since the excited atom out the N atoms is not known, the single photon state is essentially an entangled state. Recent studies [11, 12, 13, 14, 15] show that this state has very interesting features: When the sample size is less than the radiation wavelength ($R \ll \lambda$) with R being the radius of the sample and λ the wavelength, the single-photon state predominantly decays to the ground state with an enhanced rate equal to the number of atoms times the single atom spontaneous decay rate, γ. Moreover, it has been shown recently that the radiation emitted by such a system is directional [11]. From the standpoint of applications, superradiance is useful for producing coherent radiation without coherent pumping. This, in particular, is important for generating coherent radiation in x-ray and γ-ray spectral regions, where there are no effective mirrors which limit the use of ordinary stimulated emission process.

Quantum coherence has also been exploited as a resource for the emerging field of quantum information science. In this context, quantum coherence has been used to create discrete as well as continuous-variable entanglement in various quantum optical systems. For instance, coherence induced by strong laser field can create entanglement amplifier in correlated-emission laser with tens and thousands of photons [9]. Besides, coherence was shown to create entanglement between two qubits [16, 17]. From application viewpoint, quantum entanglement has proven to be the ingredient for quantum information processing For example, entanglement between photons has been used in quantum cryptography [18] and quantum teleportation [19].

In this dissertation, we present effects of quantum coherence and interference in various quantum optical systems. In Chapter II, we discuss the theory of transient Raman lasing and transient lasing without inversion in the short wavelength regimes, extreme ultra violet (XUV) and x-ray using Helium and Helium-like Boron–triply ionized Boron as a gain media. We demonstrate transient Raman lasing in Helium atoms at 58.4 nm and transient lasing without inversion in triply-ionized Boron at 6.1nm. In Chapter III, we study single-photon Dicke superradiance and show that for extended cloud of two-level atoms, where the size of the sample is larger than the radiation, a single photon collective state prepared by absorption of single photon approximately decays to the ground state with a rate the number of atoms times the single atom decay rate, $N\gamma$. In Chapter IV, we show how an position-dependent excitation phase induces quantum coherence and thereby affects the dynamics of entanglement between two qubits. In Chapter V, we propose an alternative scheme to entangle two spatially separated qubits via correlated photons in a cavity and elucidate the physics of light-to-matter entanglement. Chapter VI deals with generation of entanglement in quantum-beat laser via microwave induced coherence. Using this entangled light source we propose phase-controlled implementation of quantum lithography. In Chapter VII, we address a fundamental question, in which we study the role of dephasing on entanglement created in a quantum-beat laser. Finally, we present the summary of our main results in Chapter VIII.

A. Fundamentals of light-matter interactions

Interactions of electromagnetic radiation with matter are the pillar for this dissertation. It is then imperative to go through the fundamentals of the light-matter interactions. The analysis presented here are partially done following semiclassical

approximation, where the field is assumed be strong and treated classically while the atoms are considered quantum-mechanical objects. Although the semiclassical approximation gives remarkably good results in some systems, it is inadequate to provide information about the quantum-statistical properties of radiation. To this end, we start with a fully quantum mechanical description of interaction of multi-mode electromagnetic radiation with an atom with arbitrary energy level and then reduce it to a semiclassical approach by treating the field operators as c-number variables.

An electron of mass m and charge e interacting with external electromagnetic field is described by a minimal-coupling Hamiltonian [20]

$$H_e = \frac{1}{2}\left[\mathbf{p} - e\mathbf{A}(\mathbf{r},t)\right]^2 + eU(\mathbf{r},t) + V(r), \tag{1.1}$$

where $\mathbf{p}$ is the canonical momentum operator, $\mathbf{A}(\mathbf{r},t)$ and $U(\mathbf{r},t)$ are the vector and scalar potentials of the electromagnetic field, respectively and $V(r)$ is an electric potential that is normally the atomic binding potential. In most part of this dissertation, we apply the dipole approximation–the field wavelength is larger than the atomic size, $\mathbf{k}\cdot\mathbf{r} \ll 1$. We assume that the entire atom is immersed in an electromagnetic wave described by a vector potential $\mathbf{A}(\mathbf{r}_0+\mathbf{r},t)$, where $\mathbf{r}_0$ is the position of the nucleus. This vector potential can be written in the dipole approximation as

$$\begin{aligned}\mathbf{A}(\mathbf{r}_0+\mathbf{r}),t) &= \mathbf{A}(t)e^{i\mathbf{k}\cdot(\mathbf{r}_0+\mathbf{r})} \\ &= \mathbf{A}(t)e^{i\mathbf{k}\cdot\mathbf{r}_0}[1+i\mathbf{k}\cdot\mathbf{r}+...] \\ &\simeq \mathbf{A}(t)e^{i\mathbf{k}\cdot\mathbf{r}_0}.\end{aligned} \tag{1.2}$$

In the dipole approximation, the Schrödinger equation for this problem, with $\mathbf{A}(\mathbf{r},t) \equiv$

$\mathbf{A}(\mathbf{r}_0, t)$, is given by

$$\left\{ -\frac{\hbar^2}{2m} \left[\nabla - \frac{ie}{\hbar} \mathbf{A}(\mathbf{r}_0, t) \right]^2 + eU(\mathbf{r}, t) + V(r) \right\} \psi(\mathbf{r}, t) = i\hbar \frac{\partial \psi(\mathbf{r}, t)}{\partial t} \tag{1.3}$$

Now choosing the gauge to be the radiation gauge

$$U(\mathbf{r}, t) = 0, \qquad \nabla \cdot \mathbf{A} = 0, \tag{1.4}$$

and introducing a new wave function of the form

$$\psi(\mathbf{r}, t) = e^{ie\mathbf{A}(\mathbf{r}_0, t) \cdot \mathbf{r}/\hbar} \phi(\mathbf{r}, t) \tag{1.5}$$

the Schrödinger equation Eq. (1.3) yields

$$i\hbar \left[\frac{ie}{\hbar} \frac{\partial \mathbf{A}}{\partial t} \cdot \mathbf{r} \phi(\mathbf{r}, t) + \frac{\partial}{\partial t} \phi(\mathbf{r}, t) \right] e^{ie\mathbf{A} \cdot \mathbf{r}/\hbar} = e^{ie\mathbf{A} \cdot \mathbf{r}/\hbar} \left[\frac{p^2}{2m} + V(r) \right] \phi(\mathbf{r}, t). \tag{1.6}$$

Note that in radiation gauge the electric field is related to the vector potential as $\mathbf{E} = -\partial \mathbf{A}/\partial t$. In view of this and after cancelation of the exponential term, we get

$$i\hbar \dot{\phi}(r, t) = [H_A - e\mathbf{r} \cdot \mathbf{E}(\mathbf{r}_0, t)] \phi(\mathbf{r}, t), \tag{1.7}$$

where

$$H_A = p^2/2m + V(r)$$

is the unperturbed Hamiltonian of the electron. We then note that the total Hamiltonian, including the free Hamiltonian of the field H_F, is given by

$$H = H_F + H_A + H_I, \tag{1.8}$$

where

$$H_I = -e\mathbf{r} \cdot \mathbf{E}(\mathbf{r}_0, t) \tag{1.9}$$

is the interaction Hamiltonian. The energy of the free field H_F is given in terms of

the creation ($a_{\mathbf{k}}^{\dagger}$) and annihilation ($a_{\mathbf{k}}$) operators by

$$H_F = \sum_{\mathbf{k}} h\nu_{\mathbf{k}} \left(a_{\mathbf{k}}^{\dagger} a_{\mathbf{k}} + \frac{1}{2} \right), \tag{1.10}$$

in which ν_k is the frequency of the kth mode.

Further, the free energy of the atom H_A and $e\mathbf{r}$ can be expressed in terms of the atomic transition operators $\sigma_{ij} = |i\rangle\langle j|$. $\{|i\rangle\}$ represents a complete set of atomic energy states, that is, $\sum_i |i\rangle\langle i| = 1$. Noting that $H_A|i\rangle = E_i|i\rangle$ and using the completeness relation, the free Hamiltonian for the atom can be written as

$$H_A = IH_A = \sum_i |i\rangle\langle i|H_A = \sum_i E_i \sigma_{ii}. \tag{1.11}$$

Similarly, the term $e\mathbf{r}$ can be expressed as

$$e\mathbf{r} = I(e\mathbf{r})I = \sum_{i,j} e|i\rangle\langle i|\mathbf{r}|j\rangle\langle j| = \sum_{i,j} \wp_{ij}\sigma_{ij}, \tag{1.12}$$

where $\wp_{ij} = e\langle i|\mathbf{r}|j\rangle$ is the electric-dipole transition matrix element. The quantized electric field operator in the dipole approximation is given by

$$\mathbf{E}(\mathbf{r}_0, t) = \sum_{\mathbf{k},\lambda} \hat{\epsilon}_{\mathbf{k}}^{(\lambda)} \mathcal{E}_{\mathbf{k}} (a_{\mathbf{k},\lambda} e^{-i\nu_k t + i\mathbf{k}\cdot\mathbf{r}_0} + a_{\mathbf{k},\lambda}^{\dagger} e^{i\nu_k t - i\mathbf{k}\cdot\mathbf{r}_0}), \tag{1.13}$$

where $\hat{\epsilon}_{\mathbf{k}}^{(\lambda)}$ is a polarization vector with λ being its degrees of freedom, $\mathcal{E}_{\mathbf{k}} = \sqrt{\hbar\nu_{\mathbf{k}}/2\varepsilon_0 V}$ with ε_0 and V being the permittivity of free space and quantization volume, respectively. If we assume the position of the atom to be at the origin and linear polarization for the field, the electric field takes a simple form

$$\mathbf{E} = \sum_{\mathbf{k}} \hat{\epsilon}_{\mathbf{k}} \mathcal{E}_{\mathbf{k}} (a_{\mathbf{k}} + a_{\mathbf{k}}^{\dagger}). \tag{1.14}$$

Therefore, on account of Eqs. (1.10)-(1.12) and (1.14), the Hamiltonian of the

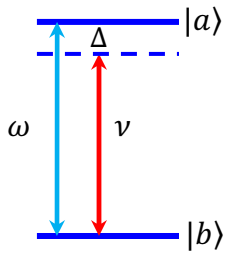

Fig. 1. A scheme of a two-level atom interacting with a single mode laser field of frequency ν and off resonant from the atomic transition frequency ω by $\Delta = \omega - \nu$. $\omega = \omega_a - \omega_b$, where $\hbar\omega_a$ and $\hbar\omega_b$ are the energy of levels $|a\rangle$ and $|b\rangle$, respectively.

system turns out to be

$$H = \sum_{\mathbf{k}} h\nu_{\mathbf{k}} a^{\dagger}_{\mathbf{k}} a_{\mathbf{k}} + \sum_{i} E_i \sigma_{ii} - \hbar \sum_{\mathbf{k},ij} \mathrm{g}^{ij} \sigma_{ij} (a_{\mathbf{k}} + a^{\dagger}_{\mathbf{k}}) \tag{1.15}$$

where $g^{ij} = \wp_{ij} \cdot \hat{\epsilon}_{\mathbf{k}} \mathcal{E}_{\mathbf{k}}/\hbar$ is the coupling constant between the atom and the field. In (1.15) we have omitted the zero-point energy and assumed that $\wp_{ij}$ is real.

Up to now we considered interaction of a multimode field with an atom with arbitrary number of energy levels. Let us now consider the simplest case in which a two-level atom is interacting with a single mode radiation field as outlined in Fig. 1. Using the Hamiltonian (1.15), we write Hamiltonian for this system as

$$H = \hbar\nu a^{\dagger} a + \hbar\omega_a |a\rangle\langle a| + \hbar\omega_b |b\rangle\langle b| - \hbar \mathrm{g}(\sigma_+ + \sigma_-)(a^{\dagger} + a). \tag{1.16}$$

Here, for the sake of simplicity, we have assumed the coupling constant to be real, $\mathrm{g}^{ab} = \mathrm{g}^{ba} = \mathrm{g}$. $\sigma_+ = |a\rangle\langle b|$ and $\sigma_- = |b\rangle\langle a|$ are the raising and lowering operator for the atom, respectively. It is worth to mention that the terms $\sigma_+ a$ and $a^{\dagger}\sigma$ describe energy conserving processes. For instance, $\sigma_+ a$ describe promotion of the atom from the lower to the upper state by absorption of a photon, while $a^{\dagger}\sigma$ represents a process

in which the atom decays from the upper to the lower state by emitting a photon. However, the other terms $\sigma_+ a^\dagger$ and $a\sigma_-$ describe energy nonconserving processes. For example, the term $\sigma_+ a^\dagger$ describes a process in which an atom is excited by emitting a photon, while term $a\sigma_-$ describe decay of an atom by absorbing a photon. These energy nonconserving processes occur due to emission and reabsorption of short-lived virtual photons. These processes are particularly important in calculating frequency (Lamb) shifts and will be discussed in more detail in Chapter III.

Another popular approximation we are going to employ in most parts of the dissertation is the rotating wave approximation, which amounts to dropping the energy nonconserving terms in the Hamiltonian (1.16). The transition frequency of the atom is defined by $\omega = \omega_a - \omega_b$. For the sake of convenience we choose the energy of the lower level $|b\rangle$ to be zero. To this end, the Hamiltonian (1.16) in the rotating wave approximation can be put in the form

$$H = H_0 + H_I, \tag{1.17}$$

where

$$H_0 = \hbar\nu a^\dagger a + \hbar\nu|a\rangle\langle a| \tag{1.18}$$

$$H_I = \hbar\Delta|a\rangle\langle a| - \hbar g(\sigma_+ a + a^\dagger \sigma_-), \tag{1.19}$$

where $\Delta = \omega - \nu$ is the detuning between the transition frequency of the atom and the field frequency.

In most instances it is more convenient to work in the interaction picture. Thus the Hamiltonian in the interaction picture is defined by

$$\mathcal{H} = e^{iH_0 t/\hbar} H_I e^{-iH_0 t/\hbar} \tag{1.20}$$

can be written in a simple form

$$\mathcal{H} = \hbar\Delta|a\rangle\langle a| - \hbar g(\sigma_+ a + a^\dagger \sigma_-). \tag{1.21}$$

It is worth to note that the above interaction Hamiltonian does not take into account the inevitable interaction of the atom as well as the field with the environment which is vital to the dynamics of the system. The dynamics of such a system is described by the time evolution of the density operator, also known as the master equation. In general, the density operator is defined as

$$\rho = \sum_\psi p_\psi |\psi\rangle\langle\psi| \tag{1.22}$$

whose time derivative together with the Schrödinger equation for state vector $|\psi\rangle$

$$i\hbar \frac{\partial|\psi\rangle}{\partial t} = \mathcal{H}|\psi\rangle \tag{1.23}$$

gives

$$\frac{\partial\rho}{\partial t} = -\frac{i}{\hbar}[\mathcal{H}\rho - \rho\mathcal{H}] = -\frac{i}{\hbar}[\mathcal{H}, \rho]. \tag{1.24}$$

The interaction of the field and the atom with the environment can be described by adding dissipation terms as [20]

$$\frac{\partial\rho}{\partial t} = -\frac{i}{\hbar}[\mathcal{H}, \rho] + \left(\frac{\partial\rho}{\partial t}\right)_{\text{atom}} + \left(\frac{\partial\rho}{\partial t}\right)_{\text{field}}, \tag{1.25}$$

where

$$\left(\frac{\partial\rho}{\partial t}\right)_{\text{atom}} = -\frac{\gamma}{2}(\sigma_+\sigma_-\rho + \rho\sigma_+\sigma_- - 2\sigma_-\rho\sigma_+), \tag{1.26}$$

$$\left(\frac{\partial\rho}{\partial t}\right)_{\text{field}} = -\frac{\kappa}{2}(a^\dagger a\rho + \rho a^\dagger a - 2a\rho a^\dagger) \tag{1.27}$$

with γ and κ being the spontaneous emission rate of the atom and the radiation decay rate, respectively. Equation (1.25) is also called *Liouville* equation and can used to

derive the density matrix elements. The diagonal elements ρ_{aa} and ρ_{bb} describe the populations in levels $|a\rangle$ and $|b\rangle$, respectively, while the off-diagonal elements $\rho_{ab} = \rho_{ba}^*$ represent the coherence developed in the system.

B. The concept of quantum coherence

In this section we consider a simple system to illustrate the physics of quantum coherence effects, which is the basis for this dissertation. As an example, we discuss the concept of coherent population trapping. Let us consider a three-level atom in a so-called Λ configuration, in which the two-lover levels ($|b\rangle$, $|c\rangle$) are coupled to upper level $|a\rangle$. The $|a\rangle \leftrightarrow |b\rangle$ and $|a\rangle \leftrightarrow |c\rangle$ transitions are dipole allowed while the transition between the two lower levels is electric dipole forbidden. The dipole allowed transitions are driven by two monochromatic fields. Other possible three-level schemes include the V and cascade (ladder) configurations. The interaction Hamiltonian for the coupling of the atom to two laser fields is given by

$$H = -\hbar\Omega_1|a\rangle\langle c| - \hbar\Omega_2|a\rangle\langle b| + \text{H.c.}, \tag{1.28}$$

where $\Omega_1 = \wp_{ac}E_1(\nu_1)/\hbar$ and $\Omega_2 = \wp_{ab}E_2(\nu_2)/\hbar$ are the Rabi frequencies corresponding to the monochromatic fields ν_1 and ν_2, respectively. The state vector of the atom has the form

$$|\psi\rangle = c_a(t)|a\rangle + c_b(t)|b\rangle + c_c(t)|c\rangle. \tag{1.29}$$

The Schrödinger equation $i\hbar\dot{\psi} = H\psi$ then gives

$$\dot{c}_a = i(\Omega_1 c_c + \Omega_2 c_b), \tag{1.30}$$

$$\dot{c}_b = i\Omega_2 c_a, \tag{1.31}$$

$$\dot{c}_c = i\Omega_1 c_a. \tag{1.32}$$

Now let us assume that the atom is initially in a coherent superposition of the two lower states

$$|0\rangle = \tilde{\Omega}_1|b\rangle - \tilde{\Omega}_2|c\rangle \tag{1.33}$$

where $\tilde{\Omega}_{1,2} = \Omega_{1,2}/\sqrt{\Omega_1^2 + \Omega_2^2}$. The state $|0\rangle$ is also know as the *dark state*, for reason that the Hamiltonian acting on this state gives nothing, that is, $H|0\rangle = 0$. In terms of the density matrix elements, the initial state can be written as

$$\rho(0) = |0\rangle\langle 0| = \tilde{\Omega}_2^2|b\rangle\langle b| - \tilde{\Omega}_1\tilde{\Omega}_2(|b\rangle\langle c| + |c\rangle\langle b|) + \tilde{\Omega}_1^2|c\rangle\langle c| \tag{1.34}$$

which yields

$$\rho_{bb}^{(0)} = \tilde{\Omega}_2^2, \rho_{cc}^{(0)} = \tilde{\Omega}_1^2, \rho_{aa}^{(0)} = 0, \rho_{bc}^{(0)} = \rho_{cb}^{(0)} = -\tilde{\Omega}_1\tilde{\Omega}_2. \tag{1.35}$$

As a special case where the two fields have the same Rabi frequency $\Omega_1 = \Omega_2$, the initial condition becomes $\rho_{bb}^{(0)} = \rho_{cc}^{(0)} = 1/2$, $\rho_{bc}^{(0)} = -1/2$. The solutions of Eqs. (1.36)-(1.38) then turn out to be

$$c_a(t) = 0, \tag{1.36}$$

$$c_b(t) = \frac{1}{\sqrt{2}}, \tag{1.37}$$

$$c_c(t) = \frac{1}{\sqrt{2}}e^{\pm i\pi}. \tag{1.38}$$

Recall that the probability of absorption by the upper state is given by

$$P_{\text{absorption}} \propto |c_a(t)|^2 = 0. \tag{1.39}$$

One can infer from this result that the two pathways that leads to the upper state $|a\rangle$ interfere destructively to cancel absorption. That means all the populations are trapped in the lower levels even though there are strong resonant lasers fields that derive the two transitions. This is the essence of quantum coherence.

CHAPTER II

USING COHERENCE TO DEMONSTRATE TRANSIENT RAMAN LASING IN XUV AND LASING WITHOUT INVERSION IN X-RAY SPECTRAL REGIONS *

A. Introduction

Gain swept superradiance (GSS) in an ensemble of two-level atoms was extensively studied in the 70's in connection with laser lethargy and coherence brightening in the X-ray laser [21, 22, 23]. In GSS, the inversion is created by injecting a short excitation pulse which produces a gain-swept medium. Among other things it was found that GSS can yield intense pulses without population inversion. This is closely related to Dicke superradiance [7, 24] in which the maximum emission rate occurs when there are equal number of atoms in the excited and ground states, i.e., when the population inversion is zero.

The quest for short wavelength lasers–XUV and x ray–has been sought since the invention of laser in connection with their potential application in fundamental science as well as real life applications. Extensive theoretical work has been done on amplification without inversion since the early work of Kocharovskaya *et al.* [4], Harris [5], and Scully *et al.* [6]. In the experimental front, LWI has been demonstrated in three level atoms, for example in Sodium (Na) and Rubidium (Rb) atoms in mid 90's [25, 26]. Those studies involved continuous pumping and were in the optical and infrared spectral regimes. LWI is rather more attractive in the short wavelength regimes

---

* Reprinted with permission from "Using quantum coherence to generate gain in the XUV and X-ray: Gain swept superradiance and lasing without inversion" by Eyob A. Sete, A. A. Svidzinsky, Y. V. Rostovtsev, H. Eleuch, P. K. Jha, S. Suckewer, and M. O. Scully, 2012. *IEEE J. Sel. Top. Quantum Electron.*, 18, 541-553, Copyright [2012] by Institute of Electrical and Electronics Engineers. For more information go to http://thesis.tamu.edu/forms/IEEE%20permission%20note.pdf/view.

where population inversion is difficult to achieve. Many schemes has been proposed to demonstrate LWI in the short wavelength spectral regimes [27, 28]. However, most of them operate in the steady state regime and requires continuous incoherent pumping. In a process where the decoherence is very fast, one always want to avoid incoherent pumping. To this end, recent proposals focus on the possibility of transient lasing without the requirement of incoherent pumping. Most recently transient lasing without inversion has been proposed [29, 30, 31, 32] in three level atomic systems.

In this Chapter, we explore connections between GSS and transient Raman lasing in helium atom (ladder scheme) with initial Raman inversion and yet the system operating without inversion in the lasing transition. In addition, we demonstrate a pure transient LWI in helium-like Boron, B^{3+} operating at 6.1nm.

B. Steady-state Raman lasing

We first discuss the concept of Raman lasing by considering three-level atom in Λ configuration shown in Fig. 2. The transitions from $|a\rangle$ to $|b\rangle$ and from $|a\rangle$ to $|c\rangle$ are dipole allowed while the transition between the two lower levels is dipole forbidden. The levels $|a\rangle$ and $|b\rangle$ are coupled by a weak field of Rabi frequency Ω_l and frequency ν_b whose amplification we are interested in. The upper level $|c\rangle$ is coupled to level $|b\rangle$ by a strong coherent field of Rabi frequency Ω and frequency ν_c.

The Hamiltonian describing the interaction between the classical laser fields and the atom, in the rotating wave and dipole approximations, is given by

$$H = \hbar\Delta_b|a\rangle\langle a| - \hbar(\Delta_b - \Delta_c)|c\rangle\langle c| - \hbar\Omega|a\rangle\langle c| - \hbar\Omega_l|a\rangle\langle b| + \text{H.c.}. \tag{2.1}$$

Here $\Delta_b = \omega_{ab} - \nu_b$ and $\Delta_c = \omega_{ac} - \nu_c$ with ω_{ac} and ω_{ab} being atomic transition frequencies for $|a\rangle$ to $|b\rangle$ and $|a\rangle$ to $|c\rangle$ transitions, respectively. Applying the Liouville

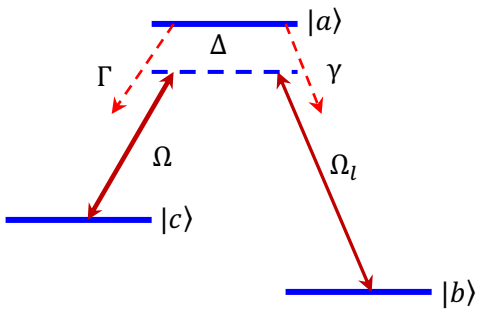

Fig. 2. A three-level atom in Λ configuration for Raman lasing.

equation and using the Hamiltonian (2.1), the equations of motion for the off-diagonal density matrix elements turn out to be

$$\frac{d}{dt}\rho_{ab} = -(i\Delta_b + \gamma_{ab})\rho_{ab} + i\Omega\rho_{bc}^* - i\Omega_l(\rho_{aa} - \rho_{bb}), \tag{2.2}$$

$$\frac{d}{dt}\rho_{ac} = -(i\Delta_c + \gamma_{ac})\rho_{ac} + i\Omega_l\rho_{bc} - i\Omega(\rho_{aa} - \rho_{cc}), \tag{2.3}$$

$$\frac{d}{dt}\rho_{bc} = -[i(\Delta_b - \Delta_c) + \gamma_{bc}]\rho_{bc} + i\Omega_l^*\rho_{ac} - i\Omega\rho_{ab}^*, \tag{2.4}$$

where $\gamma_{ab} = \gamma_{ac} = (\gamma + \Gamma)/2$, with γ and Γ being spontaneous decay rates for the upper level to levels $|b\rangle$ and $|c\rangle$, respectively, are the dephasing rates for respective off-diagonal elements; γ_{bc} is the dephasing rate for ρ_{bc} due to collisions.

We next seek to study the steady-state Raman lasing. To this end, we solve the above set of equations at steady state. Thus imposing the condition that $\dot{\rho}_{\alpha\beta} = 0$ $(\alpha, \beta = a, b, c)$ and assuming that the two detunings are the same, $\Delta_b = \Delta_c = \Delta$, we obtain

$$\rho_{ab} = \frac{i\Omega_l}{\Gamma_{ab}D^*}\left[\left(\Gamma_{bc} + \frac{|\Omega_l|^2}{\Gamma_{ac}^*}\right)n_{ba} - \frac{|\Omega|^2}{\Gamma_{ac}^*}n_{ca}\right], \tag{2.5}$$

$$\rho_{ac} = \frac{i\Omega}{\Gamma_{ac}D}\left[\left(\Gamma_{bc} + \frac{|\Omega|^2}{\Gamma_{ab}^*}\right)n_{ca} - \frac{|\Omega_l|^2}{\Gamma_{ab}^*}n_{ba}\right], \tag{2.6}$$

$$\rho_{bc} = -\frac{\Omega\Omega_l^*}{D}\left[\frac{n_{ca}}{\Gamma_{ac}} + \frac{n_{ba}}{\Gamma_{ab}^*}\right], \tag{2.7}$$

where

$$\Gamma_{ab} = i\Delta + \gamma_{ab}, \quad \Gamma_{ac} = i\Delta + \gamma_{ac}, \quad \Gamma_{bc} = \gamma_{bc},$$

$$D = \Gamma_{bc} + \frac{|\Omega_l|^2}{\Gamma_{ac}} + \frac{|\Omega|^2}{\Gamma_{ab}^*},$$

$$n_{ba} = \rho_{bb} - \rho_{aa}, \quad n_{ca} = \rho_{cc} - \rho_{aa}.$$

Note that since we have considered the lasing transition to be the $|a\rangle \rightarrow |b\rangle$ transition, the laser gain is proportional to the off-diagonal matrix element ρ_{ab}.

1. Maxwell-Schrödinger equation

In the previous section we derived the equation of motion for the density matrix elements by considering a single atom. In many problems in quantum optics, we are interested in the interaction of electromagnetic field with a large number of atoms. A typical example is the propagation of a coherent pulse through a medium, where the atoms are treated quantum mechanically and the laser field is treated classically. Throughout this Chapter we apply semiclassical theory to describe the lasing process. In this section, we derive the Maxwell-Schrödinger equation, which governs the propagation of the laser pulse through the active medium and relate it to the microscopic polarization obtained in the previous section.

The four Maxwell equations in free space read

$$\nabla \cdot \mathbf{D} = 0, \tag{2.8}$$

$$\nabla \times \mathbf{E} = -\frac{\partial \mathbf{B}}{\partial t}, \tag{2.9}$$

$$\nabla \cdot \mathbf{B} = 0, \tag{2.10}$$

$$\nabla \times \mathbf{H} = \mathbf{J} + \frac{\partial \mathbf{D}}{\partial t}, \tag{2.11}$$

with

$$\mathbf{D} = \varepsilon_0 \mathbf{E} + \mathbf{P}, \quad \mathbf{H} = \mathbf{B}/\mu_0, \quad \mathbf{J} = \sigma \mathbf{E}. \tag{2.12}$$

Here $\mathbf{P}$ is the macroscopic polarization of the medium. The conductivity σ takes into account phenomenologically any losses such as the linear response due to the background absorbing medium, and also those losses due to diffraction and mirror transmission. Now taking the curl of Eq.(2.9) and taking into account (2.10) and (2.11), we obtain the wave equation

$$\nabla \times \nabla \times \mathbf{E} + \mu_0 \sigma \frac{\partial \mathbf{E}}{\partial t} + \frac{1}{c^2} \frac{\partial^2 \mathbf{E}}{\partial t^2} = -\mu_0 \frac{\partial^2 \mathbf{P}}{\partial t^2}, \tag{2.13}$$

where $c = 1/\sqrt{\varepsilon_0 \mu_0}$ is the speed of light in free space. Note that the polarization $\mathbf{P}$ can be regarded as the source term for the radiation field $\mathbf{E}$. To obtain a simplified version of the wave equation we consider a situation in which the field is propagating along the z axis and polarized along the x axis, i.e., $\mathbf{E} = E(z,t)\hat{x}$. This assumption is valid if the field is slowly varying on the scale of optical wavelength. The wave equation thus takes a simpler form

$$\left(\frac{\partial}{\partial z} + \frac{1}{c} \frac{\partial}{\partial t} \right) \left(-\frac{\partial}{\partial z} + \frac{1}{c} \frac{\partial}{\partial t} \right) E = -\mu_0 \sigma \frac{\partial E}{\partial t} - \mu_0 \frac{\partial^2 P}{\partial t^2}. \tag{2.14}$$

The field is represented by a running wave

$$E(z,t) = \frac{1}{2} \mathcal{E}(z,t) e^{-i[\nu t - kz - \phi(z,t)]} + c.c., \tag{2.15}$$

where the amplitude $\mathcal{E}(z,t)$ and phase $\phi(z,t)$ of the field are slowly varying function of position and time. Without loss of generality we assume $\mathcal{E}(z,t)$ to be real. The macroscopic polarization for N number of atoms per unite volume can be written as

$$P(z,t) = \frac{1}{2} N p(z,t) e^{-i[\nu t - kz - \phi(z,t)]} + c.c., \tag{2.16}$$

where $p(z,t) = 2\wp_{ab}\rho_{ab}e^{-i[\nu t - kz - \phi(z,t)]} + c.c.$ is the microscopic polarization. Now plugging Eqs. (2.15) and (2.16) into (2.14) together with the slowly varying approximation where the field and polarization satisfy $\partial\mathcal{E}/\partial t \ll \nu\mathcal{E}, \partial\mathcal{E}/\partial z \ll k\mathcal{E}$, $\partial\phi/\partial t \ll \nu, \partial\phi/\partial t \ll k$, and $\partial p/\partial t \ll \nu p, \partial p/\partial z \ll kp$, we obtain the field amplitude equation to be

$$\frac{\partial\mathcal{E}}{\partial z} + \frac{1}{c}\frac{\partial\mathcal{E}}{\partial t} = \kappa\mathcal{E} - \frac{kN}{2\varepsilon}\mathrm{Im}(p), \tag{2.17}$$

where $\kappa = \sigma/2\varepsilon_0 c$ is the linear loss coefficient. In our analysis we ignore the linear loss and write the above equation for Rabi frequency $\Omega_l = \wp_{ab}\mathcal{E}/\hbar$ to make connection to the density matrix equation derived earlier

$$\frac{\partial\Omega_l}{\partial z} + \frac{1}{c}\frac{\partial\Omega_l}{\partial t} = i\eta\rho_{ab}, \tag{2.18}$$

where $\eta = 3N\lambda^2\gamma/4\pi$ with λ being the wavelength of the emitted laser light. We would like to emphasize that this classical equation will be used to describe the propagation of the laser pulse through the medium. The field, represented here by the Rabi frequency Ω_l, is directly related to the single photon coherence ρ_{ab}. In other words the gain/loss is related to this coherence, which essentially is the response of the medium to the laser pulse. As we will show shortly the gain indeed is proportional to $\mathrm{Im}(\rho_{ab})$.

We next proceed to derive the expression for gain in terms of system parameters. To that end, we write the intensity of the laser as $I = I_0 e^{Gz}$, where G being gain/absorption coefficient. We can also write the intensity as $I = A\Omega_l^2(z,t)$, where A is a constant. Then differentiating both expressions and equating the results we get

$$G = \frac{1}{\Omega_l}\frac{\partial\Omega_l}{\partial z}. \tag{2.19}$$

Now in a frame moving with the pulse, the wave equation (2.18) takes the form

$$\frac{\partial \Omega_l}{\partial z} = i\eta\rho_{ab}, \tag{2.20}$$

then the expression for the gain/absorption becomes

$$G = -\frac{1}{\Omega_l}\frac{3N\lambda^2\gamma}{4\pi}\mathrm{Im}\left(\rho_{ab}\right). \tag{2.21}$$

To demonstrate Raman lasing we go back to the results of the previous section and assume that the field detunings are large compared to the dephasing rates, i.e., $\Delta \gg \gamma_{ab}, \gamma_{ac}$ ($\Gamma_{ab} = \Gamma_{ac} = i\Delta$). In this approximation the off-diagonal density matrix element ρ_{ab} becomes

$$\rho_{ab} = -\frac{\Omega_l}{\Delta}\left[\frac{(-i\Delta\gamma_{bc} + |\Omega_l)|^2)n_{ba} - |\Omega|^2 n_{ca}}{i\Delta\gamma_{bc} - |\Omega_l|^2 + |\Omega|^2}\right]. \tag{2.22}$$

For simplicity if we choose $|\Omega_l|^2 = |\Omega|^2$, we have

$$\mathrm{Im}(\rho_{ab}) = -\frac{\Omega_l|\Omega|^2}{\Delta^2\gamma_{bc}}(\rho_{cc} - \rho_{bb}). \tag{2.23}$$

Therefore, substitution of the above expression into Eq. (2.21) yields

$$G = \frac{3N\lambda^2\gamma}{4\pi}\frac{|\Omega|^2}{\Delta^2\gamma_{bc}}(\rho_{cc} - \rho_{bb}). \tag{2.24}$$

Expression (2.24) shows that the lasing field is amplified when $\rho_{cc} > \rho_{bb}$ or Raman inversion. The corresponding lasing process is called Raman lasing.

C. Transient Raman lasing in Helium

Here we consider three-level helium atom in a cascade configuration as shown in Fig. 3. The cascade transition involves single states: $3\ ^1\mathrm{D} \rightarrow 2\ ^1\mathrm{P} \rightarrow 1\ ^1\mathrm{S}$, where the lasing transition is from $2\ ^1\mathrm{P}$ to the ground state $1\ ^1\mathrm{S}$. We show that if the system starts

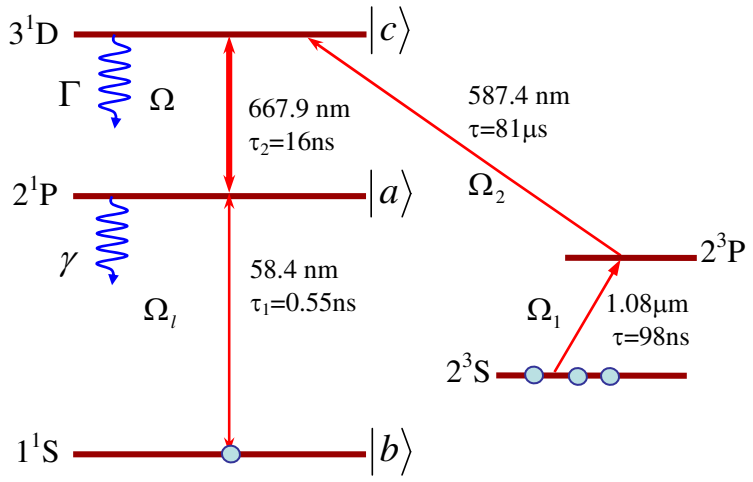

Fig. 3. XUV lasing scheme in helium. Initial population in 2 ^{3}S is driven to level 3 ^{1}D via a counter intuitive pair of pulses in which the 587.4 nm pulse is followed by the 1.08 μm pulse. Once the atom (or ion) is in the 3 ^{1}D state it is driven by a strong pulse at 668 nm to the state 2 ^{1}P. This results in Raman lasing action yielding short pulses at 58.4 nm. Energy levels of Helium [4] and transition rates are taken from Ref. [33].

with a Raman inversion $\rho_{cc}(0) = 0.56$, $\rho_{aa}(0) = 0$ and $\rho_{bb}(0) = 0.44$, strong lasing is observed at 58.4 nm without inversion in the lasing transition. This is attributed the coherence induced by the strong laser drive applied in the auxiliary transition, 3 ^{1}D $\rightarrow$ 2 ^{1}P. In the following we present the theoretical description and experimental implementation of our scheme in detail.

D. Theoretical

In order to clarify the physics and establish the connection with GSS we next briefly summarize the analysis behind ladder Raman lasing as in Fig. 3. The propagation

of the lasing field Ω_l is described by Maxwell-Schrödinger equation

$$\frac{\partial}{\partial z}\Omega_l(z,t) + \frac{1}{c}\frac{\partial}{\partial t}\Omega_l(z,t) = i\eta\rho_{ab}(z,t), \tag{2.25}$$

where $\Omega_l = \wp_{ab}\mathcal{E}_l/\hbar$ is the Rabi frequency of the laser with $\wp_{ab}$ and $\mathcal{E}_l$ being respectively the dipole matrix element for $|a\rangle \rightarrow |b\rangle$ transition and the coupling field strength. The atomic polarization is governed by the off-diagonal element of the density matrix ρ_{ab} times N, where N is the density of the atoms, $\eta = 3N\lambda^2\gamma/4\pi$ with λ being the wavelength of the radiation on the $|a\rangle \rightarrow |b\rangle$ transition and γ the radiation decay rate between these levels.

Turning to the dynamics of the atom we note that the transitions from $|c\rangle$ to $|a\rangle$ and from $|a\rangle$ to $|b\rangle$ are dipole allowed while the transition from $|c\rangle$ to $|b\rangle$ is dipole forbidden making our system a cascade scheme. The transition $|c\rangle \rightarrow |a\rangle$ is driven by a strong coherent field of Rabi frequency Ω while a weak probe field Ω_l is applied to the $|a\rangle \rightarrow |b\rangle$ transition.

The Hamiltonian describing the interaction between a three-level atom and the two classical fields in the dipole and rotating wave approximations, and at resonance is given by

$$H = -\hbar\Omega|c\rangle\langle a| - \hbar\Omega_l|a\rangle\langle b| + \text{H.c.} \tag{2.26}$$

and the master equation for the atomic density matrix has the form

$$\begin{aligned}\frac{d}{dt}\rho = -\frac{i}{\hbar}[H,\rho] &- \frac{\Gamma}{2}\left(\sigma_1^\dagger\sigma_1\rho + \rho\sigma_1^\dagger\sigma_1 - 2\sigma_1\rho\sigma_1^\dagger\right) \\ &- \frac{\gamma}{2}\left(\sigma_2^\dagger\sigma_2\rho + \rho\sigma_2^\dagger\sigma_2 - 2\sigma_2\rho\sigma_2^\dagger\right)\end{aligned} \tag{2.27}$$

in which $\sigma_1 = |a\rangle\langle c|$, $\sigma_1^\dagger = |c\rangle\langle a|$, $\sigma_2 = |b\rangle\langle a|$, $\sigma_2^\dagger = |a\rangle\langle b|$, Γ is the spontaneous emission decay rate for the $|c\rangle \rightarrow |a\rangle$ transition. Without obtaining explicit steady state solutions, some general conclusions can be drawn from the equations of motion of

the density matrix elements on the condition of gain without inversion. For instance, the steady state solution of ρ_{ab} yields

$$\mathrm{Im}(\rho_{ab}) = \frac{2\Omega_l}{\gamma}(\rho_{bb} - \rho_{aa}) + \frac{2\Omega}{\gamma}\mathrm{Re}(\rho_{cb}). \tag{2.28}$$

It follows from Eq. (2.28) that for sufficiently large negative values of $\mathrm{Re}(\rho_{cb})$ amplification ($\mathrm{Im}(\rho_{ab}) < 0$) can be obtained without population inversion.

The problem with such steady state operation is that it requires continuous pumping from $|b\rangle$ to $|c\rangle$. One might consider to use the usual incoherent sources as means of pumping. This however is a problem for the XUV transition. The most common way in such wavelength regimes is instead pumping via electron-atom collisions in a plasma. This however wipes out the coherence, ρ_{bc}, developed in the system due to electron impact. To circumvent this problem, we propose lasing in the transient regime, which does not require continuous incoherent pumping to observe laser gain. The condition for amplification of the lasing field in the transient regime is best understood in terms of the population terms only. For example, from the equation for $\dot{\rho}_{bb}$, we have

$$\mathrm{Im}(\rho_{ab}) = (\gamma\rho_{aa} - \dot{\rho}_{bb})/2\Omega_l. \tag{2.29}$$

Thus the amplification condition $\mathrm{Im}(\rho_{ab}) < 0$ implies $\dot{\rho}_{bb} > \gamma\rho_{aa}$ for the lasing field to show transient gain.

This shows that although no amplification in the steady state, it is possible to realize lasing gain in the transient regime. This is the basis for the present work, which combines several unconventional aspects of laser and atomic physics in order to produce transient lasing without inversion in various regimes. To demonstrate the feasibility of transient lasing we focus on He and He-like ions as indicated in Fig. 3.

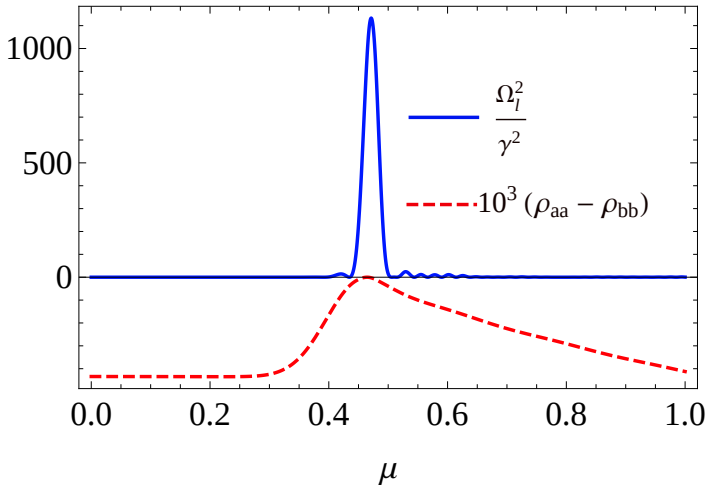

Fig. 4. Plots of the square of the lasing field Ω_l (solid curve) and scaled inversion between $|a\rangle$ to $|b\rangle$ transition (dashed curve) vs retarded time $\mu = t - z/c$ for initial condition $\rho_{cc}(0) = 0.56, \rho_{aa}(0) = 0, \rho_{bb}(0) = 0.44$. The dashed curve shows that the inversion is always negative. The unit of time is $\tau_1 = 0.55$ ns which is the $|a\rangle \rightarrow |b\rangle$ spontaneous transition lifetime. The energy output is a respectable few nanojoules compared to the input energy ~ 0.01 picojoules, other parameters are given in Table I.

In the following we present the numerical solutions to the coupled Maxwell-Schrödinger equation for various initial conditions. In the numerical simulations, we have normalized time and distance such that the equations become dimensionless. We choose the unit of time to be $\tau_1 = 0.55$ ns and the unit of length is $L = 1$ cm. For our system $\Gamma = \tau_2^{-1} = 6.4 \times 10^7$ s^{-1}, $\gamma = \tau_1^{-1} = 1.8 \times 10^9$ s^{-1} and $\lambda = 58.4$ nm. A summary of types of input pulses and parameters used in each figure is given in Table I.

We send in a very weak lasing field Ω_l and let it propagate through the medium along the $z-$axis. In Fig. 4, we plot the output lasing field intensity Ω_l^2 versus retarded time $\mu = t - z/c$ for an initial condition $\rho_{aa}^{(0)} = 0, \rho_{bb}^{(0)} = 0.44$, and $\rho_{cc}^{(0)} = 0.56$. This

Table I. Numerical values of parameters used in Figs. 4, 5 and 6. We have used $c/\gamma L = 16.5$ and $\Gamma/\gamma = 0.035$.

Fig.	Sample	Input lasing size ($\frac{z}{L}$)	Input driving field ($\frac{\Omega_l}{\gamma}$)	Output field ($\frac{\Omega}{\gamma}$)	energy (J)
4	10^{15}	13	$0.01\frac{t^2}{t^2+0.01}$	$9.9e^{-[(t-0.4)/0.1]^2}$	4.16×10^{-9}
5	10^{14}	13	$0.01\frac{t^2}{t^2+1}$	$5e^{-[(t-0.4)/0.1]^2}$	1.18×10^{-8}
6	10^{14}	13	$0.01\frac{t^2}{t^2+1}$	0	1.28×10^{-10}

figure shows that the weak input pulse is amplified by five order of magnitude when there is no inversion in the lasing transition and a little bit of inversion in the Raman transition. This attributed to the coherence induced by the strong laser derive Ω that couples levels $|c\rangle$ to $|a\rangle$.

Furthermore, to see the effect the strong driving field, we plot in Fig. 5 the lasing field intensity Ω_l^2 as a function of μ for a 13 cm long sample by pumping more atoms in the state $|c\rangle$: $\rho_{aa}^{(0)} = 0$, $\rho_{bb}^{(0)} = 0.25$, and $\rho_{cc}^{(0)} = 0.75$. The red-dotted curve shows population inversion as a function of μ in the lasing transition $a \to b$. The system starts to lase with inversion, however, after a short time it operates without inversion on the $a \to b$ transition. This is due to a combination of build up of the coherence ρ_{bc} between levels $|b\rangle$ and $|c\rangle$ and the macroscopic dipole going as ρ_{ab}. Note that the later has much in common with the effect of laser lethargy [21] and the build up of superradiance.

Now consider an initial condition in which the upper level $|c\rangle$ is empty: $\rho_{aa}^{(0)} = 0.75$, $\rho_{bb}^{(0)} = 0.25$, and $\rho_{cc}^{(0)} = 0$ and no driving field, $\Omega = 0$. Our problem essentially

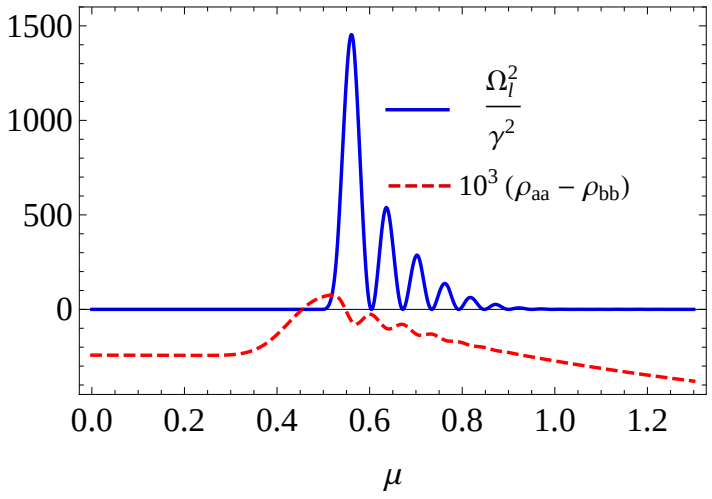

Fig. 5. Plot of the square of output lasing field Ω_l/γ, where γ is the $a \to b$ decay rate, vs retarded time $\mu = t - z/c$ for $z = 13$ and initial condition $\rho_{cc}(0) = 0.75$, $\rho_{aa}(0) = 0$, $\rho_{bb}(0) = 0.25$. The dashed curve represent the population inversion the in the lasing transition.

reduces to a two-level atom system. As can be seen from Fig. 6, most of the emission takes place well after $\rho_{aa} = \rho_{bb}$, which is the earmark of GSS. This is further discussed in section H. Note however that the output energy associated with Fig. 6 is now decreased by two orders of magnitude compared to the results of Fig. 5, where coherence induced by the drive field Ω plays an important role.

E. Experimental

In order to make clear the experimental viability of the present scheme we next discuss the two key points of excitation of 2 ^{3}S and subsequent transfer to 3 ^{1}D in He, specifically:

1. We first inject an ultrashort high power laser pulse to ionize the He gas. We then turn off the laser and rapid recombination and de-excitation follow such

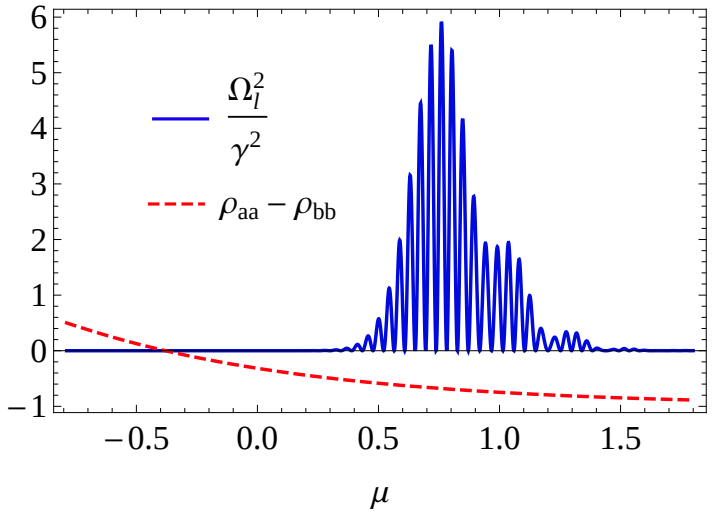

Fig. 6. Plot of the square of output lasing field Ω_l/γ vs retarded time $\mu = t - z/c$ for $z = 13$, no driving field $\Omega = 0$ and initial condition $\rho_{cc}(0) = 0$, $\rho_{aa}(0) = 0.75$, $\rho_{bb}(0) = 0.25$. The dashed curve represent the population inversion between $|a\rangle$ and $|b\rangle$.

that the lowest states of He atoms are prepared according to their statistical weights. Hence for the sake of simplicity, we take the relative population of the 2 ^{3}S and 1 ^{1}S states to be 3 to 1, as in Fig. 4.

2. The population in the 2 ^{3}S state is then transferred to the 3 ^{1}D state via the 2 ^{3}P levels by a combination of optical pumping and dark state adiabatic transfer.

Let us first consider the physics of the laser plasma. We envision a laser plasma created by Keldysh tunneling with a non Boltzmann distribution of neutral excited atoms. This involves $He^+ \rightarrow$ He electron capture via three-body recombination. Three-body recombination for H-like ions is approximately proportional to the forth power of the principal quantum number n^4 and to the square of the electron density as ${N_e}^2$. Hence for sufficiently high initial electron density three-body non-radiative

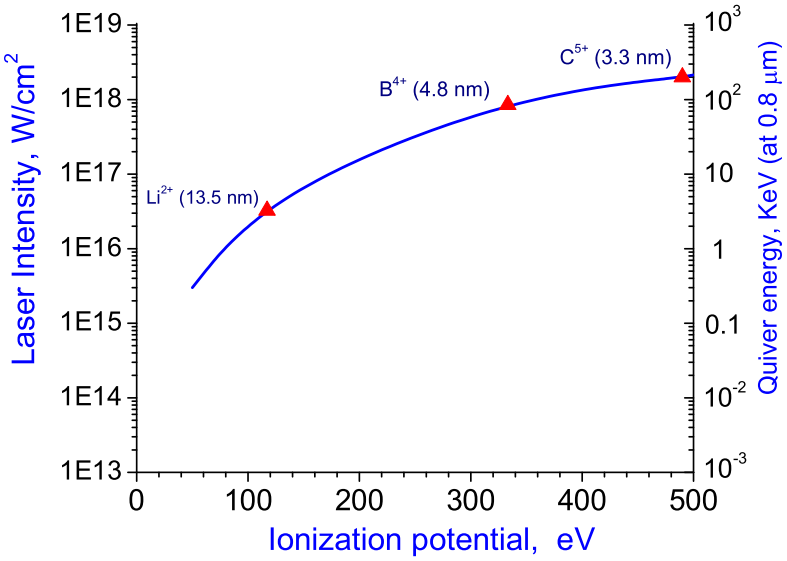

Fig. 7. Laser intensities required for an ionization rate of 10^{12}sec^{-1} versus ionization potential of H-like ions (from Ref. [35]); solid line - Keldysh theory [34]. Corresponding quiver energy ($\varepsilon_q = e^2E^2/4m_e\omega^2$) is shown on the right for laser wavelength $\lambda = 0.8\,\mu$m.

recombination will dominate two-body radiative recombination and radiative decay. However, the collisional ionization from highly excited states is also fast, thus in order for three-body recombination rates to dominate ionization rates, the recombining plasma should have a low electron temperature T_e, if its electrons have Maxwellian energy distribution, otherwise average electron energy should be low.

In order to create a fully ionized He^+ plasma at low temperature, we consider the example of a plasma capillary 10-100 μm in diameter and a few cm long. The tunneling ionization can be used to generate the plasma [34, 35, 36, 37]. In this way we can strip 1 electron from He atoms without significantly heating the plasma, especially for ultra-short laser pulses. The laser intensity needs to be in the order of 10^{15} W/cm^2 for efficient tunneling ionization of He to He^+ according to Keldysh theory [34] (see Fig. 7 [35]). For needle like plasma column such intensities can

easily be obtained from a Ti/Sapphire laser at wavelength $\lambda = 0.8$ μm with ~ 1 mJ energy per pulse in pulses of $50 - 100$ fs duration with ionization pulse propagating in plasma channel. Use of such short pulses is crucial to minimize plasma heating. In the right-hand side of Fig. 7 the vertical axis shows the quiver energy $\varepsilon_{\rm q}$, (in keV), which electrons are gaining in a laser electric field E. If electrons do not collide then their quiver energy disappears with termination of the laser pulse. Therefore it is important to use laser pulses shorter than collision times of electrons in order to minimize plasma heating during the ionization process.

It should also be noted that quiver energy, $\varepsilon_{\rm q}$ goes as λ^2, hence shorter wavelength laser beams are advantageous for creating cooler plasma as heating is proportional to quiver energy $\varepsilon_{\rm q}$ [34, 35]. Therefore it is often beneficial to use the $2^{\rm nd}$ or even $3^{\rm rd}$ harmonic of Ti/Sapphire laser even at a cost of several times less pulse energy than fundamental pulse energy. Additional plasma cooling is provided by it rapid radial expansion, for which the use of a small plasma column diameter is very important, as well as beneficial from the point of view of required laser pulse energy.

The bottom line is that we can create a cold laser plasma which recombines to produce an excited neutral gas. In particular the metastable 2 ^{3}S (8000 s radiative life time) state will be formed with a statistical weight of around 3 compared to the 1^1S state.

F. Robust population transfer and level degeneracy problem

Let us proceed to consider the transfer of population from the three 2 ^{3}S spin states to one particular magnetic sublevel of the 3 ^{1}D manifold. At time t = 0 the population resides in the three spin sublevels $\chi_{1,-1}, \chi_{1,0}$ and $\chi_{1,1}$ as per Fig. 8a. We first optically pump the atoms into one of the 2 ^{3}S spin states, say the $\chi_{1,-1}$ state as indicated in

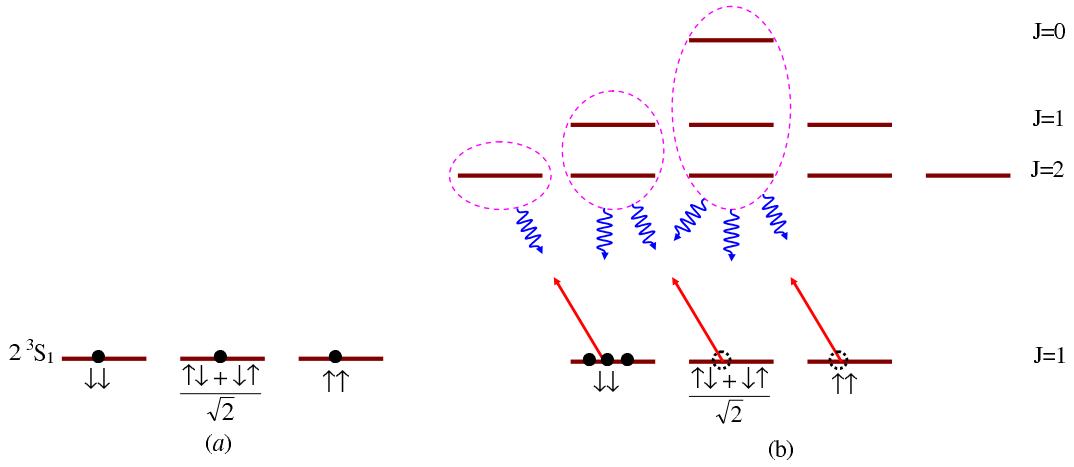

Fig. 8. (a) Atoms begin uniformly distributed in the three magnetic sublevels of the $2\ ^3S_1$ state. (b) Optical pumping by broad band left circularly polarized light to the $2\ ^3P_{2,1,0}$ states results in the transfer of all the population of the spin state $\downarrow\downarrow$.

Fig. 8b.

Robust population transfer from the triplet $2\ ^3S$ to singlet $3\ ^1D$ is then made possible by Stimulated Raman Adiabatic Passage (STIRAP) [38]. In this technique one subjects the state $2\ ^3S$ at $t = 0$ to a so-called counter intuitive pulse sequence with Rabi frequencies Ω_2 and Ω_1 in which the Ω_2 ($2\ ^3P \rightarrow 3\ ^1D$) pulse precedes the Ω_1 ($2\ ^3S \rightarrow 2\ ^3P$) pulse (see Fig. 4). This pulse sequence ideally results in a complete transfer of population to the desired state $3\ ^1D$ without necessarily populating the $2\ ^3P$ state in the process. The mechanism of STIRAP is best understood in the dressed state basis in which we introduce bright and dark states. Beginning with the dark state

$$|0\ \rangle = \frac{\Omega_2|2\ ^3S\rangle - \Omega_1|3\ ^1D\rangle}{\sqrt{\Omega_1^2 + \Omega_2^2}} \tag{2.30}$$

we apply Ω_2 before Ω_1 so that $|0\rangle \cong |2^3S\rangle$ during the early stages of transfer. Then we adiabatically turn on Ω_1 while turning off Ω_2, such that $|0\rangle \cong |3\ ^1D\rangle$ at longer

times. The condition of adiabaticity implies the following estimate of the required pulse energy

$$W \sim 1000 \frac{\hbar c S}{\lambda^3 \gamma \tau_{\rm pulse}}, \tag{2.31}$$

where S is the cross section area of the pulse, $\tau_{\rm pulse}$ is the pulse duration, λ and γ are the wavelength and the rate of the transition. For the weakest $3^1{\rm D}\rightarrow 2^3{\rm P}$ transition $\lambda = 587$ nm and $\gamma = 1.23 \times 10^4$ s^{-1}. Then for a plasma capillary of radius ~ 0.1mm and pulse duration $\tau_{\rm pulse} = 1$ ps, Eq. (2.31) yields $W \sim 0.4$mJ. Currently compact pico-second lasers are commercially available with much greater energy, i.e., a few mJ per pulse just from oscillator-regen amplifier (front-end) is well within the state of the art.

We next proceed to calculate the population transfer from 2 ^{3}S to 3 ^{1}D via STIRAP technique. First we send in a strong resonant pulsed laser (Ω_2) to couple the 2 ^{3}P to 3 ^{1}D transition. It is worth to note that 3 ^{1}D and 3 ^{3}D are essentially degenerate states (only separated by 0.2 nm) and thus the applied laser inevitably couples the 2 ^{3}P to 3 ^{3}D which is 1000 times stronger than the 2 ^{3}P to 3 ^{1}D transition. The Rabi frequencies of the two transitions are related by $\tilde{\Omega}_2 = \sqrt{(\lambda_{de}^3 \tau_{ce})/(\lambda_{ce}^3 \tau_{de})}\Omega_2 \simeq 76\Omega_2$. If one uses input pulses shorter than the spontaneous decay time of these transitions, the population will be transferred to the undesired state 3 ^{3}D. To overcome this problem it is necessary to apply pulses which are wider than the spontaneous decay times. In Fig. 9, we show that by applying ns pulses and for an optimum delay between the probe and driving pulses it is indeed possible to transfer all the initial population in 2 ^{3}S to 3 ^{1}D. However, in plasmas, due to collision of electrons with atoms, the collisional decay time can be shorter than the duration of laser pulses and thus STIRAP may not work.

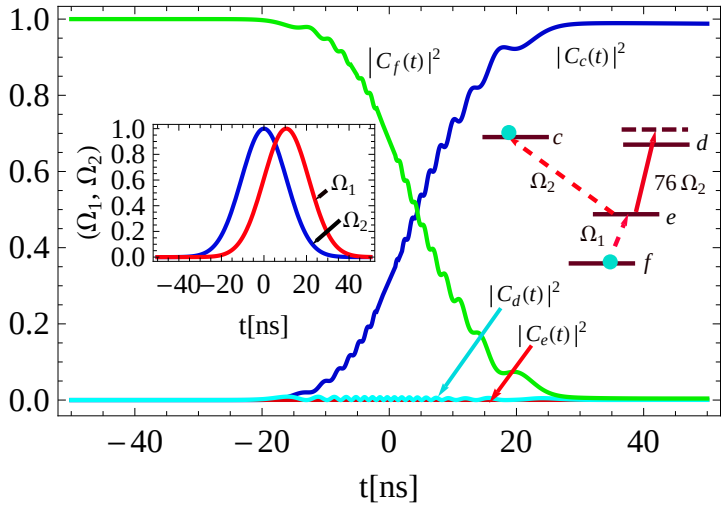

Fig. 9. Plots of probabilities for finding the system in different levels vs scaled time t. The inset on the right shows the level scheme used for the STIRAP process, which involves two Gaussian pulses (inset on the left): $\Omega_1(t) = \exp\left[-[(t+10.5)/15]^2\right]$ and $\Omega_2(t) = \exp\left[-(t/15)^2\right]$.

We thus propose to use an additional laser pulse that couples the 3 ^{3}D to the higher energy state 4 ^{3}P. This essentially cancels absorption by the 3 ^{3}D and enhances the transition to 3 ^{1}D. The equivalent scheme is sketched in the inset of Fig. 10. For sufficiently strong driving field Ω_3, the population in 2 ^{3}S can be transferred completely to the desired state 3 ^{1}D (see Fig. 10). The optimum population transfer is exhibited when the Rabi frequency Ω_3 is approximately twice stronger than $\tilde{\Omega}_2$. Results shown in Fig. 10 are obtained by numerically solving equations for C_h, C_d, C_c, C_e and C_f which are probability amplitudes to find the system in the states $|h\rangle$, $|d\rangle$, $|c\rangle$, $|e\rangle$, and $|f\rangle$, respectively and for initial condition $C_h(0) = C_d(0) = C_c(0) = C_e(0) = 0$ and $C_f(0) = 1$. For resonant driving field the evolution equations read

$$\dot{C}_h(t) = i\Omega_3(t)C_d(t), \tag{2.32a}$$

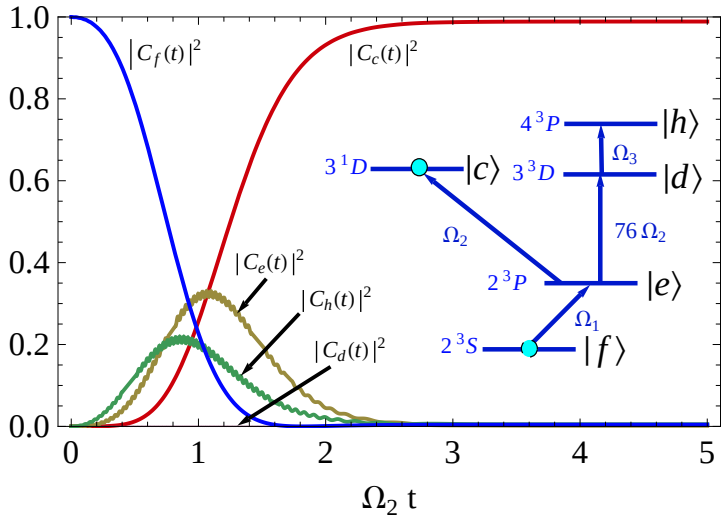

Fig. 10. Plots of probabilities of finding the system in different levels vs scaled time $\Omega_2 t$. With the help of a third laser field the population is transferred to the desired state $|c\rangle$. The inset shows the level scheme used for the STIRAP process which in this case involves three Gaussian pulses $\Omega_1 = 2\exp\left[-(t-0.3)^2/2\right]$ and $\Omega_2 = 2\exp\left[-(t-0.4)^2/2\right]$, and $\Omega_3 = 150\exp\left[-(t-1)^2\right]$.

$$\dot{C}_c(t) = i\Omega_2(t)C_e(t), \tag{2.32b}$$

$$\dot{C}_d(t) = i\tilde{\Omega}_2(t)C_e(t) + i\Omega_3(t)C_h(t), \tag{2.32c}$$

$$\dot{C}_e(t) = i\Omega_2(t)C_c(t) + i\tilde{\Omega}_2(t)C_d(t) + i\Omega_1(t)C_f(t), \tag{2.32d}$$

$$\dot{C}_f(t) = i\Omega_1(t)C_e(t), \tag{2.32e}$$

where $\tilde{\Omega}_2 \simeq 76\Omega_2$. Rabi frequencies Ω_j (j=1,2,3) given in the figures are dimensionless so that the unit of time is the inverse of the amplitude of Ω_2.

Once the population is transferred to the singlet 3 ^{1}D state a strong driving field is applied on the 3 ^{1}D to 2 ^{1}P transition. This generates coherence between 3 ^{1}D and 2 ^{1}P which in turn makes possible transient gain between 2 ^{1}P and 1 ^{1}S (see Figs. 3 and 5).

G. LWI in Helium-like Boron: B^{3+}

In this section we demonstrate transient lasing without inversion for optically thin and thick gas of Helium-like Boron ions. The scheme for B^{3+} is outlined in Fig. 11. We note that $\Lambda-$ scheme LWI is, in some ways, easier to realize than in neutral He [39]. Specifically, in B^{3+} we have the simplifying feature of direct coupling between 2^3P_1 and 1^1S_0 ($\lambda = 6.1$ nm) at the rate $\gamma = 4.2 \times 10^6$ s^{-1} [40]. Furthermore the 2^3P_1 state decays to the 2^3S_1 state ($\lambda = 282$ nm) at a rate $\Gamma = 4.5 \times 10^7$ s^{-1}. Hence, B^{3+} in an ion trap is natural for Λ LWI because $\Gamma > \gamma$, an important condition for lasing without inversion in Λ scheme. The trap should be deep enough to allow ultra short pulse excitation with excess population in the 2^3S state as in the case of neutral He. Here, however, there is no need to introduce STIRAP to transfer of population as was the case in He. The B^{3+} ions would lase at 6.1 nm.

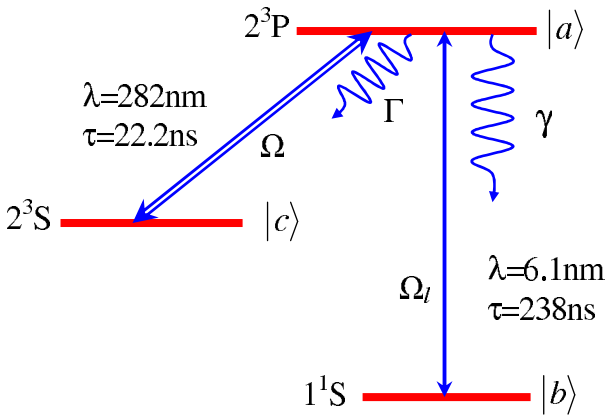

Fig. 11. Lasing without inversion scheme in B^{3+} ion.

1. Optically thin sample

We next proceed to derive an approximate analytic solution which demonstrate amplification without inversion. For a very weak lasing field the equations for the pop-

ulations ρ_{cc}, ρ_{aa}, and the coherence ρ_{ac} decouple from other equations. We thus find

$$\frac{d}{dt}\rho_{cc} = \Gamma\rho_{aa} + i\Omega(\rho_{ac} - \rho_{ca}), \tag{2.33}$$

$$\frac{d}{dt}\rho_{aa} = -(\gamma + \Gamma)\rho_{aa} - i\Omega(\rho_{ac} - \rho_{ca}), \tag{2.34}$$

$$\frac{d}{dt}\rho_{ca} = -\frac{1}{2}(\gamma + \Gamma)\rho_{ca} + i\Omega^*(\rho_{aa} - \rho_{cc}). \tag{2.35}$$

Using an initial condition where $\rho_{bb}(0) = \rho_{bb}^{(0)}$ and $\rho_{cc}(0) = \rho_{cc}^{(0)}$ and with all other elements initially zero, one can readily obtain an approximate solution

$$\rho_{aa}(t) = \frac{\rho_{cc}^{(0)}}{2}\Big[1 - e^{-3\Gamma t/4}\big(\cos 2\Omega t + \frac{3\Gamma}{8\Omega}\sin 2\Omega t\big)\Big]e^{-\gamma t/2}, \tag{2.36}$$

$$\rho_{cc}(t) = \frac{\rho_{cc}^{(0)}}{2}\Big[1 + e^{-3\Gamma t/4}\big(\cos 2\Omega t + \frac{3\Gamma + 4\gamma}{8\Omega}\sin 2\Omega t\big)\Big]e^{-\gamma t/2}, \tag{2.37}$$

$$\rho_{ac}(t) = i\frac{\rho_{cc}^{(0)}}{2}\Big[\frac{2\Gamma + \gamma}{4\Omega} + e^{-3\Gamma t/4}\big(\sin 2\Omega t - \frac{2\Gamma + \gamma}{4\Omega}\cos 2\Omega t\big)\Big]e^{-\gamma t/2}. \tag{2.38}$$

The equation for the off-diagonal density matrix element ρ_{ab} has, in first order in Ω_l, the form

$$\ddot{\rho}_{ab} + \frac{1}{2}(\Gamma + \gamma)\dot{\rho}_{ab} + \Omega^2\rho_{ab} = i\Omega_l[(2\gamma + \Gamma)\rho_{aa} - 3\Omega\mathrm{Im}(\rho_{ac})]. \tag{2.39}$$

On account of Eqs. (2.36) and (2.38), Eq. (2.39) takes the form

$$\begin{aligned}\ddot{\rho}_{ab} + \frac{1}{2}(\Gamma + \gamma)\dot{\rho}_{ab} + \Omega^2\rho_{ab} = i\frac{\Omega_l\rho_{cc}^{(0)}}{8}\Big\{&5\gamma - 2\Gamma \\ &+ [(2\Gamma - 5\gamma)\cos 2\Omega t - 12\Omega\sin 2\Omega t]e^{-3\Gamma t/4}\Big\}e^{-\frac{\gamma t}{2}}.\end{aligned} \tag{2.40}$$

The solution of this equation, taking into account the initial conditions, $\rho_{ab}(0) = 0$

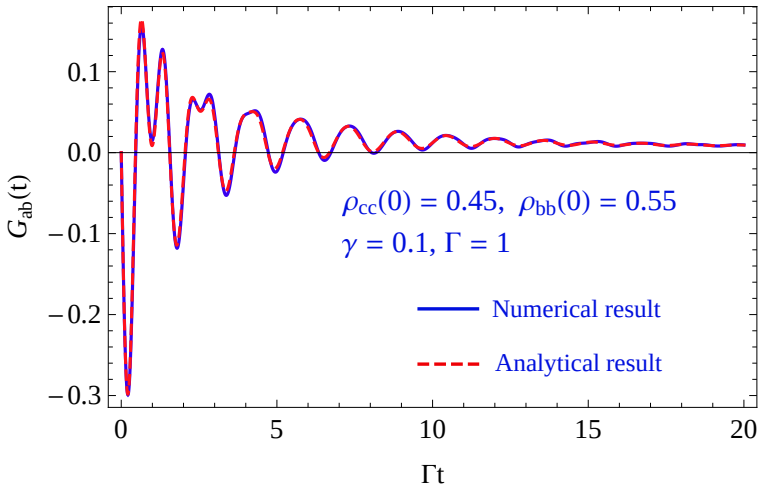

Fig. 12. Plots of dimensionless gain/absorption $G_{ab}(t) = -\frac{\eta}{\Omega_l}\mathrm{Im}[\rho_{ab}(t)]$ in the lasing transition $|a\rangle$ to $|b\rangle$ vs dimensionless time Γt. We have used $\Gamma = 1$, $\gamma = 0.1$, $\eta_b = 4.18$, $\Omega = 4$ and $\Omega_l = 0.01$ with initial condition $\rho_{aa}(0) = 0$, $\rho_{bb} = 0.55$, and $\rho_{cc} = 0.45$. All the parameters are set to be dimensionless with normalizing factors $\Gamma = 4.5 \times 10^7 \mathrm{s}^{-1}$ and $L = 10^{-2}\mathrm{m}$.

and $\dot{\rho}_{ab}(0) = \Omega_l \rho_{bb}^{(0)}$, is found to be

$$\begin{aligned}\mathrm{Im}(\rho_{ab}) \approx \frac{\Omega_l}{\Omega}\Big[\frac{2(\Gamma-\gamma)}{3\Omega}\rho_{cc}^{(0)}\cos\Omega t + (\rho_{bb}^{(0)} - \rho_{cc}^{(0)})\sin\Omega t\Big]e^{-\frac{1}{4}(\gamma+\Gamma)t} \\ + \frac{\Omega_l \rho_{cc}^{(0)}}{2\Omega}\Big[\frac{\gamma - 10\Gamma}{12\Omega}\cos 2\Omega t + \sin 2\Omega t\Big]e^{-(3\Gamma+2\gamma)t/4} \\ + \frac{\Omega_l \rho_{cc}^{(0)}}{8\Omega^2}(5\gamma - 2\Gamma)e^{-\gamma t/2}. \end{aligned} \tag{2.41}$$

The inversion between levels $|a\rangle$ and $|b\rangle$, $W(t) \equiv \rho_{aa}(t) - \rho_{bb}(t)$ is given by

$$W(t) = -(\rho_{bb}^{(0)} + \rho_{cc}^{(0)}) - \frac{\rho_{cc}^{(0)}}{2}\Big[3e^{-\gamma t/2} - (\cos 2\Omega t + \frac{3\Gamma}{8\Omega}\sin 2\Omega t)e^{-(3\Gamma+2\gamma)t/4}\Big]. \tag{2.42}$$

In general, the intensity of gain/absorption of a field with the Rabi frequency

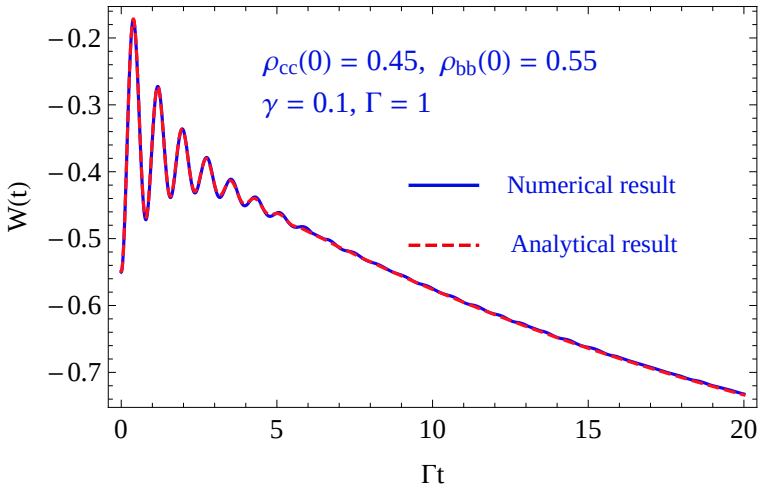

Fig. 13. Plots of inversion $W(t)$ in the lasing transition $|a\rangle$ to $|b\rangle$ vs Γt for the same parameters as in Fig. 12.

$\Omega_{\alpha\beta}$ coupling the transition $\alpha \to \beta$ with spontaneous decay rate $\gamma_{\alpha\beta}$ is given by

$$G_{\alpha\beta} \equiv -\frac{3}{4\pi} N \lambda_{\alpha\beta}^2 \gamma_{\alpha\beta} \frac{\mathrm{Im}(\rho_{\alpha\beta})}{\Omega_{\alpha\beta}} \tag{2.43}$$

where N is the density of atoms/ions in the medium, $\lambda_{\alpha\beta}$ is the wavelength of the transition, and $\rho_{\alpha\beta}$ the off-diagonal density matrix element. For the $|a\rangle$ to $|b\rangle$ transition, the expression for gain takes the form

$$G_{ab}(t) = -\eta_b \mathrm{Im}(\rho_{ab}(t))/\Omega_l, \tag{2.44}$$

in which $\eta_b = 3N\lambda^2\gamma/4\pi$. In general $\mathrm{Im}(\rho_{ab})$ is an oscillatory function which can take negative, positive or zero values. If $\mathrm{Im}(\rho_{ab}) < 0$, the system exhibits gain for the probe laser pulse while for $\mathrm{Im}\,(\rho_{ab}) > 0$ the probe laser pulse is attenuated.

In Fig. 12 we plot the analytical as well as numerical result for the gain (2.44) as a function of normalized time Γt for a density $N = 10^{15}$ ions/cm^3 and an initial condition $\rho_{aa}(0) = 0$, $\rho_{bb}(0) = 0.55$, $\rho_{cc}(0) = 0.45$. This figure shows that the analytical

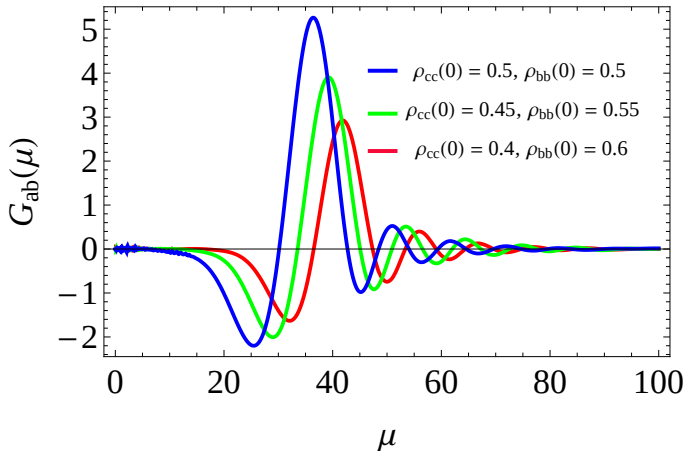

Fig. 14. Plots of dimensionless gain $G_{ab}(\mu) = -\frac{\eta}{\Omega_l}\mathrm{Im}[\rho_{ab}(\mu)]$ and vs retarded time μ for $\Omega = 3$, $\eta_b = 41.8(N = 10^{16}\mathrm{ions/cm}^3)$, $z = 10$, $\Omega_l = 10^{-2}\exp[-(t-3)^2/5]$, $\gamma = 0.1$, $\Gamma = 1$ for different initial conditions. All the parameters are set to be dimensionless with normalizing factors $\Gamma = 4.5 \times 10^7 \mathrm{s}^{-1}$ and $L = 10^{-2}\mathrm{m}$.

result is in a complete agreement with with the numerical result. Furthermore, the figure illustrates that even though there is absorption at initial moment of time, the amplification dominates at later times which leads to transient gain without population inversion as per Fig. 13. Analytical calculation which demonstrate gain without inversion using delta-function pulses is presented in Appendix A.

2. Optically thick sample

In order to obtain strong laser output it is natural to consider an optically thick sample. In this case one has to take into account the propagation of the input pulses through the medium. The dynamics of the system is described by six density matrix equations coupled to the two Maxwell-Schrödinger equations for the fields. We numerically solve these equations by assuming the strong driving field does not change appreciably in time and space.

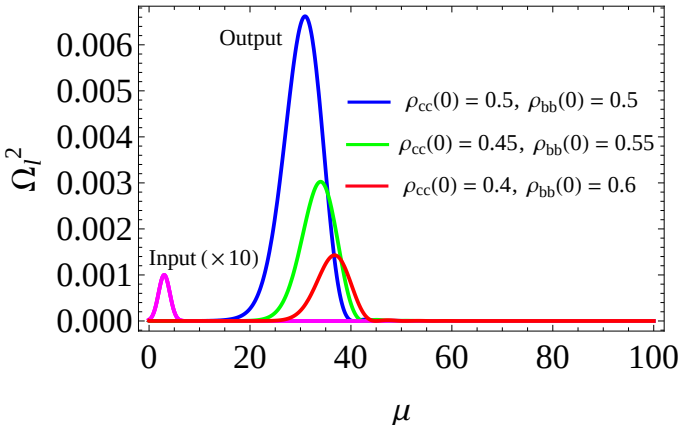

Fig. 15. Plots of the square of lasing field vs retarded time for the same parameters and initial condition as in Fig. 14. The solid red curve represent the input lasing field at $z = 0$ scaled up by a factor of 10.

Our numerical results are presented in Figs. 14 and 15. In Fig. 14 we plot the time evolution of the gain [(2.44)] in the lasing transition vs retarded time μ for a density $N = 10^{16}$ions/cm^3, sample size $L = 10$cm, and for different initial populations. This figure indicates absorption of the lasing field for some time and then gain for certain interval of time which later goes to zero in the long time limit. In support of this assertion, in Fig. 15 we plot input and output lasing pulses for the same initial populations as in Fig. 14 and show that there is indeed transient gain or amplification of the input laser pulse. Comparing the corresponding plots in Figs. 14 and 15 we observe that when the magnitude of the gain increases the amplification increases accordingly. In addition, gain depends on several parameters: density of the medium (Boron ions), the strength of the driving field and size of the sample. One can optimize the intensity of the output laser by choosing these parameters appropriately.

In Table II we present a list of parameters used in Figs. 14 and 15 and the corresponding energy of the output laser for a given initial condition. It turns out that

Table II. Numerical values of parameters used in Fig. 15 and output energy. We have used $c/\Gamma L = 666.7$ and $\gamma/\Gamma = 0.01$

Fig.	N(cm^{-3})	Sample size ($\frac{z}{L}$)	Input lasing field ($\frac{\Omega_l}{\Gamma}$)	Input driving field ($\frac{\Omega}{\Gamma}$)	Output energy (J)
15(Dotted)	10^{16}	10	$0.01e^{-[(t-3)/\sqrt{5}]^2}$	3	2.10×10^{-10}
15(Dashed)	10^{16}	10	$0.01e^{-[(t-3)/\sqrt{5}]^2}$	3	4.64×10^{-10}
15(Solid)	10^{16}	10	$0.01e^{-[(t-3)/\sqrt{5}]^2}$	3	1.12×10^{-9}

for the density of 10^{16}ions/cm^3 Boron ions, the output energy ranges approximately from 0.1 to 1nJ, which is enhanced by a factor of 2 to 3 orders of magnitude compared to the input lasing field whose energy is 5.11×10^{-12}J.

Similar Λ LWI scheme can be realized in C^{4+} for which decay rate of the $2^3P_1 \rightarrow 1^1S_0$ ($\lambda = 4.1$ nm) lasing transition is 2.7×10^7 s^{-1}, while those for the $2^3P_1 \rightarrow 2^3S_1$ ($\lambda = 227$ nm) is 5.7×10^7 s^{-1} [41].

It is worth mentioning that the results presented in this Chapter do not take into account decoherence effects due to collisions between the emitters and electron-ion collisions. The issue of line broadening in plasma and possible dephasing decay rates in our system are addressed in Appendix A.

H. Discussion

In order to better understand the key results of section D we next consider the old problem of swept gain in short wavelength (two-level atom) laser systems. For example, the following quote from [22] adopted for the present purposes, summarizes

the physics:

> "In considerations involving short-wavelength lasers, it is clear that in view of the very short spontaneous lifetimes, one would like to sweep the excitation in the direction of lasing in order that the atoms be prepared in an excited state just as the radiation from previously excited atoms reaches them.... We find that the small-signal regime of the amplifier is highly anomalous, and that superradiance plays an important role in the non-linear regime."

A coherent evolution of an ultra short pulse can be described by the coupled Maxwell-Schrödinger equations. For a pulse whose electric field is given by

$$\mathrm{E}(z,t) = \mathcal{E}_l(z,t)e^{i(kz-\omega t)}, \tag{2.45}$$

with $\mathcal{E}_l(z,t)$ being its amplitude, and an atomic polarization having an amplitude $\mathcal{P}$ and population inversion $\Delta\mathcal{N} = \rho_{aa} - \rho_{bb}$, the Maxwell-Schrödinger equations read

$$\frac{\partial}{\partial z}\Omega_l = \alpha\mathcal{P}, \tag{2.46}$$

$$\frac{\partial}{\partial \mu}\mathcal{P} = \Omega_l\Delta\mathcal{N}, \tag{2.47}$$

$$\frac{\partial}{\partial \mu}\Delta\mathcal{N} = -\Omega_l\mathcal{P}. \tag{2.48}$$

In the above equations, the Rabi frequency $\Omega_l = \wp\mathcal{E}_l/\hbar$ with $\wp$ being the atomic dipole matrix element and $\mu = t - z/c$ is the retarded time. The solutions for Eqs. (2.47) and (2.48) are given by

$$\mathcal{P} = \sin\left[\int_{-\infty}^{\mu}\Omega_l(\mu')d\mu'\right], \tag{2.49}$$

$$\Delta\mathcal{N} = \cos\left[\int_{-\infty}^{\mu}\Omega_l(\mu')d\mu'\right], \tag{2.50}$$

and therefore

$$\frac{\partial}{\partial z}\Omega_l = \alpha \sin\left[\int_{-\infty}^{\mu} \Omega_l(\mu')d\mu'\right]. \tag{2.51}$$

In particular, for a thin region of thickness Δz and a step function input pulse, we have

$$\Omega_l(z+\Delta z,\mu) = \Omega_l(z,\mu) + \alpha\Delta z \sin[\Omega_l(z)\mu]. \tag{2.52}$$

Thus the output pulse is given by the input step function with an additional emitted field whose envelope oscillates at a frequency Ω_l. It should be noted that this emitted field is not governed by the population inversion $\Delta\mathcal{N}$. We have here a simple example of laser gain without inversion. The pulse is gaining energy at a maximal rate when $\Omega_l\mu = \pi/2$ at which point the population inversion $\Delta\mathcal{N} = \cos(\Omega_l\mu)$ vanishes.

If we consider the case where Ω_l is slowly varying in μ, one can write Eq. (2.51) as

$$\frac{d}{dz}\Omega_l = \alpha \sin\left[\mu\Omega_l(\mu,z)\right] \tag{2.53}$$

which can be written in the form

$$\int_{\Omega_l(\mu,0)}^{\Omega_l(\mu,z)} \frac{d\Omega_l}{\sin(\mu\Omega_l)} = \int_0^z \alpha dz. \tag{2.54}$$

Performing the integration, we obtain

$$\ln\Big[\tan\Big(\frac{\mu\Omega_l(\mu,z)}{2}\Big)\Big] - \ln\Big[\tan\Big(\frac{\mu\Omega_l(\mu,0)}{2}\Big)\Big] = \alpha\mu z. \tag{2.55}$$

This yields

$$\Omega_l(\mu,z) = \frac{2}{\mu}\arctan\Big[\tan\big(\mu\Omega_l(\mu,0)/2\big)e^{\alpha\mu z}\Big]. \tag{2.56}$$

As an example, if we take $\alpha = 0.06$, $z = 5$cm and input pulse $\Omega_l(\mu,0) = 0.1\exp[-(t/0.2)^2]$ the output pulse is amplified approximately by a factor of one order of magnitude as shown in Fig. 16.

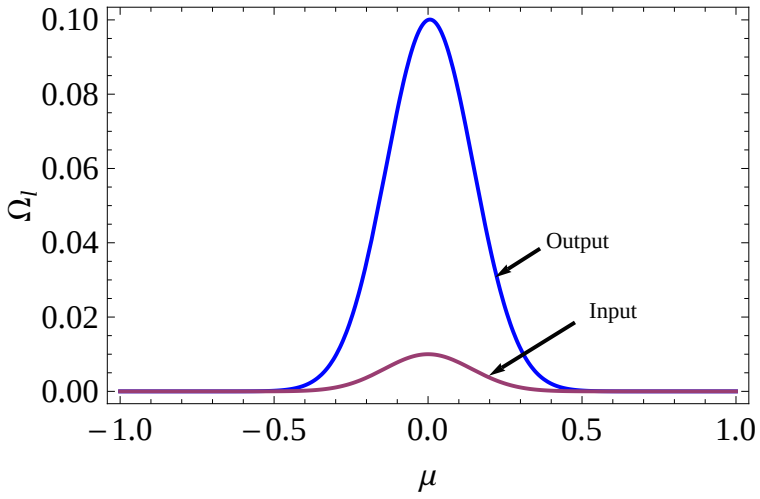

Fig. 16. Plots of $\Omega_l(\mu, z)$ vs μ for $\alpha = 0.06$ and $z = 5$cm and for an initial input pulse $\Omega_l(\mu, 0) = 0.1\exp(-t^2/0.4)$.

To put the present XUV scheme in context we note that there are several methods for producing extreme ultra-violet and soft x-ray lasing: for example, using a capillary discharge [42], a free-electron laser [43], optical field ionization of a gas cell [44] or plasma-based recombination lasers [45]. Coherent XUV and soft x-ray radiation can also be produced by the generation of harmonics of an optical laser in a gas or plasma medium. Our goal in the present work is to investigate the extent to which (transient) LWI might be useful in this problem.

Electron excitation has been the mechanism of choice for the pumping of a wide variety of XUV lasers. Alternatively, high-intensity ultrashort (with pulse duration less then 100 fs) optical pulses can be used to pump recombination lasers [35]. In this method, intense circularly polarized light ionizes atoms via tunneling process. Then atoms recombine yielding species in excited electron states.

The three-body recombination scheme is attractive due to its potential of achieving lasing at XUV and soft x-ray wavelengths with relatively moderate pumping re-

quirements. Several experiments have demonstrated gain and lasing in such scheme [46, 47, 48]. Recombination mechanism relies on obtaining ions in a relatively cold plasma which is possible due to short duration of the pump pulse. Then rapid recombination and de-excitation processes follow during which transient population inversion can be created.

In this Chapter we focused on lasing in He and He-like ions which utilizes advantages of the recombination XUV and soft x-ray lasers and the effects of quantum coherence. The later, for example, is the key for lasing without inversion wherein quantum coherence created in the medium by means of strong driving field helps to partially eliminate resonant absorption on the transition of interest and to achieve gain without population inversion. Such an effect holds promise for obtaining short wavelength lasers in the XUV and x-ray spectral domains, where inverted medium is difficult to prepare due to fast spontaneous decay.

CHAPTER III

SINGLE-PHOTON DICKE SUPERRADIANCE *

A. Introduction

When a gas molecules, confined in volume of dimensions less than the wavelength of the emitted radiation, are interacting with a common radiation field, the spontaneous emission process can not be described by treating each molecule separately. One should rather consider the gas as a single quantum mechanical system involving collective states. This leads to spontaneous emission of coherent radiation as a result of transition between such collective states. For a system of N spin-1/2 particles and when the system is initially in state in which half of the molecules are in excited and the other half in the ground state, Dicke [7] showed that the collective system emits maximum radiation intensity proportional N^2. Extension of this phenomenon for a gas confined in volume whose dimension is larger than the radiation wavelength is later generalized by Dicke himself [49] and several other authors [50].

From the physical standpoint, cooperative spontaneous emission is an example of many-body quantum problem of N atoms collectively interacting with electromagnetic field. Emission from a weakly excited group of atoms is, in some ways, even more interesting than the case of a highly excited system. In the case of a weakly excited ensemble (e.g. single-photon state–one atom out of N is excited) it might be thought that the radiation rate would go as the single atom decay rate γ; however, the such state radiates at a rate $\Gamma_N \propto N\gamma$.

---

* Reprinted with permission from "Correlated spontaneous emission on the Danube" by Eyob A. Sete, A. A. Svidzinsky, H. Eleuch, Z. Yang, R. D. Nevels, and M. O. Scully, 2010. *J. Mod. Opt.*, 57, 1311-1330, Copyright [2010] by Taylor and Francis Ltd.

Recent calculations [11, 12] focus on the problem in which a single photon is stored in a gas cloud and then retrieved at a later time. The temporal, directional, and spectral characteristics of the cooperatively reemitted radiation is then of interest. Synchrotron radiation experiments involving N nuclei excited by weak ray pulse have features in common with the present problem. In such experiments a thin disk of nuclei can easily be prepared in a superposition in which all the atoms are predominantly in the ground state together with a small probability of being in the excited state.

In the optical domain cooperative spontaneous emission is a subject of fundamental and applied interest. For instance, quantum beat phenomena provide a good example of a situation in which a quantized electromagnetic field yields a radically different result from a classic field plus vacuum fluctuation analysis. An ensemble of N two-level atoms with one excitation also plays an important role in quantum memory and quantum networking. Relevant experiments have been carried out by the groups of Kuzmich [51], Kimble [52], and Vuletic [53].

More recently the dynamical evolution of a large cloud with one atom excited out of N atoms undergoing cooperative spontaneous emission has been considered [54]. It is found that the decay of such a state depends on the relation between an effective Rabi frequency $\Omega = \sqrt{N}\Omega_0$ and the time of photon flight through the cloud R/c. If $R < c/\Omega$ the state exponentially decays with the rate $\Omega^2 R/c$. In the opposite limit $R \gg c/\Omega$, the coupled atom-radiation system oscillates with frequency Ω between the collective Dicke state (with no photons) and the atomic ground state (with one photon) while decaying at a rate c/R. We call such a regime a new kind of "cavity" QED because dynamical oscillations in the evolution of the quantum state exist without a cavity. It is as if the atomic cloud acts to form a "cavity" with the atom cloud volume V replacing the virtual photon (cavity) volume V_{ph}, such that the usual

vacuum Rabi frequency $\Omega_{vac} = (\wp/\hbar)\sqrt{\hbar\omega/\epsilon_0 V_{vac}}$ is replaced by $\Omega_0 = (\wp/\hbar)\sqrt{\hbar\omega/\epsilon_0 V}$ in the present problem. Here $\wp$ is the electric-dipole transition matrix element, $\hbar\omega$ is the photon energy and ϵ_0 is free space permittivity.

Cooperative effects of N atoms in a cavity were investigated in 1980's by Cummings [55, 56, 57] and others [58, 59]. Buzek [60] studied the dynamics of an excited atom in the presence of $N-1$ atoms in the free space and predicted radiation suppression. Dynamics of the system in free space and spatial anisotropy of the emitted radiation have been re-explored in the past few years [11, 12, 14, 15, 54, 61, 62].

When interatomic distances are small compared to the radiation wave length λ the exchange of virtual photons induces strong dipole-dipole interaction between atoms [63, 64]. Such effects can have interesting consequences, for example, can destroy superradiance. Recently, it was shown that virtual photons modify time evolution of the system [61] and dramatically change evolution of the trapped states [14]. One way to overcome the undesired effects of nearby atoms is to replace the small sample by an extended cloud. Unfortunately this tends to destroy superradiance since it brings in subradiant states $|B_1\rangle$, $|B_2\rangle$, ..., $|B_{N-1}\rangle$ (see Fig. 17). In a recent paper [13], it was shown to a good approximation however that small sample Dicke superradiance carries over to large sample.

Effects of virtual photons on evolution of N two-level atom states with two initial conditions, namely symmetric state $|B_0\rangle_{\rm sym} = \frac{1}{\sqrt{N}}\sum_{j=1}^{N}|\downarrow_1\downarrow_2 \ ... \uparrow_j \ ... \downarrow_N\rangle$ and timed Dicke state $|B_0\rangle = \frac{1}{\sqrt{N}}\sum_{j=1}^{N} e^{i\mathbf{k}_0\cdot\mathbf{r}_j}|\downarrow_1\downarrow_2 ... \uparrow_j ... \downarrow_N\rangle$ in the large sample limit ($R \gg \lambda$) has been analyzed. For symmetric state the effect of virtual processes appear to be essentially negligible on the time scale of a few $1/\Gamma$ as illustrated in Fig. 18 (here $\Gamma = 3N\gamma/2(k_0R)^2$). As shown in the same figure, for fast decaying state $|B_0\rangle$, such processes excite other states with $10-20\%$ probability which can be observed experimentally. The catch is that the evolution of the timed Dicke state can

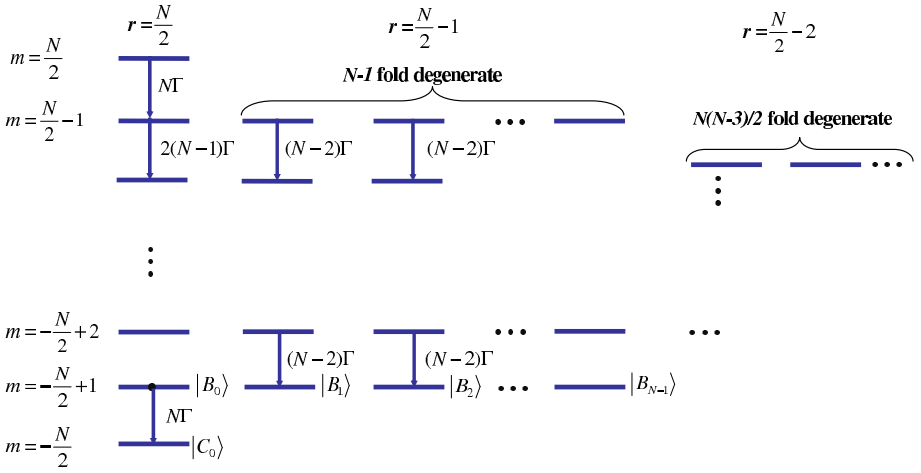

Fig. 17. Dicke energy level representation of N two-level atoms.

be described to a good approximation by real processes.

In this Chapter, we consider N two-level atoms interacting with the continuum of vacuum modes. We take an initial state such that one atom is excited out of the N atoms. We investigate how this state evolves in time both in small sample ($R \ll \lambda$) and large sample ($R \gg \lambda$) limits. Moreover, we calculate the collective Lamb shift corresponding to the symmetric state.

B. Single-photon Dicke superradiance

Here we consider N identical two-level atoms whose upper and lower levels are represented by $|a_j\rangle$ and $|b_j\rangle$ (with $j = 1, ..., N$) initially prepared in the single-photon state by absorption of a single photon of wave vector $\mathbf{k_0}$. That is the atomic system is prepared in a collective initial state

$$|B_0\rangle = \frac{1}{\sqrt{N}} \sum_{j=1}^{N} e^{i\mathbf{k_0}\cdot\mathbf{r}_j} |\downarrow_1 \downarrow_2 \ldots \uparrow_j \ldots \downarrow_N\rangle, \tag{3.1}$$

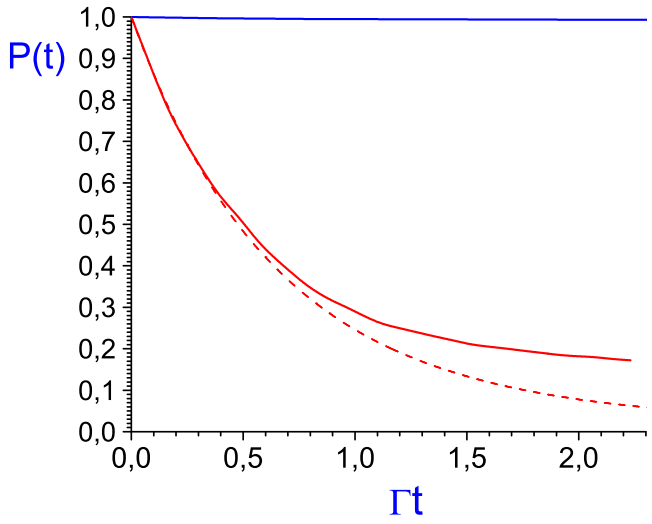

Fig. 18. Probability that atoms are excited as a function of time for $R = 5\lambda$ calculated taking into account virtual processes (solid lines). Upper solid curve shows evolution of the symmetric state $|B_0\rangle_{\rm sym}$ which practically does not decay on the time scale of a few $1/\Gamma$. Lower lines show evolution of the $|B_0\rangle$ state with (solid line [65]) and without (dash line [14]) taking into account virtual processes.

where we have introduced a notation $|a_j\rangle \equiv |\uparrow_j\rangle$ and $|b_j\rangle \equiv |\downarrow_j\rangle$, and $\mathbf{r}_j$ denotes the position of the j^{th} atom. It is worth mentioning that the term in the phase factor $\mathbf{k}_0 \cdot \mathbf{r}_j = (\omega/c)\mathbf{n}_0 \cdot \mathbf{r}_j = \omega t_j$ describes the timing of the excitation of atoms located at $\mathbf{r}_j$ [11]. Hence we call the state $|B_0\rangle$ a timed Dicke state and the corresponding complete set of states shown in Fig. 17 timed Dicke basis.

The Hamiltonian describing interaction between the atoms and the radiation field in the rotating wave approximation is given by

$$\hat{V}(t) = \sum_{j,\mathbf{k}} \hbar g_{\mathbf{k}} \hat{\sigma}_j \hat{a}^\dagger_{\mathbf{k}} e^{-i\mathbf{k}\cdot\mathbf{r}_j} e^{i(\nu_k - \omega)t} + \text{H.c.}, \tag{3.2}$$

where $g_{\mathbf{k}} = (\omega\wp/\hbar)\sqrt{\hbar/\epsilon_0 V_{\rm ph}\nu_k}$ is the atom-field coupling constant, $\wp$ is the atomic dipole matrix element, ϵ_0 is the permittivity of free space, $V_{\rm ph}$ is the quantization volume, $\nu_k = ck$ is the frequency of the kth mode, $\hat{a}_{\mathbf{k}}$ ($\hat{a}^\dagger_{\mathbf{k}}$) is annihilation (creation) operator of a photon with wave vector $\mathbf{k}$ and $\hat{\sigma}_j$ ($\hat{\sigma}^\dagger_j$) is the lowering (raising) operator of the jth atom.

1. Small sample

Next we calculate the evolution of the $|B_0\rangle$ state for N identical atoms confined in a spherical volume of radius R much less than the radiation wavelength λ. In this limit, one can write the exponential factor in Eq. (4.1) as $\exp(i\mathbf{k_0}\cdot\mathbf{r}) \cong 1$ and hence the initial state takes the form

$$|B_0\rangle_{\rm sym} = \frac{1}{\sqrt{N}}\sum_{j=1}^{N} |\downarrow_1\downarrow_2 \ldots \uparrow_j \ldots \downarrow_N\rangle. \tag{3.3}$$

In terms of Dicke basis the corresponding state vector can be written as

$$|\Psi(t)\rangle = \beta_0(t)|0\rangle|B_0\rangle_{\rm sym} + \sum_{\mathbf{k}} \gamma_{\mathbf{k}}(t)|C_0, 1_{\mathbf{k}}\rangle. \tag{3.4}$$

To calculate matrix elements in the rate equation it is convenient to use the angular momentum approach. As Dicke pointed out, the atomic states can be mapped onto angular momentum states with $r = N/2$ and $m = (n_a - n_b)/2$ with n_a and n_b being the number of atoms in the excited and ground states, respectively. If we denote the initial state by $|B_0\rangle_{\rm sym} = |r, m\rangle$ then other states can be obtained by applying the raising $\hat{L}_+ \equiv \sum_{j=1}^{N}\hat{\sigma}^\dagger_j$ and lowering $\hat{L}_- \equiv \sum_{j=1}^{N}\hat{\sigma}_j$ operators on $|r, m\rangle$ (see Fig. 17). The Schrödinger equation yields

$$\frac{d}{dt}\beta_0(t) = -i\langle 0|_{\rm sym}\langle B_0|\hat{V}(t)|\Psi(t)\rangle = -i\sum_{\mathbf{k}} g_{\mathbf{k}} e^{-i(\nu_{\mathbf{k}}-\omega)t}\gamma_{\mathbf{k}}\langle r, m|\hat{L}_+|r, m-1\rangle. \tag{3.5}$$

Recalling that $\hat{L}_+|r,m-1\rangle = \big[r(r+1)-m(m-1)\big]^{1/2}|r,m\rangle$, the above equation takes the form

$$\frac{d}{dt}\beta_0(t) = -i\sqrt{N}\sum_{\mathbf{k}} g_{\mathbf{k}} e^{-i(\nu_{\mathbf{k}}-\omega)t}\gamma_{\mathbf{k}}. \tag{3.6}$$

In a similar way one can verify that

$$\frac{d}{dt}\gamma_{\mathbf{k}}(t) = -i\sqrt{N} g_{\mathbf{k}} e^{i(\nu_{\mathbf{k}}-\omega)t}\beta_0. \tag{3.7}$$

Plugging formal solution of Eq. (3.7) into (3.6), we find

$$\frac{d}{dt}\beta_0(t) = -N\sum_{\mathbf{k}} g_{\mathbf{k}}^2 \int_0^t dt'\ e^{i(\nu_{\mathbf{k}}-\omega)(t'-t)}\beta_0(t'). \tag{3.8}$$

Applying Markov approximation in which we replace $\beta_0(t')$ by $\beta_0(t)$ and noting that $\int_0^t dt'\ e^{i(\nu_{\mathbf{k}}-\omega)(t'-t)} \cong \pi\delta[c(k-k_0)]$, we obtain

$$\frac{d}{dt}\beta_0(t) = -\frac{\pi N}{c}\sum_{\mathbf{k}} g_{\mathbf{k}}^2 \delta(k-k_0)\beta_0(t). \tag{3.9}$$

Using the transformation

$$\sum_{\mathbf{k}} \to \frac{V_{\rm ph}}{(2\pi)^3}\int d^3\mathbf{k} = \frac{V_{\rm ph}}{2\pi^2}\int_0^\infty k^2 dk, \tag{3.10}$$

Equation (3.9) can be written as

$$\frac{d}{dt}\beta_0(t) = -\Gamma\beta_0(t), \tag{3.11}$$

where $\Gamma = N\gamma$ and $\gamma = \wp^2\omega^3/2\pi\hbar\epsilon_0 c^3$ is the single atom decay rate. Therefore, the initial state $|B_0\rangle_{\rm sym}$ decays exponentially to the ground state as $\beta_0(t) = \exp(-N\gamma t)$ with a decay rate N times faster than that of an isolated two-level atom. This result was obtained by Dicke [7]. Since only one photon is involved in the system, we call this process single-photon Dicke superradiance.

2. Large sample

In this section we discuss single-photon Dicke superradiance in the large sample limit, $R \gg \lambda$. We first consider the three atom example and extend it to N atoms case and show that, to a good approximation, the time Dicke state decays exponentially to the ground state with a rate $\Gamma_N = N\gamma$.

a. Three atoms

First let us consider three atoms and calculate the evolution of the state $|B_0\rangle$. The state vector at time t can be written in terms of the Dicke basis set (see Fig. 19) as

$$|\Psi(t)\rangle = \beta_0(t)|B_0, 0\rangle + \beta_1(t)|B_1, 0\rangle + \beta_2(t)|B_2, 0\rangle + \sum_{\mathbf{k}} \gamma_{\mathbf{k}}(t)|C_0, 1_{\mathbf{k}}\rangle.$$

Now applying Schrödinger equation, we obtain

$$\frac{d}{dt}\beta_0(t) = -\frac{i}{\sqrt{3}} \sum_{\mathbf{k}} g_{\mathbf{k}} \sum_{j=1}^{3} e^{i(\mathbf{k}-\mathbf{k_0})\cdot\mathbf{r_j}} e^{-i(\nu_{\mathbf{k}}-\omega)t} \gamma_{\mathbf{k}}(t), \tag{3.12}$$

$$\begin{aligned}\frac{d}{dt}\gamma_{\mathbf{k}}(t) = -ig_{\mathbf{k}}\Big[\frac{\beta_0}{\sqrt{3}} \sum_{j=1}^{3} e^{-i(\mathbf{k}-\mathbf{k_0})\cdot\mathbf{r_j}} + \frac{\beta_1}{\sqrt{2}}\big(e^{-i(\mathbf{k}-\mathbf{k_0})\cdot\mathbf{r_1}} - e^{-i(\mathbf{k}-\mathbf{k_0})\cdot\mathbf{r_2}}\big) \\ + \frac{\beta_2}{\sqrt{6}}\big(-e^{-i(\mathbf{k}-\mathbf{k_0})\cdot\mathbf{r_1}} - e^{-i(\mathbf{k}-\mathbf{k_0})\cdot\mathbf{r_2}} + 2e^{-i(\mathbf{k}-\mathbf{k_0})\cdot\mathbf{r_3}}\big)\Big] e^{i(\nu_{\mathbf{k}}-\omega)t}.\end{aligned} \tag{3.13}$$

Substituting Eq. (3.13) into Eq. (3.12) and using approximately valid relation $\int_0^t dt' e^{i(\nu_{\mathbf{k}}-\omega)(t'-t)} \cong \pi\delta[c(k-k_0)]$, we obtain

$$\dot{\beta}_0 = -\gamma_{00}\beta_0 - \gamma_{01}\beta_1 - \gamma_{02}\beta_2, \tag{3.14}$$

where

$$\gamma_{00} = \frac{1}{3}\sum_{\mathbf{k}} g_{\mathbf{k}}^2 \delta[c(k-k_0)] \sum_{j=1}^{3} e^{i(\mathbf{k}-\mathbf{k_0})\cdot\mathbf{r_j}} \Big[\sum_{j=1}^{3} e^{-i(\mathbf{k}-\mathbf{k_0})\cdot\mathbf{r_j}}\Big], \tag{3.15a}$$

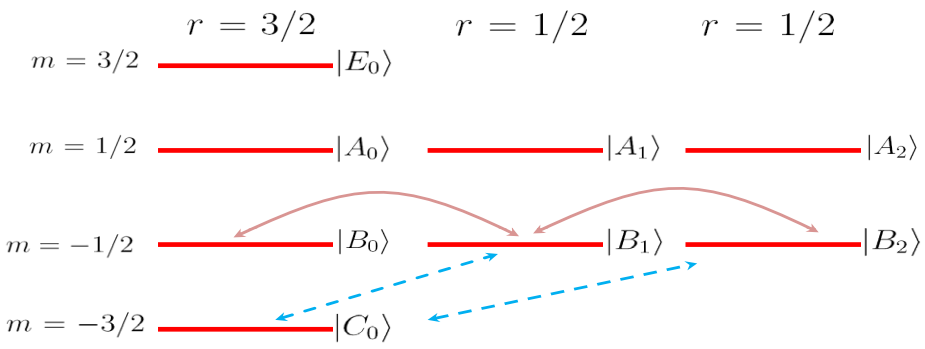

$$
\begin{aligned}
|E_0\rangle &= |\uparrow\uparrow\uparrow\rangle\, e^{i\mathbf{k}_0\cdot(\mathbf{r}_1+\mathbf{r}_2+\mathbf{r}_3)} \\
|A_0\rangle &= \frac{1}{\sqrt{3}}\left[|\uparrow\uparrow\downarrow\rangle\, e^{i\mathbf{k}_0\cdot(\mathbf{r}_1+\mathbf{r}_2)} + |\uparrow\downarrow\uparrow\rangle\, e^{i\mathbf{k}_0\cdot(\mathbf{r}_1+\mathbf{r}_3)} + |\downarrow\uparrow\uparrow\rangle\, e^{i\mathbf{k}_0\cdot(\mathbf{r}_2+\mathbf{r}_3)}\right] \\
|A_1\rangle &= \frac{1}{\sqrt{2}}\left[|\uparrow\uparrow\downarrow\rangle\, e^{i\mathbf{k}_0\cdot(\mathbf{r}_1+\mathbf{r}_2)} - |\uparrow\downarrow\uparrow\rangle\, e^{i\mathbf{k}_0\cdot(\mathbf{r}_1+\mathbf{r}_3)}\right] \\
|A_2\rangle &= \frac{1}{\sqrt{6}}\left[-|\uparrow\uparrow\downarrow\rangle\, e^{i\mathbf{k}_0\cdot(\mathbf{r}_1+\mathbf{r}_2)} - |\uparrow\downarrow\uparrow\rangle\, e^{i\mathbf{k}_0\cdot(\mathbf{r}_1+\mathbf{r}_3)} + 2|\downarrow\uparrow\uparrow\rangle\, e^{i\mathbf{k}_0\cdot(\mathbf{r}_2+\mathbf{r}_3)}\right] \\
|B_0\rangle &= \frac{1}{\sqrt{3}}\left[|\uparrow\downarrow\downarrow\rangle\, e^{i\mathbf{k}_0\cdot\mathbf{r}_1} + |\downarrow\uparrow\downarrow\rangle\, e^{i\mathbf{k}_0\cdot\mathbf{r}_2} + |\downarrow\downarrow\uparrow\rangle\, e^{i\mathbf{k}_0\cdot\mathbf{r}_3}\right] \\
|B_1\rangle &= \frac{1}{\sqrt{2}}\left[|\uparrow\downarrow\downarrow\rangle\, e^{i\mathbf{k}_0\cdot\mathbf{r}_1} - |\downarrow\uparrow\downarrow\rangle\, e^{i\mathbf{k}_0\cdot\mathbf{r}_2}\right] \\
|B_2\rangle &= \frac{1}{\sqrt{6}}\left[|\uparrow\downarrow\downarrow\rangle\, e^{i\mathbf{k}_0\cdot\mathbf{r}_1} + |\downarrow\uparrow\downarrow\rangle\, e^{i\mathbf{k}_0\cdot\mathbf{r}_2} - 2|\downarrow\downarrow\uparrow\rangle\, e^{i\mathbf{k}_0\cdot\mathbf{r}_3}\right] \\
|C_0\rangle &= |\downarrow\downarrow\downarrow\rangle
\end{aligned}
$$

Fig. 19. Dicke basis representation of three two-level atoms far apart compared to the wavelength of emitted radiation. In this limit, $|B_0\rangle$ state is coupled to degenerate states $|B_1\rangle$ and $|B_2\rangle$.

$$\gamma_{01} = \frac{1}{\sqrt{3\times 2}}\sum_{\mathbf{k}} g_{\mathbf{k}}^2\delta[c(k-k_0)]\sum_{j=1}^{3} e^{i(\mathbf{k}-\mathbf{k_0})\cdot\mathbf{r_j}}\Big[\left(e^{-i(\mathbf{k}-\mathbf{k_0})\cdot\mathbf{r_1}} - e^{-i(\mathbf{k}-\mathbf{k_0})\cdot\mathbf{r_2}}\right)\Big], \quad (3.15b)$$

$$\gamma_{02} = \frac{1}{\sqrt{3\times 6}}\sum_{\mathbf{k}} g_{\mathbf{k}}^2\delta[c(k-k_0)]\sum_{j=1}^{3} e^{i(\mathbf{k}-\mathbf{k_0})\cdot\mathbf{r_j}}\Big[\Big(-e^{-i(\mathbf{k}-\mathbf{k_0})\cdot\mathbf{r_1}} - e^{-i(\mathbf{k}-\mathbf{k_0})\cdot\mathbf{r_2}} + 2e^{-i(\mathbf{k}-\mathbf{k_0})\cdot\mathbf{r_3}}\Big)\Big]. \quad (3.15c)$$

Note that state $|B_0\rangle$ is coupled to degenerate states $|B_1\rangle$ and $|B_2\rangle$ which was first pointed out by Agarwal [66]. It is also closely related to earlier work of Fano [67]

and thus we call it Fano-Agarwal coupling. In the small sample limit, however, $\exp(\pm i\mathbf{k}\cdot\mathbf{r}) \simeq \mathbf{1}$ and coefficients $\Gamma_{0,1}$ and $\Gamma_{0,2}$ vanish, which results in decoupling of the degenerate levels. Note also that for small sample, $\gamma_{00} = 3\gamma$ and thus Eq. (3.14) reduces to $\dot{\beta}_0 = -3\gamma\beta_0$ which agrees with Eq. (3.11) for $N = 3$. This shows that going from small to large sample limits leads to coupling of degenerate states. A natural question that follows is–can this be the case for large number of atoms? We address this question in Section b.

b. N atoms: $R \gg \lambda$

We now consider N identical two-level atoms and calculate the evolution of $|B_0\rangle$ state in the large sample limit. We assume that the time of photon flight through the atomic cloud R/c is smaller than the state decay time. In this regime one can apply Markov approximation. The state vector given in terms of the Dicke basis has the form

$$|\Psi(t)\rangle = \sum_{l=0}^{N-1} \beta_l |B_l, 0\rangle + \sum_{\mathbf{k}} \gamma_k |C_0, 1_k\rangle. \tag{3.16}$$

Applying Schrödinger equation and using (B), one finds

$$\dot{\beta}_l = -i \sum_{j,\mathbf{k}} g_{\mathbf{k}} \langle B_l|\sigma_j^+|C_0\rangle e^{i\mathbf{k}\cdot\mathbf{r}_j} e^{-i(\nu_k-\omega)t} \gamma_k(t), \tag{3.17}$$

$$\dot{\gamma}_k = -i \sum_{j,l'} g_{k'} \langle C_0|\sigma_j|B_{l'}\rangle e^{-i\mathbf{k}\cdot\mathbf{r}_j} e^{i(\nu_k-\omega)t} \beta_{l'}(t). \tag{3.18}$$

Integrating Eq. (3.18) and plugging the result into Eq. (3.17) yields

$$\dot{\beta}_l = -\sum_{\mathbf{k}} g_{\mathbf{k}}^2 \sum_{l'} \sum_{i,j} \langle B_l|\sigma_j^\dagger|C_0\rangle \langle C_0|\sigma_i|B_{l'}\rangle e^{i\mathbf{k}\cdot(\mathbf{r}_j-\mathbf{r}_i)} \int_0^t dt' e^{-i(\nu_k-\omega)(t-t')} \beta_{l'}(t'). \tag{3.19}$$

Here we are interested in the time evolution of the $|B_0\rangle$ state. To this end, setting $l = 0$ in the above equation and in view of Eq. (B.7) and (B.11), Eq. (3.19) reduces

to

$$\dot{\beta}_0 = -\sum_{\mathbf{k}} g_{\mathbf{k}}^2 \int_0^t dt' \Big(r_{00}(t,t')\beta_0(t') + \sum_l r_{0l}(t,t')\beta_l(t') \Big), \tag{3.20}$$

where

$$r_{00} = \Big(1 + \frac{1}{N}\sum_{i\neq j} e^{i(\mathbf{k}-\mathbf{k}_0)\cdot(\mathbf{r}_i-\mathbf{r}_j)}\Big) e^{-ic(k-k_0)(t-t')},$$

$$r_{0l} = \frac{1}{\sqrt{Nl(l+1)}} \sum_{i=1}^{N} e^{i(\mathbf{k}-\mathbf{k}_0)\cdot\mathbf{r}_i} \Big[\sum_{j=1}^{l} e^{-i(\mathbf{k}-\mathbf{k}_0)\cdot\mathbf{r}_j} - l e^{-i(\mathbf{k}-\mathbf{k}_0)\cdot\mathbf{r}_{l+1}} \Big] e^{-ic(k-k_0)(t-t')}. \tag{3.22}$$

For very large N, invoking the ansatz $\sum_i e^{i(\mathbf{k}-\mathbf{k}_0)\cdot\mathbf{r}_i} \Rightarrow \delta(\mathbf{k}-\mathbf{k}_0)$ the square bracketed terms in Eq. (3.22) vanish. Therefore the off-diagonal terms in Eq. (7.19) vanish and we are left with

$$\dot{\beta}_0 = -\sum_{\mathbf{k}} g_{\mathbf{k}}^2 \int_0^t dt' \Big(1 + \frac{1}{N}\sum_{i\neq j} e^{i(\mathbf{k}-\mathbf{k}_0)\cdot(\mathbf{r}_j-\mathbf{r}_i)}\Big) e^{-ic(k-k_0)(t-t')}\beta_0(t').$$

We thus note that for a very large number of atoms, the coupling of the state $|B_0\rangle$ to degenerate states vanishes and the state decays exponentially to the ground state.

3. A delta function ingression

In order to estimate the contribution of $|B_l\rangle$ states to the time evolution of the symmetric state $|B_0\rangle$ for finite number of atoms without doing rigorous calculation, we invoke the ansatz

$$\sum_i e^{i(\mathbf{k}-\mathbf{k}_0)\cdot\mathbf{r}_i} \Rightarrow \frac{(2\pi)^3 N}{Vk^2}\delta(\hat{\Omega}_{\mathbf{k}} - \hat{\Omega}_{\mathbf{k}_0})\delta(k-k_0) \Rightarrow \frac{8\pi^2 R}{Vk^2}\delta(\hat{\Omega}_{\mathbf{k}} - \hat{\Omega}_{\mathbf{k}_0}) \sum_i e^{i(k-k_0)r_i}. \tag{3.23}$$

Now let us first change the summation over k to integration in Eq. (7.19) and use the ansatz (3.23) to we obtain

$$\dot{\beta}_0(t) = -\frac{RV_{ph}}{\pi V} \int_0^\infty dk g_k^2 \sum_{i=1}^{N} e^{i(k-k_0)r_i} \int_0^t dt' e^{-ic(k-k_0)(t-t')}$$

$$\times\Big[\frac{1}{N}\sum_j e^{-i(k-k_0)r_j}\beta_0(t')+\frac{1}{\sqrt{Nl(l+1)}}\Big(\sum_{j=1}^{l} e^{-i(k-k_0)r_j}-le^{-i(k-k_0)r_{l+1}}\Big)\beta_l(t')\Big]. \quad (3.24)$$

Consider only the contribution of one of the trapped states ($l = 1$) to the time evolution of the symmetric state $|B_0\rangle$. Taking only the $l = 1$ term in Eq. (3.24), we have

$$\left(\frac{\partial\beta_0}{\partial t}\right)_{i,j} = -\frac{RV_{ph}}{\pi V}\frac{1}{\sqrt{2N}}\int_0^\infty dk g_k^2\int_0^t dt' e^{-ic(k-k_0)(t-t')} \times\sum_{n=1}^{N} e^{i(k-k_0)r_n}\left(e^{-i(k-k_0)r_i}-e^{-i(k-k_0)r_j}\right)\beta_1(t'). \quad (3.25)$$

For simplicity we further assume that atoms are uniformly distributed along the radial direction from $r = 0$ to $r = R$ so that $r_n = n\Delta$, where $n = 1, 2, ..., N$ and Δ is the spacing between consecutive atoms. It can be verified that

$$\sum_{n=1}^{N}[e^{i(k-k_0)\Delta}]^n = \frac{1-e^{i(k-k_0)N\Delta}}{e^{-i(k-k_0)\Delta}-1} = -\sum_{n=0}^{\infty} e^{-i(k-k_0)n\Delta}(1-e^{i(k-k_0)R}). \quad (3.26)$$

Plugging (3.26) into (3.25), we obtain

$$\left(\frac{\partial\beta_0}{\partial t}\right)_{i,j} = -\frac{RV_{ph}}{\pi V}\frac{1}{\sqrt{2N}}\sum_{\mathbf{k}} g_{\mathbf{k}}^2\int_0^t dt' e^{-ic(k-k_0)(t-t')}\sum_{n=0}^{\infty}\left[e^{-i(k-k_0)n\Delta}-e^{i(k-k_0)(R-n\Delta)}\right] \times\left(e^{-i(k-k_0)r_i}-e^{-i(k-k_0)r_j}\right)\beta_1(t'). \quad (3.27)$$

Evaluating the coupling constant $g_{\mathbf{k}}$ at k_0, Eq. (3.27) takes the form

$$\left(\frac{\partial\beta_0}{\partial t}\right)_{i,j} = \frac{3\gamma}{2\pi(k_0R)^2}\frac{c}{\sqrt{2N}}\sum_{n=0}^{\infty}\int_0^t dt'\int_{-k_0}^{\infty} d\kappa\Big\{\big(e^{-i\kappa[c(t-t')+n\Delta+r_i]} - e^{-i\kappa[c(t-t')+(n\Delta-R)+r_i]}\big)-(r_i\to r_j)\Big\}\beta_1(t'), \quad (3.28)$$

where $\kappa = k - k_0$. Noting that $k_0 = \omega/c \gg \gamma/c$ the limit of integration over κ can be extended to $-\infty$. Thus performing the integration over κ gives

$$\left(\frac{\partial\beta_0}{\partial t}\right)_{i,j} = \frac{3\gamma}{(k_0R)^2}\frac{1}{\sqrt{2N}}\sum_{n=0}^{\infty}\int_0^t dt'\Big\{\delta\left[t + \frac{n\Delta}{c} + \frac{r_i}{c} - t'\right] - \delta\left[t + \frac{n\Delta - R}{c} + \frac{r_i}{c} - t'\right] - (r_i \to r_j)]\Big\}\beta_1(t'). \tag{3.29}$$

Considering the r_i integral and writing $r_i = n_i\Delta$, we have

$$\sum_{n=0}^{\infty}\int_0^t dt'\Big\{\delta\left[t + \frac{(n+n_i)\Delta}{c} - t'\right] - \delta\left[t - \frac{(N-n-n_i)\Delta}{c} - t'\right]\Big\}\beta_1(t'). \tag{3.30}$$

Performing the integration, one readily obtains

$$\sum_{n=0}^{\infty}\int_0^t dt'\left\{\delta\left[t - \frac{(n+n_i)\Delta}{c} - t'\right] - \delta\left[t - \frac{(N-n-n_i)\Delta}{c} - t'\right]\right\}\beta_1(t') = -n_i\beta_1. \tag{3.31}$$

Therefore, in the limit $ct > R$, Eq. (3.29) takes the form

$$\left(\frac{\partial\beta_0}{\partial t}\right)_{i,j} \cong -\frac{3\gamma}{2(k_0R)^2}\frac{1}{\sqrt{2N}}(n_i - n_j)\beta_1.$$

We can then write Eq. (3.24) as

$$\dot{\beta}_0 \cong -\Gamma_{00}\beta_0 - \sum_{l=1}^{N-1}\Gamma_{0l}\beta_l, \tag{3.32}$$

where

$$\begin{aligned}
\Gamma_{00} &\cong \frac{3N\gamma}{2(k_0R)^2}, \\
\Gamma_{01} &= \frac{3\gamma}{2(k_0R)^2}\frac{1}{\sqrt{2N}}(n_2 - n_1) \\
&\vdots \\
\Gamma_{0l} &= \frac{3\gamma}{2(k_0R)^2}\frac{1}{\sqrt{Nl(l+1)}}\sum_{j=1}^{l}(n_l - n_j).
\end{aligned} \tag{3.33}$$

The atom label n_i tells us which site (not which atom).

Keeping only the first two terms in Eq. (3.32), we have

$$\dot{\beta}_0(t) \cong -\Gamma_{00}\beta_0(t) - \Gamma_{01}\beta_1(t). \tag{3.34}$$

In similar way one can establish that

$$\dot{\beta}_1(t) \cong -\Gamma_{11}\beta_1(t) - \Gamma_{10}\beta_0(t),$$

where $\Gamma_{10} = \Gamma_{01} \propto 1/\sqrt{N}$ and $\Gamma_{11} \propto 1$. Solving for β_1, we obtain

$$\beta_1(t) \cong \Gamma_{10}\frac{e^{-\Gamma_{00}t} - e^{-\Gamma_{11}t}}{\Gamma_{00} - \Gamma_{11}} \simeq -\frac{\Gamma_{10}}{\Gamma_{00}}e^{-\Gamma_{11}t}. \tag{3.35}$$

Substituting Eq. (3.35) into the formal solution of Eq. (3.34) and using the initial condition $\beta_0(0) = 1$, we find

$$\beta_0(t) \cong e^{-\Gamma_{00}t} + \frac{\Gamma_{10}^2}{\Gamma_{00}(\Gamma_{00} - \Gamma_{11})}(e^{-\Gamma_{00}t} - e^{-\Gamma_{11}t}) \cong e^{-\Gamma_{00}t} + \frac{1}{N}e^{-\Gamma_{11}t}. \tag{3.36}$$

We immediately notice that the contribution of the first nonsymmetric state $|B_1\rangle$ to the time evolution of the initial state $|B_0\rangle$ goes like $1/N$ which is negligible for large N. Therefore, the $|B_0\rangle$ state decays exponentially as in the small sample limit with an enhanced rate Γ_{00}.

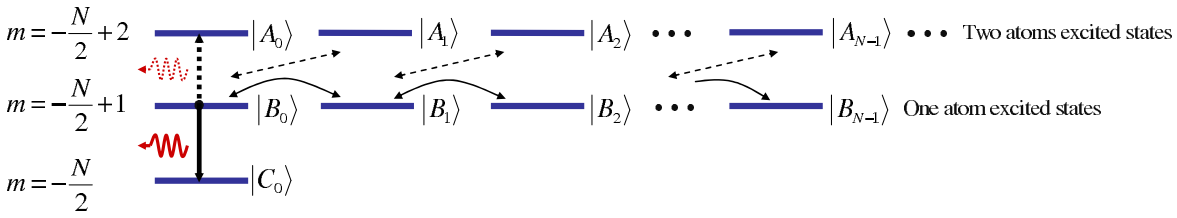

Fig. 20. Relevant Dicke states for calculation of collective Lamb shift in single photon Dicke superradiance. The solid arrows describe the coupling between degenerate states, that is, between $|B_0\rangle$ and $|B_l\rangle$ ($l \geq 1$) and the dashed arrows indicate the virtual processes which arise due to the counter-rotating terms going as $\exp[i(\nu_k + \omega)t]$ in the Hamiltonian [Eq. (3.37)].

Rigorous consideration, however, must take into account possible coupling to all other states and include counter-rotating terms in the interaction Hamiltonian. As shown in [14, 65], Eq. (3.36) remains valid only approximately and other states are excited with about $10 - 20\%$ probability in the large sample limit. For small time the state $|B_0\rangle$ decays exponentially with a rate $\Gamma_{00} = 3N\gamma/2(k_0R)^2$. In the long time limit, the state $|B_0\rangle$ exhibits power-law decay [14].

C. The effect of virtual processes on single photon Dicke superradiance

Frequency or Lamb shift arises due to repeated emission and absorption of short-lived virtual photons. It was originally observed by Lamb and Retherford between two "degenerate" states $2p_{1/2}$ and $2s_{1/2}$ of a hydrogen atom [68]. Here we discuss the effect of virtual processes on the time evolution of the $|B_0\rangle$ (see Fig. 20) state for atoms distributed in a spherical cloud of radius R following Ref. [13]. We focus on evolution of the $|B_0\rangle$ state in the large sample limit $R \gg \lambda$ (but $R \ll c/\Gamma$, where Γ is the state decay rate). The Hamiltonian (B) written in the rotating wave approximation cannot fully describe virtual processes. One should rather go beyond the rotating wave approximation in order to properly account for both the real and virtual processes.

To this end, we write the Hamiltonian beyond rotating wave approximation as

$$V(t) = \sum_{j,\mathbf{k}} \hbar g_{\mathbf{k}} \left(\sigma_j a_{\mathbf{k}}^\dagger e^{-i\mathbf{k}\cdot\mathbf{r}_j} e^{i(\nu_{\mathbf{k}}-\omega)t} + \sigma_j^\dagger a_{\mathbf{k}}^\dagger e^{-i\mathbf{k}\cdot\mathbf{r}_j} e^{i(\nu_{\mathbf{k}}+\omega)t} \right) + \text{H.c.} \tag{3.37}$$

For the system initially prepared in the $|B_0\rangle$ state, an atom may emit a photon in the $\mathbf{k}$ mode and decay to the ground state $|C_0\rangle$ which is described by the term in the Hamiltonian $\sigma a_{\mathbf{k}}^\dagger$. An equally possible transition, represented by $a_{\mathbf{k}}\sigma^\dagger$, is when an atom in the ground state absorbs a photon and jumps to the next excited states, i.e., either of the $|B_l\rangle$ states. These two processes are real and energy conserving in a sense that the atom absorbs some energy and get excited to higher energy level or vice versa. On the other hand, the term $\sigma^\dagger a_{\mathbf{k}}^\dagger$ describes a process in which an atom makes a transition to the next excited state, i.e., $|A_l\rangle$, by emitting a short-lived virtual photon in the $\mathbf{k}$ mode. Then one of the atoms absorbs this photon and decays back to either of $|B_l\rangle$ states in a short time, which is described by the term $\sigma a_{\mathbf{k}}$ in the Hamiltonian. These processes, opposed to the former ones, are virtual and energy non-conserving. As we will demonstrate below both processes contribute to evolution of the initial state $|B_0\rangle$.

In the limit $R \gg \lambda$, the state vector at time t can be written as

$$|\Psi(t)\rangle = \sum_{n=0}^{m} \sum_{\mathbf{k}} \alpha_{n,\mathbf{k}} |A_n, 1_{\mathbf{k}}\rangle + \sum_{l=0}^{N-1} \beta_l |B_l, 0\rangle + \sum_{\mathbf{k}} \gamma_{\mathbf{k}} |C_0, 1_{\mathbf{k}}\rangle, \tag{3.38}$$

where $m = (N-1)(N-2)/2$. Applying Schrödinger equation and using the Hamiltonian (3.37) and the state vector (3.38), one can readily obtain equations of evolution for probability amplitudes to be

$$\begin{aligned} \dot{\beta}_l = &-i \sum_{j,\mathbf{k}} g_{\mathbf{k}} \langle B_l | \sigma_j^+ | C_0 \rangle e^{i\mathbf{k}\cdot\mathbf{r}_j} e^{-i(\nu_k-\omega)t} \gamma_{\mathbf{k}}(t) \\ &- i \sum_{j,\mathbf{k}} g_{\mathbf{k}} \sum_{n'} \langle B_l | \sigma_j | A_{n'} \rangle e^{i\mathbf{k}\cdot\mathbf{r}_j} e^{-i(\nu_k+\omega)t} \alpha_{n',\mathbf{k}}(t), \end{aligned} \tag{3.39}$$

$$\dot{\gamma}_{\mathbf{k}} = -i \sum_{j,l'} g_{\mathbf{k}'} \langle C_0|\sigma_j|B_{l'}\rangle e^{-i\mathbf{k}\cdot\mathbf{r}_j} e^{i(\nu_k-\omega)t} \beta_{l'}(t), \tag{3.40}$$

$$\dot{\alpha}_{n,\mathbf{k}} = -i \sum_{j,l'} g_{\mathbf{k}} \langle A_n|\sigma_j^\dagger|B_{l'}\rangle e^{-i\mathbf{k}\cdot\mathbf{r}_j} e^{i(\nu_k+\omega)t} \beta_{l'}(t). \tag{3.41}$$

Now plugging formal solutions of Eqs. (3.41) and (3.40) into (3.39) we get

$$\begin{aligned}\dot{\beta}_l = &- \sum_{\mathbf{k}} g_{\mathbf{k}}^2 \sum_{l'} \sum_{i,j} \langle B_l|\sigma_j^\dagger|C_0\rangle\langle C_0|\sigma_i|B_{l'}\rangle e^{i\mathbf{k}\cdot(\mathbf{r}_j-\mathbf{r}_i)} \int_0^t dt' e^{-i(\nu_k-\omega)(t-t')} \beta_{l'}(t') \\ &- \sum_{\mathbf{k}} g_{\mathbf{k}}^2 \sum_{l'} \sum_{i,j} \langle B_l|\sigma_j \sum_{n'} |A_{n'}\rangle\langle A_{n'}|\sigma_i^\dagger|B_{l'}\rangle e^{i\mathbf{k}\cdot(\mathbf{r}_j-\mathbf{r}_i)} \int_0^t dt' e^{-i(\nu_k+\omega)(t-t')} \beta_{l'}(t').\end{aligned} \tag{3.42}$$

We are interested in the time evolution of the initial state $|B_0\rangle$. Thus setting $l = 0$ in Eq. (3.42), noting that $|A_{n'}\rangle\langle A_{n'}| = \mathbf{1}$ and performing the summation we readily establish that (see Appendix A for detailed calculation)

$$\dot{\beta}_0(t) = -\sum_{\mathbf{k}} g_{\mathbf{k}}^2 \int_0^t dt' \left[R_{00}(t,t')\beta_0(t') + \sum_{l=1}^{N-1} R_{0l}(t,t')\beta_l(t') \right], \tag{3.43}$$

where R_{00} and R_{0l} are given by Eqs. (B.9) and (B.13), respectively. Further, applying Markov approximation and performing the integration over time, we obtain

$$\dot{\beta}_0(t) = -\Gamma_{00}\beta_0 - \sum_{i=1}^{N-1} \Gamma_{0l}\beta_l, \tag{3.44}$$

where

$$\begin{aligned}\Gamma_{00}(t) = &\sum_{\mathbf{k}} g_{\mathbf{k}}^2 \Big(1 + \frac{1}{N} \sum_{i\neq j} e^{i(\mathbf{k}-\mathbf{k}_0)\cdot(\mathbf{r}_j-\mathbf{r}_i)}\Big) \frac{e^{-ic(k-k_0)t}}{ic(k-k_0)} \\ &+ \sum_{\mathbf{k}} g_{\mathbf{k}}^2 \Big(N - 1 + \frac{1}{N} \sum_{i\neq j} e^{i(\mathbf{k}+\mathbf{k}_0)\cdot(\mathbf{r}_j-\mathbf{r}_i)}\Big) \frac{e^{-ic(k+k_0)t}}{ic(k+k_0)},\end{aligned} \tag{3.45}$$

$$\Gamma_{0l}(t,t') = \frac{1}{\sqrt{Nl(l+1)}} \sum_{\mathbf{k}} g_{\mathbf{k}}^2 \sum_j e^{i(\mathbf{k}-\mathbf{k}_0)\cdot\mathbf{r}_j}$$
$$\times \Big[\sum_{i=1}^{l} e^{-i(\mathbf{k}-\mathbf{k}_0)\cdot\mathbf{r}_i} - l e^{-i(\mathbf{k}-\mathbf{k}_0)\cdot\mathbf{r}_{l+1}} \Big] \frac{e^{-ic(k-k_0)t}}{ic(k-k_0)}$$
$$+ \frac{1}{\sqrt{Nl(l+1)}} \sum_{\mathbf{k}} g_{\mathbf{k}}^2 \sum_j e^{-i(\mathbf{k}+\mathbf{k}_0)\cdot\mathbf{r}_j}$$
$$\times \Big[\sum_{i=1}^{l} e^{i(\mathbf{k}+\mathbf{k}_0)\cdot\mathbf{r}_i} - l e^{i(\mathbf{k}+\mathbf{k}_0)\cdot\mathbf{r}_{l+1}} \Big] \frac{e^{-ic(k+k_0)t}}{ic(k+k_0)}. \tag{3.46}$$

As per the result of Appendix B, all terms in Γ_{0l} vanish and only the Γ_{00} term in (3.44) survives. Calculating the expression for Γ_{00}, Eq. (3.44) becomes

$$\dot{\beta}_0 = -\gamma\beta_0 - \left(\frac{\gamma}{2\pi} \frac{N-1}{V} \lambda^2 R \right) \beta_0(t) + i \frac{\gamma}{\pi k_0} \int_0^K k dk \Big[\frac{1}{k-k_0} + \frac{N-1}{k+k_0} \Big] \beta_0(t)$$
$$+ i \frac{\gamma}{k_0} \frac{N-1}{V} \int_0^\infty \frac{dk}{k} \int_{-R}^{R} dr\, e^{i(k-k_0)r} \Big[\frac{1}{k-k_0} + \frac{1}{k+k_0} \Big] \beta_0(t), \tag{3.47}$$

where K is the cutoff wave vector. We proceed to carry out the first integral by subtracting off the electron self energy terms, i.e., replace $(k \pm k_0)^{-1}$ by $(k \pm k_0)^{-1} - k_0^{-1}$ as it appears in the square bracket. The third integral is finite due to the exponential factor $\exp[i(k-k_0)r]$ and yields a simple result in the limit $k_0 R \gg 1$ (see Appendix B). Thus using the results in Appendix B, Eq. (3.47) takes the form

$$\dot{\beta}_0 = -(\gamma + \Gamma)\beta_0 + \frac{i}{\pi} \left(\gamma \ln \frac{K^2 - k_0^2}{k_0^2} - N\gamma \ln \frac{K+k_0}{k_0} - \frac{\Gamma}{\pi} \frac{\lambda}{4R} S \right) \beta_0, \tag{3.48}$$

where

$$\Gamma = \frac{3\gamma(N-1)}{2(k_0 R)^2} \tag{3.49}$$

and the shape factor

$$S = 1 - \frac{2\cos k_0 R}{\pi k_0 R}.$$

A similar calculation for the ground state yields

$$\dot{\gamma}_0 = -i\left(\frac{\gamma}{\pi} N \ln\frac{K+k_0}{k_0}\right)\gamma_0 \tag{3.50}$$

so that the frequency shift between $|B_0\rangle$ and $|C_0\rangle$ is

$$\delta\omega_\beta - \delta\omega_\gamma = -\frac{\gamma}{\pi}\ln\frac{K^2-k_0^2}{k_0^2} + \frac{\Gamma}{\pi}\frac{\lambda}{4R}S. \tag{3.51}$$

In the above equation, the first term is the single atom Lamb shift while the second term is the collective Lamb shift due to the many particle effect. The amplitude of the $|B_0\rangle$ state (4.1) has been shown to decay exponentially even though the collective Lamb shift can be large. In addition, when the sample is large enough, $|B_0\rangle$ decays to $|C_0\rangle$ with a high probability. The many particle contribution to the Lamb shift, $\mathcal{L}_N \sim \Gamma\lambda/4R \sim N\gamma(\lambda/R)^3$ can be much larger than the single particle shift (which is of order γ); for example, for a gas at one torr $N/R^3 \sim 10^{16}\text{atom/cm}^3$ and wavelength $\lambda = 1\mu m$ yields $\mathcal{L}_N \sim 10^4\gamma$.

One should mention that results obtained in this section are only approximate because replacement of summation over atoms by delta function (in Appendix B) is not rigorous for a finite size of the atomic cloud. Proper treatment of the problem shows that the $|B_0\rangle$ state decays exponentially only for $t \sim 1/\Gamma$, for large time the decay becomes power-law [14].

D. Conclusion

We have analyzed evolution of cooperative spontaneous emission from a collection of N identical two-level atoms which are uniformly distributed in a sphere and initially prepared by absorption of a single photon–timed Dicke state. In particular, we have discussed the time evolution this state in both small and large sample limits. We have

also calculated the frequency or Lamb shift associated with the timed Dicke state for the large sample limit.

It turns out that if one takes into account energy conserving processes only, the timed Dicke state, to a good approximation, decays exponentially to the ground state. On the other hand, when the virtual processes are taken into account the result depends crucially on the initial state of the system. For instance, if a large atomic cloud is initially prepared in the rapidly decaying timed Dicke state, virtual processes lead to excitation of the other states with 10-20 % probability. This relatively small but intersecting effect can be observed experimentally. However, when the system is initially in a trapped state then virtual processes qualitatively change the time evolution yielding new decay channels. As a consequence, the initial trapped state is no longer trapped and slowly decays via photon emission.

CHAPTER IV

PROTECTING FAST DECAY OF ENTANGLEMENT BETWEEN DIPOLE-COUPLED QUBITS VIA QUANTUM INTERFERENCE *

A. Introduction

Quantum interference (QI), an intriguing consequence of the superposition principle has led to numerous fascinating phenomena [1, 4, 69, 70, 71]. Application of QI in generation of bipartite entanglement both in discrete [72, 73] and continuous-variable [9, 10, 74] settings has been the focus of current investigation. Note that bipartite entanglement involving two atoms, extensively used for implementations of various quantum information protocols [75, 76, 77, 78, 79, 80], is known to be quite fragile in the face of decoherence [75, 81]. In view of this, in the past few years considerable effort has been devoted to the study of dynamical aspect of two-atom entanglement in presence of decoherence [16, 82, 83, 84, 85, 86, 87, 88, 89]. In one such study [16], it was found that in contrary to the adverse effect of spontaneous emission on atomic entanglement [87], cooperative spontaneous emission in two atom systems can generate entanglement between the atoms. It is worth mentioning here that the problem of cooperative spontaneous emission first addressed by Dicke [7] is known to exhibit several counter-intuitive phenomena [66] namely, directed spontaneous emission [11], Lamb shift [13], and single-photon Dicke superradiance [15] as discussed in previous Chapter. In recent times, with the discovery of atom like behavior of semiconductor quantum dots [90, 91] and their utilization towards solid state quantum computing [90, 91, 92], we have a new class of systems where the phenomenon of cooperative

---

* Reprinted with permission from "Quantum interference in timed Dicke basis and its effect on bipartite entanglement" by Eyob A. Sete and S. Das, 2011. *Phys. Rev. A*, 83, 042301, Copyright [2011] by American Physical Society.

spontaneous emission can be of immense importance from the context of quantum information sciences.

As pointed out in Chapter III, the state of an atom acquires a phase shift $\exp(i\mathbf{k}_0 \cdot \mathbf{r}_j)$ when it is excited by a photon of wave vector $\mathbf{k}_0$. The term $\mathbf{k}_0 \cdot \mathbf{r}_j = \nu_0 t_j$ encodes the information that when and where the atom is excited. Such a position-dependent phase factor in a system of large number of atoms was shown to exhibit fascinating features. For example, it can lead to Fano-Agarwal-type coupling between degenerate levels and creates coherence between them [66, 67]. Moreover, it determines the directionality of the emitted radiation in single-photon Dicke superradiance [11]. Recently, Ooi and co-workers [93] studied the effect of position-dependant excitation phase on the population dynamics, intensity, and spatial and angular correlations in two two-level atoms interacting via their dipoles. The results show that the excitation phase considerably modifies the dynamics of the system. Later, Das *et al.* [94] investigated the effect of the position-dependent excitation phase on the Dicke cooperative emission spectrum. A strong quantum correlation among the atoms was reported in presence of the excitation phase. This was attributed to a vacuum mediated QI generated in the two-atom system. The result of [94] qualitatively indicates that the spatial variation of the excitation phase can affect the generation and evolution of entanglement in the system. It may be added that, such vacuum mediated QI and its effect has been earlier studied in atomic systems [66, 95, 96, 97]. While these earlier works utilize the quantum interference that comes about due to the configuration of the atomic system, we are motivated at studying the effect of quantum interference induced by the position-dependent excitation phase.

To understand the effects of such QI on the two atom entanglement, we present a systematic study of the time evolution of entanglement measure for two strongly dipole-coupled atoms undergoing a cooperative spontaneous emission. We consider

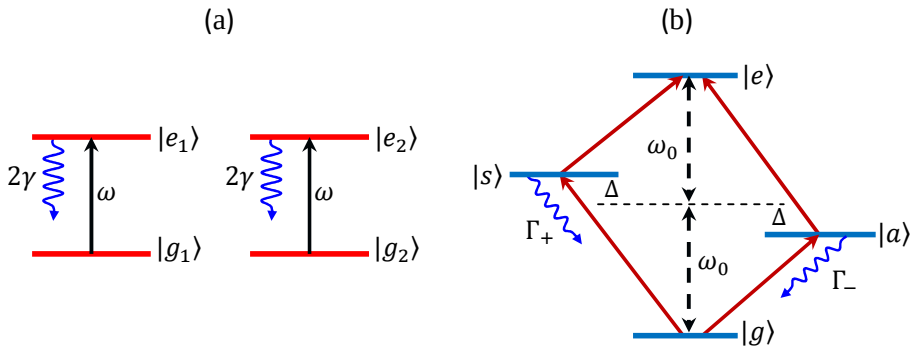

Fig. 21. Energy level diagram for two two-level atoms in bare basis (a) and in the timed Dicke basis (b). The frequency shift $\Delta = \Omega_{12}\cos\varphi$ occurs as a result of dipole-dipole interaction between the two atoms. The collective states $|s\rangle$ and $|a\rangle$ decays at a rate of Γ_+ and Γ_-, respectively, where $\Gamma_\pm = 2(\gamma \pm \gamma_{12}\cos\varphi)$.

various initial quantum states in which the two atoms can be prepared and explore the effects on the dynamical behavior of entanglement due to the quantum interference. We explicitly take into account the position-dependent excitation of the atoms by introducing *timed Dicke basis* [11]. It is important to understand that the entanglement in a two-atom system crucially depends on the cooperative decay rates, the initial conditions, and the dipole-dipole interactions [84], all of which get modified due to the quantum interference. We show that for the system initially prepared in the symmetric timed Dicke state, a coherence between the symmetric and antisymmetric states is dynamically generated as a result of the QI between the two pathways leading to the ground state. This coherence considerably slows down decay of the entanglement between the qubits.

B. Model and equations of evolution

We consider a system of two qubits formed by the excited states $|e_i\rangle$ and ground states $|g_i\rangle$ $(i = 1, 2)$ of two identical two level atoms, see Fig. 21a. The qubits are

fixed at positions r_1 and r_2 and the interqubit distance is less than the wavelength of the radiation field, λ. We further assume that the qubits are coupled to one another by a dipole-dipole interaction and are coupled to the environment via an interaction with a common vacuum reservoir. The time evolution of the density operator for such a two-qubit system is given by [66]

$$\frac{d}{dt}\rho = -i\omega_0 \sum_{i=1}^{2}[\sigma_i^z, \rho] - i\sum_{i\neq j}^{2}\Omega_{ij}[\sigma_i^\dagger \sigma_j, \rho] - \sum_{i,j=1}^{2}\gamma_{ij}(\rho\sigma_i^\dagger\sigma_j + \sigma_i^\dagger\sigma_j\rho - 2\sigma_j\rho\sigma_i^\dagger). \quad (4.1)$$

Here

$$\omega_0 = \omega + \omega_L \quad (4.2)$$

is the normalized atomic transition frequency with ω being the bare atomic transition frequency and $\omega_L = -(\gamma/\pi)\ln[|\omega_c/\omega - 1|(1 + \omega_c/\omega)]$ the relative single-atom Lamb shift between the bare levels; ω_c is the cut-off frequency. $\sigma_i^z = (\sigma_i^\dagger\sigma_i - \sigma_i\sigma_i^\dagger)/2$ is the energy operator with $\sigma_i^\dagger(\sigma_i)$ being the raising (lowering) operator for ith atom, Ω_{ij} and γ_{ij} for $i \neq j$ are, respectively, the dipole-dipole interaction term and the cooperative decay rate given by

$$\Omega_{ij} = \frac{3}{2}\gamma\left[(1 - 3\cos^2\theta)\left(\frac{\sin(k_0 r_{ij})}{(k_0 r_{ij})^2} + \frac{\cos(k_0 r_{ij})}{(k_0 r_{ij})^3}\right) - (1 - \cos^2\theta)\frac{\sin(k_0 r_{ij})}{k_0 r_{ij}}\right] \quad (4.3)$$

and

$$\gamma_{ij} = \frac{3}{2}\gamma\left[(1 - \cos^2\theta)\frac{\sin(k_0 r_{ij})}{k_0 r_{ij}} + (1 - 3\cos^2\theta)\left(\frac{\cos(k_0 r_{ij})}{(k_0 r_{ij})^2} - \frac{\sin(k_0 r_{ij})}{(k_0 r_{ij})^3}\right)\right], \quad (4.4)$$

where $2\gamma \equiv 2\gamma_{11} = 2\gamma_{22} = 2|\vec{\wp}_{eg}|^2\omega^3/3\pi\varepsilon_0\hbar c^3$ is the spontaneous decay rate of the individual qubits. $\vec{\wp}_{eg}$ is the dipole moment, $k_0 = 2\pi/\lambda$ with λ being the wavelength of the emitted radiation and θ is the angle between the direction of the dipole moment and the line joining the ith and the jth qubits, and $r_{ij} = |\mathbf{r}_i - \mathbf{r}_j|$ is the interqubit distance. In this work, we assume that the orientation of the dipole moment is random

and hence Eqs. (4.3) and (4.4) simplifies considerably and take a simple form

$$\Omega_{ij} = -\gamma \cos(k_0 r_{ij})/k_0 r_{ij}, \tag{4.5}$$

$$\gamma_{ij} = \gamma \sin(k_0 r_{ij})/k_0 r_{ij}. \tag{4.6}$$

We next consider the preparation of initial state of the qubits. For this purpose, we assume that the qubits interacts with a very weak laser field (almost at a single-photon level) propagating with a wave vector $\mathbf{k}_0$. The interaction with the weak field can lead to a resonant single photon absorption process. It is important to note that we consider the direction of the wave vector to be different to that of the interqubit axis. This thus generate a position-dependent excitation phase of the qubits whenever a photon is absorbed. The excitation process, with the laser field treated classically and in the rotating wave approximation, can be described by the Hamiltonian

$$V = -\hbar\Omega \sum_{j=1}^{2} (\sigma_j^+ e^{i\mathbf{k}_0 \cdot \mathbf{r}_j} \; e^{-i(\nu_0 - \omega)t} + \text{H.c.}), \tag{4.7}$$

where $\Omega = \mathbf{d}_{e_1 g_1} \cdot \mathcal{E}/\hbar = \mathbf{d}_{e_2 g_2} \cdot \mathcal{E}/\hbar$ is the Rabi frequency and ν_0 is the frequency of the incident radiation. Note that the position-dependent phase factors in the Hamiltonian would substantially affect the dynamical behavior of the correlation in the two-qubit system. We except that this in turn will lead to modification of entanglement between the qubits. The investigation of such modification in the entanglement feature is the key focus of this work. To study the effect of position-dependent excitation phase on the dynamics, it proves to be convenient to work in a basis defined by the phase factors. Such a basis was introduced in Ref. [11] in context to directed spontaneous emission from an ensemble of atoms and is also known as the *timed Dicke basis*. To

this end, for our system of two qubits there are four timed Dicke states:

$$|e\rangle = |e_1 e_2\rangle e^{i\mathbf{k}_0\cdot\mathbf{r}_1 + i\mathbf{k}_0\cdot\mathbf{r}_2}, \tag{4.8a}$$

$$|s\rangle = \frac{1}{\sqrt{2}}(|e_1 g_2\rangle e^{i\mathbf{k}_0\cdot\mathbf{r}_1} + |g_1 e_2\rangle e^{i\mathbf{k}_0\cdot\mathbf{r}_2}), \tag{4.8b}$$

$$|a\rangle = \frac{1}{\sqrt{2}}(|e_1 g_2\rangle e^{i\mathbf{k}_0\cdot\mathbf{r}_1} - |g_1 e_2\rangle e^{i\mathbf{k}_0\cdot\mathbf{r}_2}), \tag{4.8c}$$

$$|g\rangle = |g_1 g_2\rangle. \tag{4.8d}$$

In terms of this basis the equations of evolution for the elements of the density operator read:

$$\dot{\rho}_{ee} = -4\gamma\rho_{ee}, \tag{4.9a}$$

$$\dot{\rho}_{es} = -[3\gamma + \gamma_{12}\cos\varphi + i(\omega_0 - \Omega_{12}\cos\varphi)]\rho_{es} + i\sin\varphi(\gamma_{12} - i\Omega_{12})\rho_{ea}, \tag{4.9b}$$

$$\dot{\rho}_{ea} = -[3\gamma - \gamma_{12}\cos\varphi + i(\omega_0 + \Omega_{12}\cos\varphi)]\rho_{ea} + i\sin\varphi(\gamma_{12} + i\Omega_{12})\rho_{es}, \tag{4.9c}$$

$$\dot{\rho}_{eg} = -2(\gamma + i\omega_0)\rho_{eg}, \tag{4.9d}$$

$$\begin{aligned}\dot{\rho}_{ss} =& -2(\gamma + \gamma_{12}\cos\varphi)\rho_{ss} - i\sin\varphi(\gamma_{12} + i\Omega_{12})\rho_{as} + i\sin\varphi(\gamma_{12} - i\Omega_{12})\rho_{sa} \\ &+ 2(\gamma + \gamma_{12}\cos\varphi)\rho_{ee},\end{aligned} \tag{4.9e}$$

$$\begin{aligned}\dot{\rho}_{aa} =& -2(\gamma - \gamma_{12}\cos\varphi)\rho_{aa} - i\sin\varphi(\gamma_{12} - i\Omega_{12})\rho_{as} + i\sin\varphi(\gamma_{12} + i\Omega_{12})\rho_{sa} \\ &+ 2(\gamma - \gamma_{12}\cos\varphi)\rho_{ee},\end{aligned} \tag{4.9f}$$

$$\dot{\rho}_{as} = -2(\gamma - i\Omega_{12}\cos\varphi)\rho_{as} + i\sin\varphi(\gamma_{12} + i\Omega_{12})\rho_{ss} + i\sin\varphi(\gamma_{12} - i\Omega_{12})\rho_{aa} - 2i\gamma_{12}\sin\varphi\rho_{ee}, \tag{4.9g}$$

$$\dot{\rho}_{gs} = -[\gamma + \gamma_{12}\cos\varphi - i(\omega_0 + \Omega_{12}\cos\varphi)]\rho_{gs} + i\sin\varphi(\gamma_{12} - i\Omega_{12})\rho_{ga} + 2(\gamma + \gamma_{12}\cos\varphi)\rho_{se} + 2i\gamma_{12}\sin\varphi\rho_{ae}, \tag{4.9h}$$

$$\dot{\rho}_{ga} = -[\gamma - \gamma_{12}\cos\varphi - i(\omega_0 - \Omega_{12}\cos\varphi)])\rho_{ga} - i\sin\varphi(\gamma_{12} - i\Omega_{12})\rho_{gs} - 2(\gamma - \gamma_{12}\cos\varphi)\rho_{ae} + 2i\gamma_{12}\sin\varphi\rho_{se}, \tag{4.9i}$$

$$\dot{\rho}_{gg} = 2(\gamma + \gamma_{12}\cos\varphi)\rho_{ss} + 2(\gamma - \gamma_{12}\cos\varphi)\rho_{aa} + 2i\gamma_{12}\sin\varphi(\rho_{as} - \rho_{sa}), \tag{4.9j}$$

where $\varphi = \mathbf{k}_0 \cdot (\mathbf{r}_i - \mathbf{r}_j) = \frac{2\pi}{\lambda} r_{ij}\cos\xi$ with ξ being the angle between the laser propagation direction and the line joining the two atoms.

Inspection of Eqs. (4.9b) and (4.9c) shows that the presence of dipole-dipole interaction gives rise to collective frequency (Lamb) shift, which is as a result of repeated emission and absorption of short-lived virtual photons [13, 15, 98]. The shifts are only observed for symmetric and antisymmetric states. The former is shifted up while the later shifted down by an equal amount $\Delta = \Omega_{12}\cos\varphi$ from the single photon resonance line as shown in Fig. 21b. It is interesting to note that one can manipulate the frequency shift by only orienting the laser field appropriately with respect to the line joining the two atoms. For example, $\varphi = \pi/2$, i.e., when the angle between the laser propagation direction and the line joining the two atoms is $\xi = \pi/3$ and the interatomic distance equal to half of the radiation wavelength, $r_{12} = \lambda/2$, the level shift vanishes. Thus it is possible to control the level shift by applying a laser field in a particular direction without turning off the dipole-dipole interaction.

Furthermore, we note that the transition probability from the excited state $|e\rangle$

to the one photon states, $|s\rangle$ and $|a\rangle$, is the sum of the probability of each transition. Since it is the probability, not the probability amplitudes that add up we don't expect quantum interference phenomenon to occur. However, the transition probability from the one photon states, $|s\rangle$ and $|a\rangle$ to the ground state $|g\rangle$ is obtained by squaring the sum of the amplitude of each transition. When there is a coherence between the two states ($|s\rangle$ and $|a\rangle$), this can lead to quantum interference yielding coherent population transfer between $|s\rangle$ and $|a\rangle$. Indeed, the populations in $|s\rangle$ and $|a\rangle$ are coupled to the coherence ρ_{as} as per Eqs. (4.9e)-(4.9g). It is worth to note that this coupling disappears when the direction of propagation of the laser field is perpendicular to the interqubit axis $\xi = \pi/2$ ($\varphi = 0$). Therefore, a nonzero ϖ result in creation of two-photon coherence ρ_{as}. In this work, we explore the extent to which this coherence affects the dynamical evolution of bipartite entanglement between the qubits.

C. Entanglement measure

In general a state of a quantum system is said to be entangled when the density operator of the composite system cannot factorize into that of the individual subsystems. There are several entanglement measures for two-qubit system in the literature. However, we use the concurrence, a widely used entanglement monotone, for our purpose. The concurrence, first introduced by Wooters [99], is defined as

$$\mathcal{C}(t) = \max(0, \sqrt{\lambda_1} - \sqrt{\lambda_2} - \sqrt{\lambda_3} - \sqrt{\lambda_4}), \tag{4.10}$$

where $\lambda_1 > \lambda_2 > \lambda_3 > \lambda_4$. $\{\lambda i\}$ are the eigenvalues of the matrix $\rho\tilde{\rho}$ in which $\tilde{\rho} = \sigma_y \otimes \sigma_y \rho^* \sigma_y \otimes \sigma_y$ with σ_y being the Pauli matrix. The concurrence takes values ranging from 0 to 1. For maximally entangled state $\mathcal{C}(t) = 1$ and for separable state $\mathcal{C}(t) = 0$.

For a dissipative system, without any external driving field, the density matrix of the qubits system has the form

$$\rho(t) = \begin{pmatrix} \rho_{11} & 0 & 0 & \rho_{14} \\ 0 & \rho_{22} & \rho_{23} & 0 \\ 0 & \rho_{32} & \rho_{33} & 0 \\ \rho_{41} & 0 & 0 & \rho_{44} \end{pmatrix} \tag{4.11}$$

in the basis set $|1\rangle = |e_1 e_2\rangle e^{i\mathbf{k}_0\cdot(\mathbf{r}_1+\mathbf{r}_2)}$, $|2\rangle = |e_1 g_2\rangle e^{i\mathbf{k}_0\cdot\mathbf{r}_1}$, $|3\rangle = |g_1 e_2\rangle e^{i\mathbf{k}_0\cdot\mathbf{r}_2}$, and $|4\rangle = |g_1 g_2\rangle$. Note that for a quantum state initially prepared in a block form of (4.11), the time-evolved density matrix will have the same block form, i.e., the zeros remain zero and the nonzero components evolve in time [84, 89].

We next proceed to calculate the concurrence for the qubits initially prepared in the form of (4.11). To do so, one has to determine the matrix $\tilde{\rho}$ in the basis where ρ is expressed. Using the definition of the density matrix $\tilde{\rho}$, we obtain

$$\tilde{\rho}(t) = \begin{pmatrix} \rho_{44} & 0 & 0 & \rho_{14} \\ 0 & \rho_{33} & \rho_{23} & 0 \\ 0 & \rho_{32} & \rho_{22} & 0 \\ \rho_{41} & 0 & 0 & \rho_{11} \end{pmatrix}. \tag{4.12}$$

Thus the square root of the eigenvalues of the matrix $\rho\tilde{\rho}$ are:

$$\{\sqrt{\lambda_i}\} = \{\sqrt{\rho_{22}\rho_{33}} \pm |\rho_{23}|, \sqrt{\rho_{11}\rho_{44}} \pm |\rho_{14}|\}. \tag{4.13}$$

There are two possible expressions for the concurrence, depending on the values of the eigenvalues. The first case is that when $|\rho_{23}| + \sqrt{\rho_{22}\rho_{33}}$ be the largest eigenvalue. This leads to a concurrence

$$\mathcal{C}_1(t) = 2(|\rho_{23}| - \sqrt{\rho_{11}\rho_{44}}). \tag{4.14}$$

While if $|\rho_{14}| + \sqrt{\rho_{11}\rho_{44}}$ is the largest eigenvalue then the concurrence takes the form

$$\mathcal{C}_2(t) = 2(|\rho_{14}| - \sqrt{\rho_{22}\rho_{33}}). \tag{4.15}$$

Depending on the initial condition used, one of the concurrence expressions suffices to quantify the entanglement between the qubits. Further, inspection of (4.14) and (4.15) shows that $\mathcal{C}_1(t)$ would be positive and hence the measure of entanglement when the two-photon coherence ρ_{23} is larger than the square root of the product of the populations in the excited and ground states. On the other hand, for $\mathcal{C}_2(t)$ to be a measure of entanglement for the system the two-photon coherence ρ_{14} should be greater than the square root of the product of the populations in one-photon excited states.

In order to gain insight into the physics it is convenient to express the concurrences in terms of timed Dicke basis introduced earlier. To do so, one has to apply a unitary transformation $U\rho U^\dagger$ on the density matrix given by (4.11). The matrix U is given by

$$U = \begin{pmatrix} 1 & 0 & 0 & 0 \\ 0 & \frac{1}{\sqrt{2}} & -\frac{1}{\sqrt{2}} & 0 \\ 0 & \frac{1}{\sqrt{2}} & \frac{1}{\sqrt{2}} & 0 \\ 0 & 0 & 0 & 1 \end{pmatrix}. \tag{4.16}$$

The elements of the density matrix $U\rho U^\dagger$ is related to that of ρ by

$$\begin{aligned} &\rho_{ee} = \rho_{11}, \quad \rho_{eg} = \rho_{14}, \\ &\rho_{aa} = \frac{1}{2}(\rho_{22} + \rho_{33} - (\rho_{23} + \rho_{32})), \quad \rho_{ss} = \frac{1}{2}(\rho_{22} + \rho_{33} + \rho_{23} + \rho_{32}), \\ &\rho_{as} = \frac{1}{2}(\rho_{22} - \rho_{33} + \rho_{23} - \rho_{32}), \quad \rho_{sa} = \frac{1}{2}(\rho_{22} - \rho_{33} - (\rho_{23} - \rho_{32})). \end{aligned} \tag{4.17}$$

Therefore the concurrence can be expressed in terms of the timed Dicke basis as

$$\mathcal{C}(t) = \max(0, \mathcal{C}_1(t), \mathcal{C}_2(t)), \tag{4.18}$$

where

$$\mathcal{C}_1(t) = \sqrt{(\rho_{ss} - \rho_{aa})^2 + 4[\mathrm{Im}(\rho_{as})]^2} - 2\sqrt{\rho_{ee}\rho_{gg}}, \tag{4.19}$$

$$\mathcal{C}_2(t) = 2|\rho_{eg}| - \sqrt{(\rho_{ss} + \rho_{aa})^2 + 4[\mathrm{Re}(\rho_{as})]^2}. \tag{4.20}$$

This expression for concurrence will be used in the following section to study the dynamical evolution of entanglement in the two-qubit system by considering various initial conditions.

D. Entanglement dynamics of two identical qubits

1. Initial pure state

In the two-qubit system one might consider a pure separable or entangled state as an initial condition. For instance, for pure separable state, one can take the two atom excited state, $|e\rangle$. Even though this is unentangled state at the initial time, the interaction of the atoms with the environment leads to weak transient entanglement [16, 84]. The effect of quantum interference induced by position-dependent excitation phase is unimportant in this case we thus instead focus on pure entangled state as an initial condition.

We take the initial state of the two-qubit system to be the symmetric state $|s\rangle$. This state is a pure maximally entangled state and can be prepared using correlated pair of photons generated from a parametric down-conversion process in which one of the photons is sent to a detector D_1 and the other is directed towards the atoms. A click on the detector D_1 tells us that the other photon is sent to the atoms. If the second detector D_2 registrars a count then no atom is excited. However, if D_1

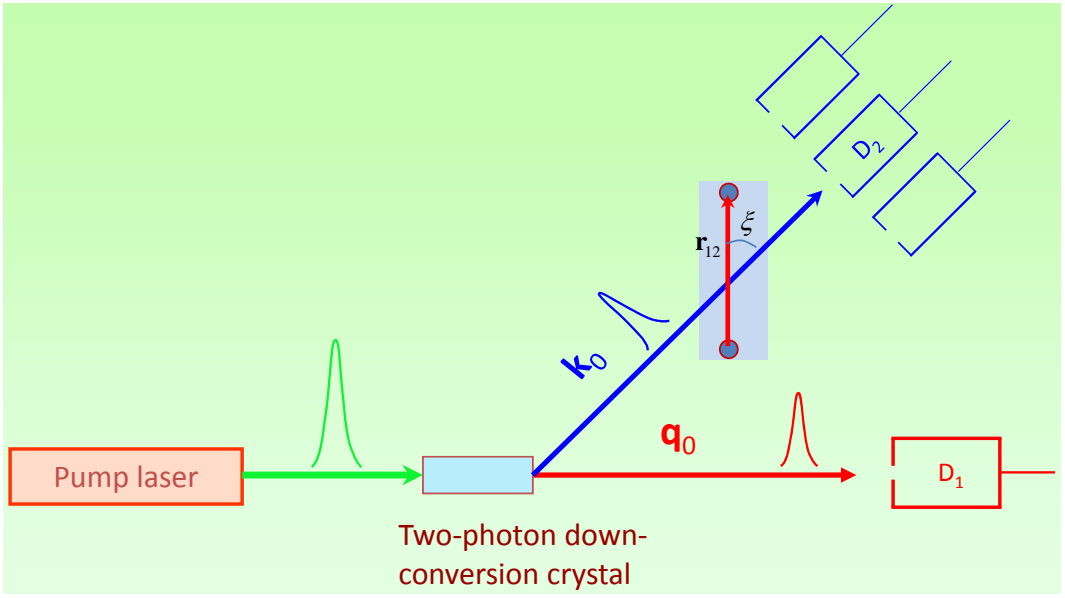

Fig. 22. A scheme illustrating a proposed method to prepare symmetric timed Dicke state $|s\rangle$. A similar scheme has been proposed to excite one atom in a cloud of N atoms [11]. The two-photon down conversion crystal converts the a pump photon into signal-idler pair of photons of wave vectors $\mathbf{k}_0$ and $\mathbf{q}_0$. A click on detector D_1 indicates generation of the pair and hence no click on the second detector D_2–assuming a perfect detector–means the photon of wave vector $\mathbf{k}_0$ conditionally excite one of the atoms.

registers a click and D_2 does not then we know that one of the atoms is excited, but we don't know which one (see Fig. 22). This leads to a superposition state $|s\rangle$. Recently, Thiel *et al.* [100] proposed a method to prepare all the symmetric states using a linear optical tools.

In terms of the timed Dicke basis the initial density matrix has only one nonzero element namely, $\rho_{ss}(0) = 1$; all other matrix elements are zero. Since there is no initial two-photon coherence, $\rho_{eg}(0) = 0$, according to Eq. (4.9d), it remains zero all the times. As a consequence the expression given by (4.20) will be negative and hence cannot be used as an entanglement measure. Moreover, it is easy to see that

for initial condition that, the population in the doubly excited state is zero, i.e., $\rho_{ee}(t) = 0$. Thus Eq. (4.19) is the entanglement measure for the initial condition considered here. In view of this, expression given by (4.19) takes the form

$$\mathcal{C}_1(t) = \sqrt{(\rho_{ss} - \rho_{aa})^2 + 4[\mathrm{Im}(\rho_{as})]^2} > 0 \tag{4.21}$$

and thus the concurrence can be written as

$$\mathcal{C}(t) = \max(0, \mathcal{C}_1(t)). \tag{4.22}$$

This expression shows that the concurrence is unity at $t = 0$ as it should be.

To clearly see the effect of the position-dependent excitation phase on the entanglement, we first consider the case for which $\varphi = 0$. In this respect, disregarding the relative phase shift ($\varphi = 0$) the solutions of the elements of the density matrix in Eq. (4.21) turn out to be $\rho_{ss}(t) = \exp[-2(\gamma + \gamma_{12})t]$, $\rho_{aa}(t) = 0$, and $\rho_{as} = 0$, which leads to

$$\mathcal{C}(t) = \max(0, e^{-2(\gamma+\gamma_{12})t}). \tag{4.23}$$

We immediately see that the concurrence depends only on the symmetric state population, $\rho_{ss}(t)$. As there is no single photon coherence generated in this case, population transfer between levels $|s\rangle$ and $|a\rangle$ does not occur. As a result the initial entanglement experiences an enhanced decay due to the collective decay rate (γ_{12}) and goes asymptotically to zero as $t \to \infty$. For nonidentical atoms, however, even though the entanglement has the same behavior as identical atoms at the initial time, it exhibits revival at later times [16]. Here the detuning plays an important role in creating coherence between the symmetric and antisymmetric states, which is the basis for entanglement in the two-qubit system. In the following we rather show, by taking into account the spatial phase dependence of the atomic states, that quantum in-

terference in the system leads to a population transfer between the symmetric and antisymmetric states and hence generation of coherence, ρ_{as}.

As mentioned in the Introduction, the phase shift that an atom experiences during the excitation process contain physical information about the excited atom. For example, in the phase factor associated with an excited atom $\exp(i\mathbf{k}_0 \cdot \mathbf{r}_j)$ the term $\mathbf{k}_0 \cdot \mathbf{r}_j = \nu_0 \hat{n} \cdot \mathbf{r}_j / c \equiv \nu_0 t_j$ indicates that the atom located at position r_j is excited at time t_j. This has been discussed in the context of directed spontaneous emission and collective Lamb shift in recent years [11, 13]. Here, we present how this phase factor can be used to improve the entanglement at later times.

In one photon subspace [$\rho_{ss}(0) = 1$] and for nonzero position-dependent excitation phase the important equations read

$$\dot{\rho}_{ss} = -2(\gamma + \gamma_{12}\cos\varphi)\rho_{ss} - i\sin\varphi(\gamma_{12} + i\Omega_{12})\rho_{as} + i\sin\varphi(\gamma_{12} - i\Omega_{12})\rho_{sa}, \quad (4.24)$$

$$\dot{\rho}_{aa} = -2(\gamma - \gamma_{12}\cos\varphi)\rho_{aa} - i\sin\varphi(\gamma_{12} - i\Omega_{12})\rho_{as} + i\sin\varphi(\gamma_{12} + i\Omega_{12})\rho_{sa}, \quad (4.25)$$

$$\dot{\rho}_{as} = -2(\gamma - i\Omega_{12}\cos\varphi)\rho_{as} + i\sin\varphi(\gamma_{12} + i\Omega_{12})\rho_{ss} + i\sin\varphi(\gamma_{12} - i\Omega_{12})\rho_{aa}. \quad (4.26)$$

These equations fully describe the dynamical behavior of the population transfer between the symmetric and antisymmetric states and the coherence developed between them under the given initial condition. We particularly note that the coherence critically depends on the position-dependent excitation phase (φ). It is not difficult to see from these equations that for a laser propagating perpendicular to the interqubit axis ($\varphi = 0$) there will be no coherence, which in turn implies the initial population in the symmetric state directly decays to the ground state without ever being transferred to the antisymmetric state. In this decay process, the maximum entanglement present at the initial time will be washed out in short time. Therefore, for this particular

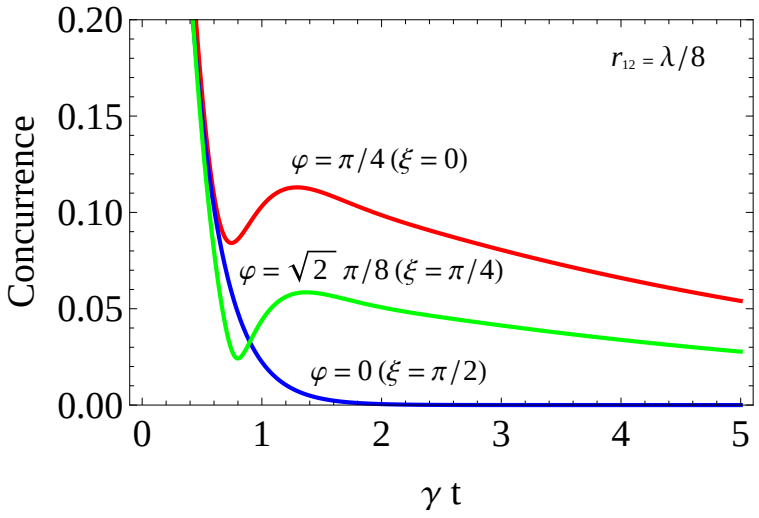

Fig. 23. Plots of the time evolution of concurrence $\mathcal{C}_1(t)$ with initial condition $\rho_{ss}(0) = 1$, for interatomic distance $r_{12} = \lambda/8$ $(\gamma_{12}/\gamma = 0.9, \Omega_{12}/\gamma = -0.9)$ for different values of the position-dependent phase φ.

initial condition, one has to play around with the position-dependent excitation phase to avoid enhanced decay of the entanglement.

Using the analytical solutions of the Eqs. (4.24)-(4.26), the concurrence can be expressed as

$$\mathcal{C}(t) = \max(0, \mathcal{C}_1(t)), \tag{4.27}$$

where

$$\mathcal{C}_1(t) = e^{-2\gamma t}[(\cos\varphi \cosh 2\gamma_{12}t - \sinh 2\gamma_{12}t)^2 + \sin^2\varphi \cos^2 2\Omega_{12}t]^{1/2}. \tag{4.28}$$

Inspection of (4.28) shows that the presence of the excitation phase brings in the dipole-dipole interaction (Ω_{12}) into the dynamics. This is in contrast to the case where $\varphi = 0$, in which the concurrence is independent of the interqubit interaction. Note that it is, in part, the initial preparation of the state that determines the dynamical behavior of the two-qubit system.

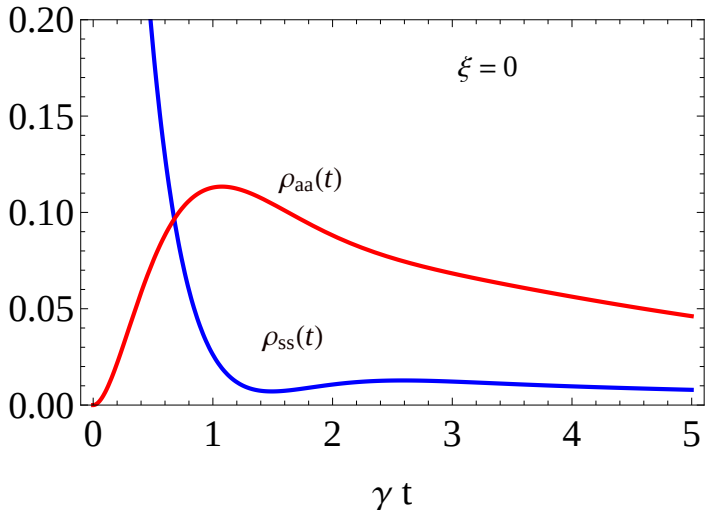

Fig. 24. Plots of the population in the symmetric (blue curve) and asymmetric (red curve) states versus γt when the excitation phase is maximum $\xi = 0(\varphi = \pi/4)$ and $r_{12} = \lambda/8$.

In Fig. 23, we show the evolution of the concurrence as a function of the position-dependent excitation phase which is determined by the angle between the direction of propagation of the laser and the line joining the two atoms (ξ) for the two-qubit system prepared initially in the symmetric state $|s\rangle$ and for interatomic distance $r_{12} = \lambda/8$. As mentioned earlier, the concurrence corresponding to $\varphi = 0$ exhibits a sharp decrease and ultimately goes to zero for $t \to \infty$. The situation for nonzero excitation phase is different; the concurrence sharply diminishes during the decay time of the symmetric state $[2\gamma + \gamma_{12}\cos\varphi]^{-1}$ and shows a bit of revival and decays slowly before it goes to zero as $t \to \infty$. This can be understood by looking at Fig. 24, where we plotted the time evolution of populations in the symmetric and antisymmetric states. As can be clearly seen from this figure, for $\varphi \neq 0(\xi = 0)$, quantum interference leads to coherent transfer of population from the initially populated state $|s\rangle$ to antisymmetric state $|a\rangle$ and hence generation of coherence between these levels as

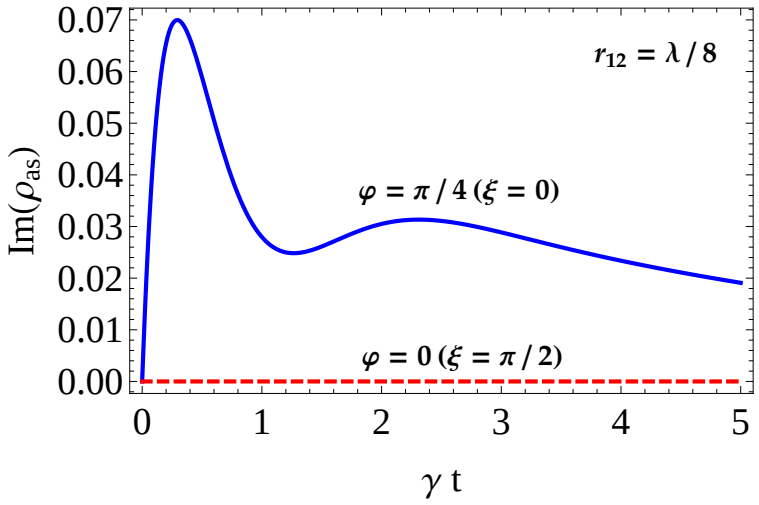

Fig. 25. Plots the imaginary part of coherence between the symmetric and antisymmetric states ρ_{as} with initial condition $\rho_{ss}(0) = 1$, for interatomic distance $r_{12} = \lambda/8$ ($\gamma_{12}/\gamma = 0.9, \Omega_{12}/\gamma = -0.9$) and for $\xi = 0$. The coherence ρ_{as} is generated only when $\varphi \neq 0$ for case of identical atoms.

illustrated in Fig. 25. This coherence is responsible for the entanglement observed between the qubits.

2. Initial mixed state

We next consider an initial state in which the two qubits are prepared in a mixed entangled state [87] given by the density matrix

$$\rho(0) = \frac{1}{3}(a|1\rangle\langle 1| + (1-a)|4\rangle\langle 4| + (b+c)|\Phi\rangle\langle\Phi|) \tag{4.29}$$

in which $|\Phi\rangle = \frac{1}{\sqrt{b+c}}(\sqrt{b}|2\rangle + e^{i\chi}\sqrt{c}|3\rangle)$ and the normalization condition reads $(1+b+c)/3 = 1$. Here a, b, c and χ are independent parameters which determine the initial state of the two entangled qubits. Note that the above state is a form of generalized Werner state. The initial condition given by (4.29) can be written in the basis of

(4.11) as

$$\rho(0) = \frac{1}{3}\begin{pmatrix} a & 0 & 0 & 0 \\ 0 & b & z & 0 \\ 0 & z^* & c & 0 \\ 0 & 0 & 0 & 1-a \end{pmatrix}, \tag{4.30}$$

where $z = \sqrt{bc}\, e^{i\chi}$ is some initial two-photon coherence in the system and χ is the respective phase of the coherence. Now applying the transformation given by (4.17), the initial density matrix elements for $b = c = |z| = 1$ become

$$\rho_{ee}(0) = a/3, \quad \rho_{aa}(0) = (1-\cos\chi)/3, \quad \rho_{gg}(0) = (1-a)/3,$$
$$\rho_{ss}(0) = (1+\cos\chi)/3, \quad \rho_{as}(0) = \frac{i}{3}\sin\chi.$$

Since $\rho_{es}(0) = \rho_{ea}(0) = \rho_{gs}(0) = \rho_{ga}(0) = 0$, the form of the initial density matrix remain the same, i.e., all the zero elements remain zero and the all the rest evolves in time. Under this scenario the expression given by (4.20) will be negative and hence cannot be an entanglement measure for the two-qubit system. Therefore, (4.19) is the only candidate left to quantify the entanglement between the qubits. For $\varphi = 0$ the system of equations governing the dynamics of the two qubits can be solved analytically. Using these solutions, solved under the initial condition (4.30), the expression that describes the entanglement between the qubits, $\mathcal{C}_1(t)$, turns out to be

$$\mathcal{C}_1(t) = \frac{2}{3}e^{-2\gamma t}\Big\{\Big[\left(\cos\chi\cosh 2\gamma_{12}t - \sinh 2\gamma_{12}t + a\eta_1(t)\right)^2 + \sin^2\chi\cosh 2\Omega_{12}t\Big]^{1/2} - \sqrt{3a(1-\eta_2(t))}\Big\}, \tag{4.31}$$

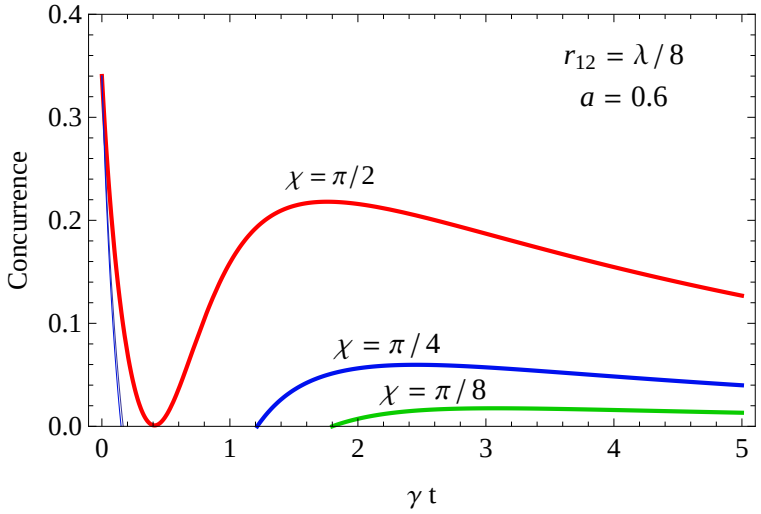

Fig. 26. Plots of the time evolution of concurrence $\mathcal{C}(t)$ with initial condition $b = c = |z| = 1$ and for $a = 0.6$, $r_{12} = \lambda/8$, and for different values of the initial phase χ.

where

$$\eta_1(t) = \frac{(\gamma^2 + \gamma_{12}^2)}{\gamma_{12}^2 - \gamma^2} \sinh 2\gamma_{12}t + \frac{2\gamma\gamma_{12}}{\gamma_{12}^2 - \gamma^2}(e^{-2\gamma t} - \cosh 2\gamma_{12}t), \tag{4.32}$$

$$\begin{aligned}\eta_2(t) = \frac{a}{3}e^{-4\gamma t} + \frac{2}{3}e^{-2\gamma t}\big[&\cosh 2\gamma_{12}t - \cos\chi \sinh 2\gamma_{12}t \\ &+ a\frac{(\gamma^2 + \gamma_{12}^2)}{\gamma_{12}^2 - \gamma^2}(e^{-2\gamma t} - \cosh 2\gamma_{12}t) - a\frac{2\gamma\gamma_{12}}{\gamma_{12}^2 - \gamma^2}\sinh 2\gamma_{12}t)\big].\end{aligned} \tag{4.33}$$

We immediately see from this result that the concurrence depends on the parameters a, which characterizes the initial populations of the doubly excited state and on the phase parameter χ which determines the initial populations in the symmetric and antisymmetric states as well as the coherence between them. If we assume that the qubits are coupled independently to their respective vacuum environment ($\gamma_{12} = 0$) and are well separated in position ($r_{12} \gg \lambda$) so that the dipole-dipole interaction

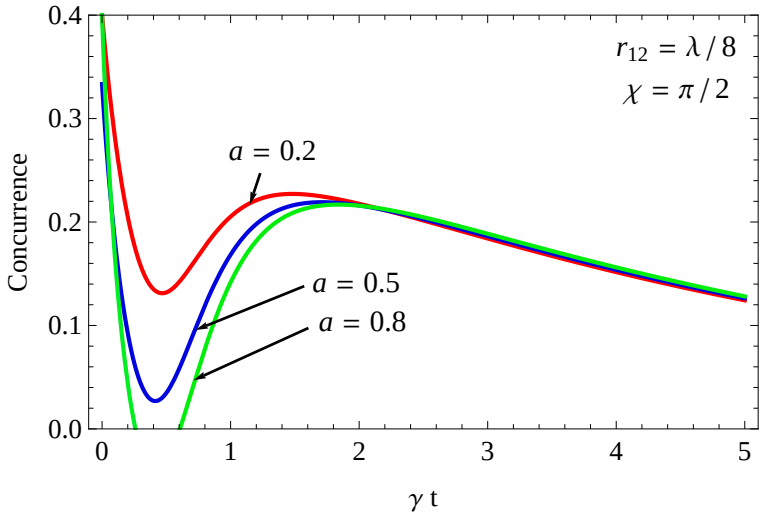

Fig. 27. Plots of the time evolution of concurrence with initial condition $b = c = |z| = 1$ and for $\chi = \pi/2$, $r_{12} = \lambda/8$ ($\gamma_{12}/\gamma = 0.9, \Omega_{12}/\gamma = -0.9$), and for different values of the initial population a.

($\Omega_{12} \to 0$), $\mathcal{C}_1(t)$ reduces to

$$\mathcal{C}_1(t) = \frac{2}{3}e^{-2\gamma t}\Big[1 - \sqrt{a(1 - a + 2\alpha^2 + \alpha^4 a)}\Big],$$

where $\alpha(t) = \sqrt{1 - \exp(-2\gamma t)}$. Note that $\mathcal{C}_1(t)$ is independent of the initial phase χ. This coincides with the earlier results of Yu and Eberly [87]. In the following we study the dependence of the concurrence and hence the entanglement between the qubits on various system parameters. Figure 26 shows the time evolution of the concurrence for $r_{12} = \lambda/8$ and $a = 0.6$ and for different values of the initial phase angle, χ. We observe from this figure that the initial entanglement between the qubits vanishes and exhibits revival. The amplitude of revival and the revival time (the time at which the entanglement revive in the system) are directly related to the initial coherence in the system. The higher the initial coherence the higher the amplitude of revival and the shorter the revival time is. Not surprisingly the magnitude of revival diminishes when

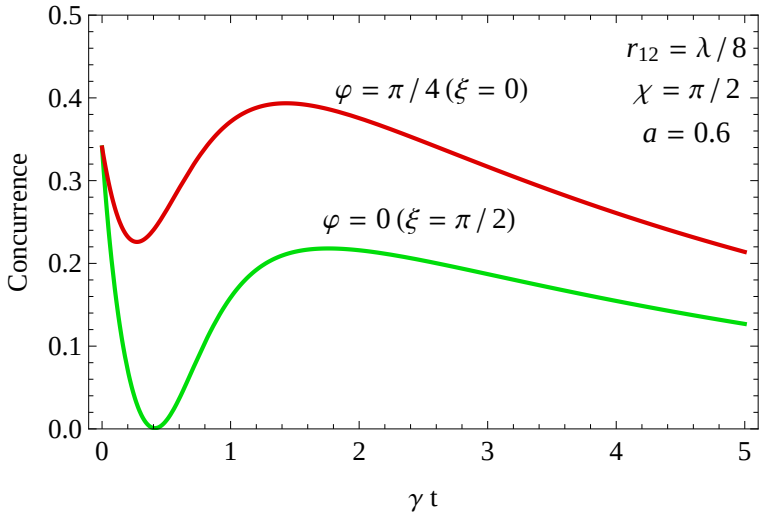

Fig. 28. Plots of the evolution of concurrence with initial condition $b = c = |z| = 1$ and for $r_{12} = \lambda/8$ ($\gamma_{12}/\gamma = 0.9, \Omega_{12}/\gamma = -0.9$), $\chi = \pi/2$ and for $\varphi = \pi/4$ (red curve) and $\varphi = 0$ (green curve).

the initial coherence decreases. Now keeping the initial coherence at its maximum value ($\chi = \pi/2$), we investigate the influence of the population distribution between the excited and ground states on the concurrence. Figure 27 shows the evolution of the concurrence for $\chi = \pi/2$ and for different values of a. This figure indicates that when the initial population in the excited state grows the transient entanglement falls sharply and even disappears for $a = 0.8$ ($\rho_{ee}(0) \approx 0.27$) in the short time window. The entanglement then shows revival and a slowly damping behavior afterwards for all values of initial populations.

We next analyze the evolution of entanglement in the system by introducing the position-dependent excitation phase φ into the dynamics. By comparing the previous results for $\varphi = 0$ with the numerical plots for $\varphi = \pi/4$, we discuss the effect of the excitation phase on the entanglement dynamics. Our results are summarized in Figs. 28 and 29. In Fig. 28, we present a comparison of concurrence taking into account the

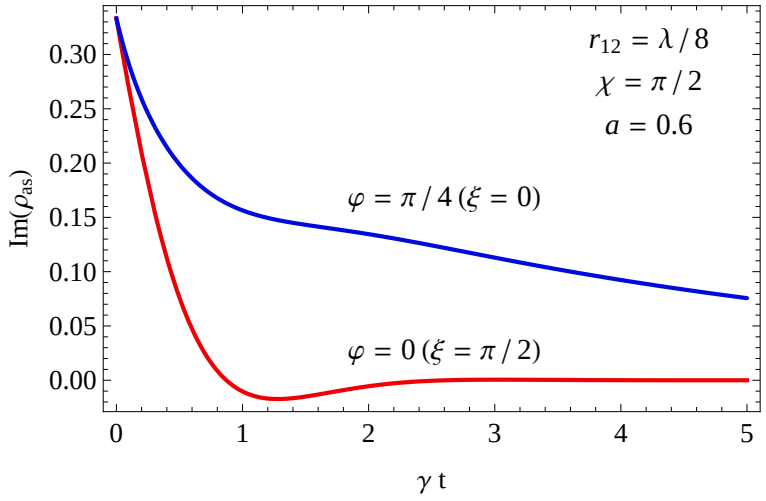

Fig. 29. Plots of the imaginary part of the one photon coherence ρ_{as} with initial condition $b = c = |z| = 1$ and for $r_{12} = \lambda/8$ $(\gamma_{12}/\gamma = 0.9, \Omega_{12}/\gamma = -0.9)$, $\chi = \pi/2$ and for $\varphi = 0$ (red curve) and $\varphi = \pi/4$ (blue curve).

excitation phase $\varphi = \pi/4$ $(\xi = 0)$ and in the absence of excitation phase, $\varphi = 0$ $(\xi = \pi/2)$ for interatomic distance less than the radiation wavelength, $r_{12} = \lambda/8$. Recall that $\varphi = (2\pi/\lambda) r_{12} \cos\xi$, where ξ is the angle between the laser propagation direction and the line joining the two atoms. These plots clearly show that the excitation phase effectively protects the initial entanglement from experiencing a sudden death and even enhances the entanglement from its initial value during the revival period. The amount of entanglement then drops gradually and approaches zero as $t \to \infty$. It is worth noting that the position-dependent excitation phase creates additional coherence and hence improves the revival magnitude over that observed for the case $\varphi = 0$. This enhanced coherence, as shown in Fig. 29, is a signature of stronger entanglement between the qubits.

E. Conclusion

We have investigated the effect of quantum interference induced by position-dependent excitation phase on the evolution of entanglement between two dipole-coupled qubits and undergoing a cooperative spontaneous emission. Our results show that for the atoms initially prepared in a symmetric state, the excitation phase induces quantum interference in the two-qubit system that leads to coherent population transfer between the symmetric and antisymmetric states. This thus creates a coherence which, in effect, slows down the otherwise fast decay of two-qubit entanglement considerably. We find that the evolution of entanglement crucially depends on the coherence between the symmetric and antisymmetric states. Furthermore, when the qubits are prepared in a Werner-type mixed entangled state the entanglement is known to suffer sudden death. However, if one takes into account the excitation phase into the dynamics the entanglement exhibits revival. This revival is attributed to the strong coherence dynamically developed between the symmetric and antisymmetric states. A viable candidate for realization of our findings would be semiconductor quantum dots. Note that coupled quantum dots with interdot distance less than the radiation wavelength has already been investigated in context to photoluminescence spectra [90] and quantum gates [101].

CHAPTER V

ENTANGLEMENT OF TWO SPATIALLY SEPARATED QUBITS VIA CORRELATED PHOTONS *

A. Introduction

In the Chapter IV we have discussed how the quantum interference induced by position dependent excitation phase affects entanglement between two dipole-coupled qubits undergoing cooperative spontaneous emission. Here we consider an alternative scheme to create entanglement between two initially uncoupled qubits in a cavity QED setup.

In discrete variable entanglement, a key aspect has been the dependence of entanglement on the direct coupling of the qubits, whose physical origin differs from one system to other. For example, dipolar coupling plays an important role in atoms, ions, molecules and quantum dots [16, 17, 102], whereas waveguides are coupled by evanescent waves [71] and superconducting qubits via their mutual inductance [103]. An essential drawback of the schemes dependent in particular on dipolar coupling is that the entanglement relies on the interqubit separations and is prominent only when separation is less than the operational wavelength [84]. For quantum computing applications and quantum networks, one however needs entanglement between qubits to be long-lived for separations more than the operational wavelength. In recent years, schemes based on cavity quantum electrodynamics (QED) [104, 105], virtual photons [106], and nonclassical radiation in superconducting charge qubits [107, 108] has been proposed in achieving this.

---

* Reprinted with permission from "Entanglement of two spatially separated qubits via correlated photons" by Eyob A. Sete and S. Das, 2012. *Opt. Lett.*, in press, Copyright [2012] by Optical Society of America.

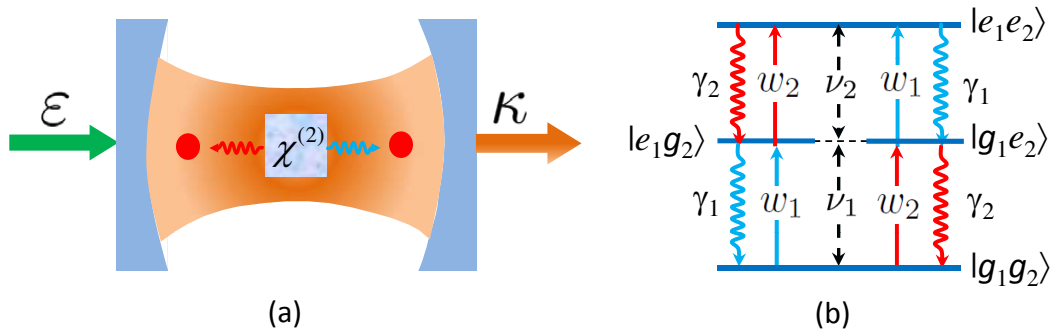

Fig. 30. (a) Schematic of interaction of two qubits with squeezed light in a cavity. When the pump laser of amplitude ε and frequency ν drives the nonlinear crystal of susceptibility $\chi^{(2)}$ correlated signal-idler photon pairs of frequency ν_1, ν_2 ($\nu = \nu_1 + \nu_2$) are generated. The two-photon correlation is then transferred to the two-qubit system mediated by the cavity (b) Collective state energy level diagram for the two-qubit system including incoherent pumping rates (w_1 and w_2).

In this Chapter, we propose an alternative scheme for generating steady state entanglement between two uncoupled qubits via interaction with squeezed light in a cavity QED setup. The two-photon correlation properties of the squeezed light is found to be effective in generating two-qubit entanglement even for interqubit separations more than the operational wavelength. Incoherently pumping the less dissipative qubit [109] then leads to significant steady state concurrence [99]. In our scheme the optimum concurrence turns out to be ~ 0.8 for asymmetric and ~ 0.6 for identical qubits in realistic parameter regime.

B. Model and master equation

We consider two qubits in a nondegenerate optical parametric oscillator cavity as shown in Fig. 30a. It is well known that in a parametric oscillator a pump photon of frequency ν impinging on a nonlinear crystal of susceptibility $\chi^{(2)}$ is down con-

verted into two photons of lower frequencies ν_1 and ν_2 so that $\nu = \nu_1 + \nu_2$. The down converted photons are known to show strong correlation, which translates into nonclassical properties such as squeezing and entanglement. The idea is to exploit the correlation between the photons to create entanglement between the qubits in the cavity. We assume that the qubits are spatially separated more than a wavelength so that the dipole-dipole interaction is unimportant. Effectively, the qubits are initially uncoupled and has no correlation between them. In this work, we investigate how the correlation between the photons is transferred to the qubits and realize light-to-matter entanglement transfer in such a scheme.

The interaction Hamiltonian of the qubit-cavity field system can be written, in rotating wave and dipole approximations, as

$$\hat{H}_I = \sum_{j=1,k\neq j}^{2} \Delta_j \hat{\sigma}_j^\dagger \hat{\sigma}_j + \mathrm{g}_j(c\hat{\sigma}_j^\dagger \hat{a}_j + s\hat{\sigma}_j^\dagger \hat{a}_k^\dagger + \mathrm{H.c.}), \tag{5.1}$$

where H.c. stands for hermitian conjugate, $c \equiv \cosh(\varepsilon t)$ and $s \equiv \sinh(\varepsilon t)$ with ε being the coupling strength proportional to the nonlinear susceptibility $\chi^{(2)}$ of the nonlinear crystal and the strength of the coherent drive field. The operators σ_j and a_j represent the lowering operator for jth qubit and annihilation operator for the jth cavity mode, respectively. g_j and Δ_j are the jth qubit-cavity mode coupling constant and detuning, respectively. Note that the above Hamiltonian is obtained by applying the transformation

$$\hat{H}_I = e^{i\hat{H}_1 t}\hat{H}_2 e^{-i\hat{H}_1 t}, \tag{5.2}$$

where

$$\hat{H}_1 = i\varepsilon(\hat{a}_1^\dagger \hat{a}_2^\dagger - \hat{a}_1\hat{a}_2), \tag{5.3}$$

$$\hat{H}_2 = \sum_{j=1}^{2}[\Delta_j |e_j\rangle\langle e_j| + \mathrm{g}_j(\hat{\sigma}_j^\dagger \hat{a}_j + \hat{\sigma}_j \hat{a}_j^\dagger)]. \tag{5.4}$$

For our scheme the third term and its hermitian conjugate in (5.1) are of utmost

importance and is the basis for the present work. Note that these terms are proportional to $\sinh \varepsilon t$ and disappear when we turn off the two-photon source or squeezing ($\varepsilon = 0$). The physical interpretation of these terms will become clearer in the master equation.

To study the dynamics of the cavity-qubit system we write down a master equation for qubit-field operator ρ_{AF}

$$\dot{\rho_{AF}} = -i[H_I, \rho_{AF}] + \mathcal{L}_{1A}\rho_{AF} + \mathcal{L}_{2A}\rho_{AF} + \mathcal{L}_{a_1}\rho_{AF} + \mathcal{L}_{a_2}\rho_{AF}, \tag{5.5}$$

where

$$\mathcal{L}_{jA}\rho_{AF} = \frac{\gamma_j}{2}(2\sigma_j\rho_{AF}\sigma_j^\dagger - \sigma_j^\dagger\sigma_j\rho_{AF} - \rho_{AF}\sigma_j^\dagger\sigma_j),$$

$$\mathcal{L}_{aj}\rho_{AF} = \kappa_j(2a_j\rho_{AF}a_j^\dagger - a_j^\dagger a_j\rho_{AF} - \rho_{AF}a_j^\dagger a_j),$$

and γ_j and $2\kappa_j$ $(j = 1, 2)$ are spontaneous emission rate of the jth qubit and damping rate of the jth cavity mode, respectively. The master equation (5.5) can be solved exactly using numerical methods. However, in order to obtain a closed from analytical solution for the concurrence and elucidate the physics of light-to-matter entanglement transfer, we make the bad-cavity approximation ($\kappa \gg g, \gamma$). In this limit, the cavity field reaches steady state faster than the qubits. This permits one to adiabatically eliminate the field variables and obtain an exactly solvable master equation for the qubits. Following the procedure outlined in [110] the master equation for the qubits alone (in the bad-cavity limit) reads

$$\begin{aligned}\dot{\rho} = -i\sum_{j=1}^{2}\Delta_j[\sigma_j^\dagger\sigma_j, \rho] - \sum_{j=1}^{2}\frac{\Gamma_j}{2}\left([\sigma_j^\dagger, \sigma_j\rho] + [\rho\sigma_j^\dagger, \sigma_j]\right) \\ - \frac{\varepsilon}{2\kappa}\sqrt{\gamma_{1c}\gamma_{2c}}\left\{[\sigma_1^\dagger, \rho\sigma_2^\dagger] + [\sigma_2^\dagger, \rho\sigma_1^\dagger] + \text{H.c.}\right\},\end{aligned} \tag{5.6}$$

where $\Gamma_j = \gamma_j + \gamma_{jc}$ and $\gamma_{jc} = \gamma_{0j}/(1 - \varepsilon^2/\kappa^2)$ are the total decay rate and modified

cavity-induced (due to squeezed field) decay rate of the jth qubit with $\gamma_{0j} = 2g_j^2/\kappa$ being the unmodified cavity-induced qubit decay rate. The second line in Eq. (5.6) is due to the squeezed light and describes two-qubit excitation by absorption of two-correlated photons emerging from the nonlinear crystal. This leads to creation of coherence between the doubly excited and ground states, which as we will show later, is crucial for entanglement generation between the qubits. We thus investigate how the non-local correlations between photons in the squeezed light is transferred to the qubits. To quantify the entanglement, we use concurrence [99] as the measure of entanglement in this work. The relevant concurrence expression in the basis of the two-qubit collective state (see Fig. 30b): $|e\rangle = |e_1e_2\rangle$, $|g\rangle = |g_1g_2\rangle$, $|s\rangle = (|e_1g_2\rangle + |g_1e_2\rangle)/\sqrt{2}$, and $|a\rangle = (|e_1g_2\rangle - |g_1e_2\rangle)/\sqrt{2}$) is given by

$$\mathcal{C} = 2|\rho_{eg}| - \sqrt{(\rho_{ss} + \rho_{aa})^2 - (\rho_{as} + \rho_{sa})^2}. \tag{5.7}$$

This expression clearly shows that for entanglement to exist there has to be strong two-photon coherence ρ_{eg} between the qubits. Note that even though the qubits in our scheme are separated by more than a wavelength, we do consider the two qubit collective basis for the theoretical analysis. The justification of this lies in the fact that the qubits do get coupled eventually via interaction with the cavity modes.

C. Transient entanglement

To elucidate the physics of entanglement transfer from continuous to discrete variables or light-to-matter, we first consider a simplest case of identical qubits ($\Gamma_1 = \Gamma_2 = \Gamma$), and equal cavity damping rates ($\kappa_1 = \kappa_2 = \kappa$) and qubit-cavity detunings $\Delta = \Delta_1 = \Delta_2$. We further assume that the two qubits are initially in a pure product state $|e_1g_2\rangle$.

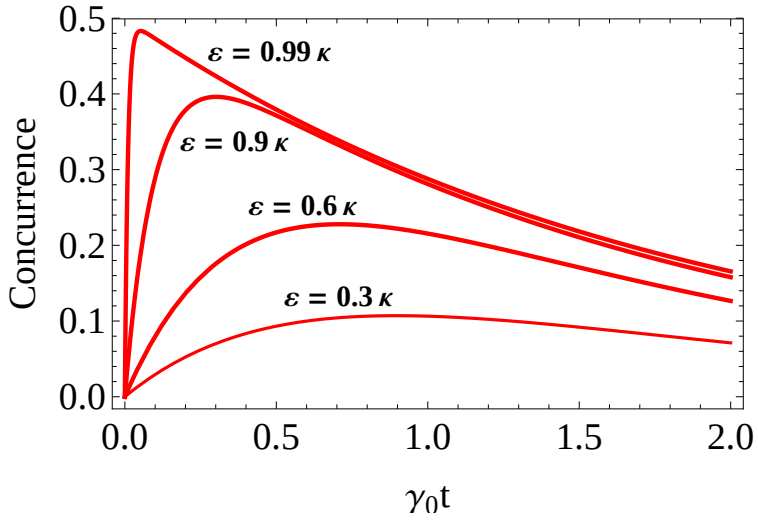

Fig. 31. Time dependent concurrence [Eq. (5.10)] for various values of ε, at resonance ($\Delta = 0$), and for $\gamma/\gamma_0 = 0.05$ [$\kappa = 80$MHz,g $= 35$MHz,$\gamma = 1.5$MHz].

For this initial condition we readily obtain

$$\rho_{aa} = \rho_{ss} = \rho_{as} = \frac{e^{-\Gamma t}}{2\alpha^2}\left[\Delta^2 - \left(\frac{\varepsilon\gamma_c}{2\kappa}\right)^2 \cos 2\alpha t\right], \tag{5.8}$$

$$\rho_{eg} = \frac{\varepsilon\gamma_c\ e^{-\Gamma t}}{4\kappa\alpha^2}\left[i\Delta(\cos 2\alpha t - 1) + \alpha \sin 2\alpha t\right], \tag{5.9}$$

where

$$\alpha = \sqrt{\Delta^2 - (\varepsilon\gamma_c/2\kappa)^2}.$$

The concurrence (5.7) then only depends on the two-photon coherence, i.e., $\mathcal{C} = 2|\rho_{eg}|$ and take a simple form

$$\mathcal{C} = \frac{\varepsilon\gamma_c e^{-\Gamma t}}{2\sqrt{2}\kappa}\left\{\left[2\Delta^2 - \left(\frac{\varepsilon\gamma_c}{2\kappa}\right)^2 (1 + \cos 2\alpha t)\right]\frac{\sin^2 \alpha t}{\alpha^4}\right\}^{\frac{1}{2}}. \tag{5.10}$$

We immediately see from Eq. (5.10) that the two qubits remain disentangled ($\mathcal{C} = 0$) in absence of the squeezed light ($\varepsilon = 0$). Figure 31 shows the temporal behavior of $\mathcal{C}$ as a function of the amplitude of the pump laser ε and for realistic parameter

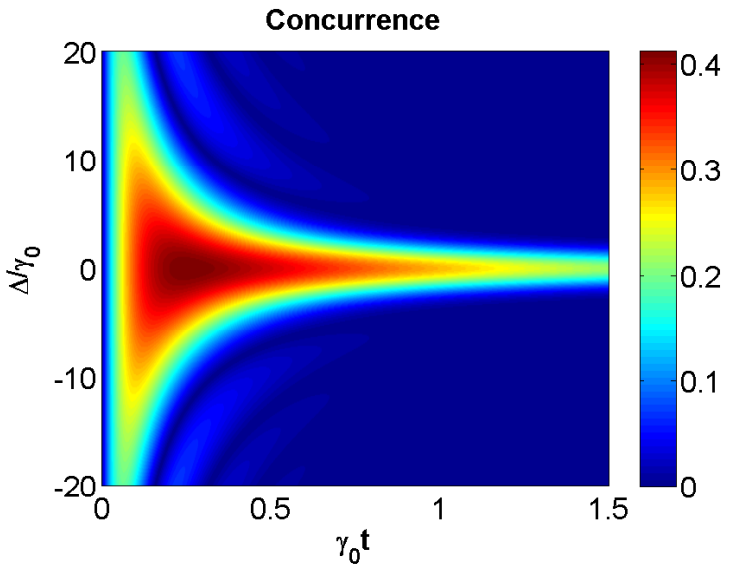

Fig. 32. Concurrence [Eq. (5.10)] versus $\gamma_0 t$ and detuning Δ/γ_0 for $\gamma/\gamma_0 = 0.05$ and $\varepsilon/\kappa = 0.92$.

$\gamma/\gamma_0 = 0.05$. We see that the concurrence increases with increasing ε for initial times and then decays exponentially in the long time limit. As the degree of squeezing in a subthreshold parametric down conversion depends on the pump laser amplitude ε, it thus means that the degree of entanglement between the qubits is directly proportional to degree of squeezing (correlation between the photons) in the transient regime. This behavior hence clearly demonstrate the transfer of entanglement from light to matter. Furthermore, as illustrated in Fig. 32, the entanglement depends on the qubit-cavity detuning. Strong entanglement is achieved when the qubits are at resonance with the cavity modes. For larger detunings, the entanglement decreases and shows damped oscillation as given by (5.10) as shown in Fig. 32.

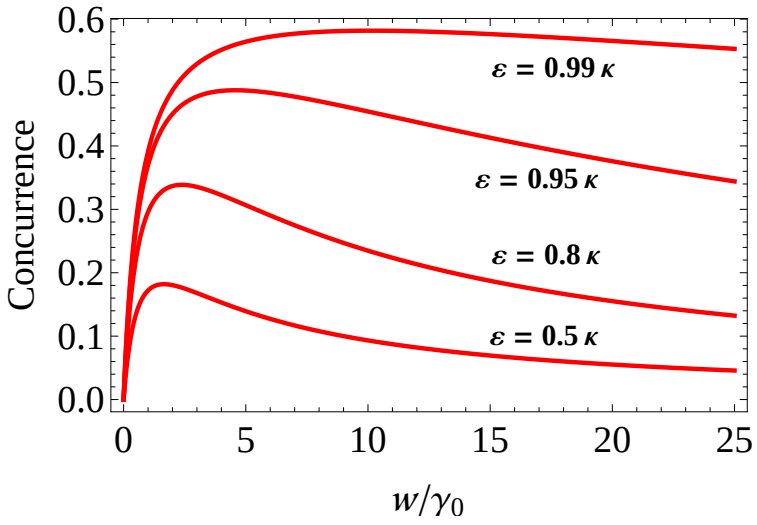

Fig. 33. Steady-state concurrence versus w/γ_0, at resonance, for $\gamma/\gamma_0 = 0.02$ and various values of ε.

D. Steady-state entanglement

In practical implementation of many quantum information processing, achieving steady-state entanglement is sometimes important. In light of this, we next focus on generation of steady-state entanglement. For this purpose, we consider incoherent pumping of the qubits, for example, by means of a flash lamp. The effect of the incoherent pump can be included by adding the following term to the master equation (5.6):

$$\mathcal{L}_p\rho = -\sum_{m=1}^{2} \frac{w_m}{2}(\hat{\sigma}_m\hat{\sigma}_m^\dagger\hat{\rho} + \hat{\rho}\hat{\sigma}_m\hat{\sigma}_m^\dagger - 2\hat{\sigma}_m^\dagger\hat{\rho}\hat{\sigma}_m), \tag{5.11}$$

where w_1 and w_2 are incoherent pumping rates for qubits 1 and 2, respectively. Note that creation of steady-state entanglement between two qubits using incoherent pump has been recently proposed for initially coupled qubits through their electric dipoles. It was shown that optimum entanglement is obtained when the less dissipative qubit is pumped [109]. Here we explore the effect of incoherent pump in creating steady-

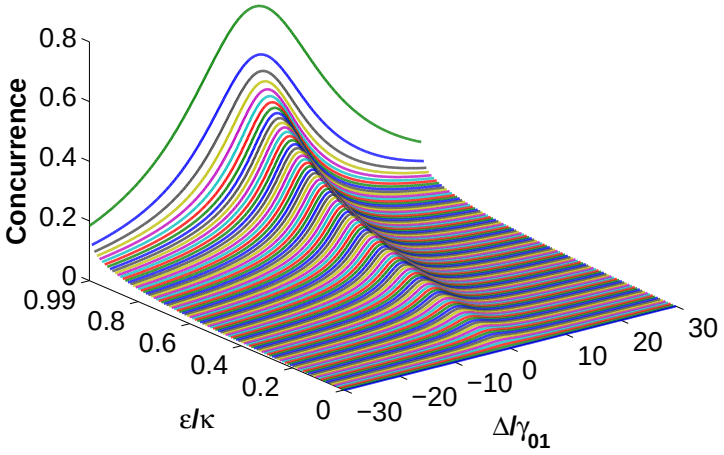

Fig. 34. Concurrence ($\mathcal{C}$) versus ε/κ and Δ/γ_{01} for $\gamma_1/\gamma_{01} = 0.01$, $\gamma_2/\gamma_{02} = 0.05$, $\gamma_{02} = 1.08\gamma_{01}$ and $w_1 = 3.5\gamma_{01}$, $w_2 = 0$.

state entanglement between two spatially separated and initially uncoupled qubits interacting with nonclassical radiation.

We first consider, for simplicity, identical qubits with one qubit incoherently pumped and the other dissipates. The concurrence in this case at resonance has a simple form:

$$\mathcal{C} = \frac{2w\varepsilon\gamma_c}{\kappa}\frac{1}{|(w+\Gamma)(w+2\Gamma) - 2(\varepsilon\gamma_c/\kappa)^2|}. \tag{5.12}$$

Figure 33 shows the steady-state concurrence versus w/γ_0 for various values of ε. This figure clearly shows that the two qubits exhibit substantially high steady-state entanglement, $\mathcal{C} \approx 0.6$. As previously noted, strong entanglement is achieved close to the threshold ($\varepsilon/\kappa = 1$). The incoherent pump works in such a way that for higher squeezing source, the qubit should be pumped at stronger rate in order to reach the optimum entanglement. Since the source of entanglement in our scheme is two-photon coherence, the generated entanglement in the steady state is of the form

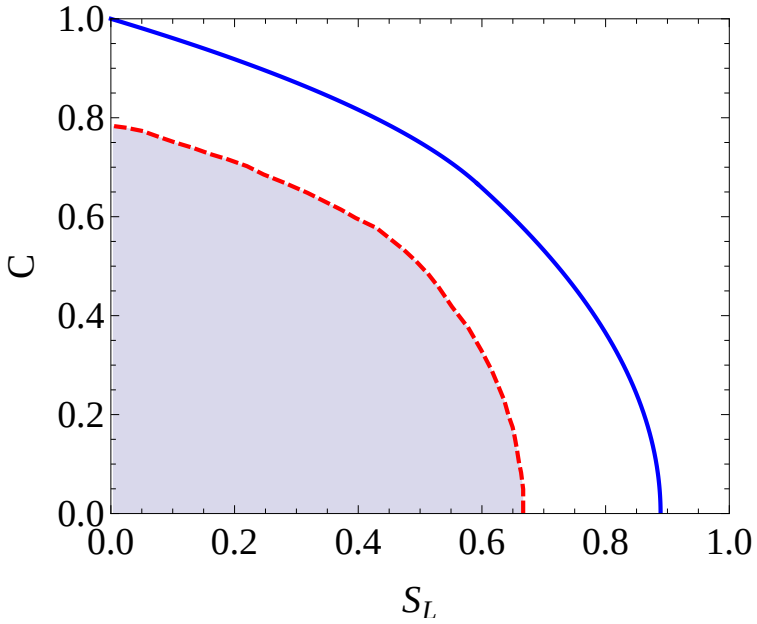

Fig. 35. Plot of concurrence $\mathcal{C}$ versus linear entropy for randomly generated points using realistic parameters for the present system (red-dashed curve) and for maximally entangled mixed state (blue-solid curve).

$(\alpha|e_1e_2\rangle + \beta|g_1g_2\rangle)$ with α and β being complex amplitudes.

In line with the previous studies [109] we next consider asymmetric qubits with the less dissipative qubit pumped incoherently. The steady-state concurrence now becomes

$$\mathcal{C} = 4w_1\Lambda\left[\frac{\upsilon^2 + 4\Delta^2}{[(\upsilon^2 + 4\Delta^2)(w_1 + \Gamma_1) - 8\upsilon\Lambda^2)]^2}\right]^{\frac{1}{2}} \tag{5.13}$$

where $\upsilon = w_1 + \Gamma_1 + \Gamma_2(\Gamma_1 < \Gamma_2), \Lambda = (\varepsilon/2\kappa)\sqrt{\gamma_{1c}\gamma_{2c}}$. Here we observe that the steady-state entanglement only exists when both the pump rate (w_1) and squeezed pump field amplitude (ε) are non zero. As can be seen from Fig. 34, entanglement is maximum at resonance and increases when one approaches to the threshold point. The optimum entanglement achieved in this case is quite high, $\mathcal{C} \approx 0.8$ for $\varepsilon = 0.99\kappa$. In order to get further insight into the formation of entangled state of the

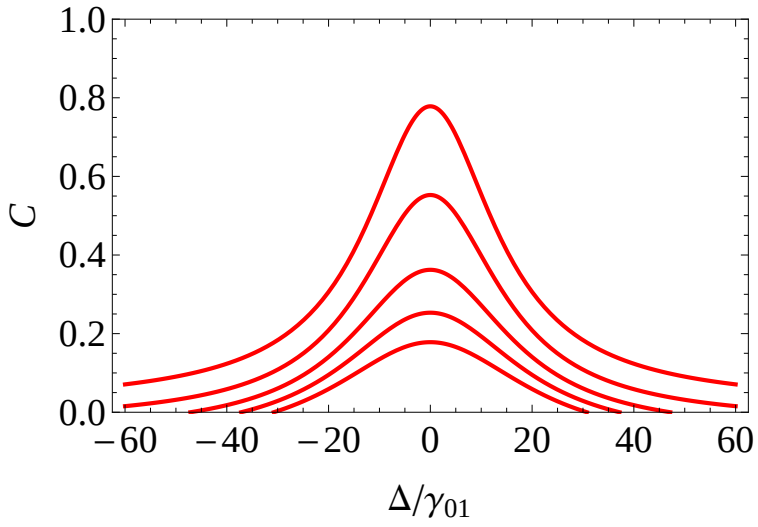

Fig. 36. Concurrence ($\mathcal{C}$) versus Δ/γ_{01} for $\varepsilon/\kappa = 0.99$ and for various values of w_2: $w_2 = 0, 0.5, 1.5, 2.5, 3.5\gamma_{01}$ from top to bottom. All other parameters are the same as in Fig. 34.

two qubits, we examine the region of concurrence-linear entropy plane accessible to our scheme. The shaded region in Fig. 35 represent randomly generated points of $\mathcal{C}$ and linear entropy $S_L = \frac{4}{3}[1 - \mathrm{Tr}(\rho^2)]$ [75] for realistic system parameters ($S_L = 0$ and 1 corresponds to pure and maximally mixed states, respectively). The dashed line gives the upper bound on $\mathcal{C}$ and S_L achievable in our scheme. It is interesting to note that maximum entanglement is achieved when the state of the qubits is pure, which is markedly different from earlier models based on coupled qubits [109]. Another interesting question is whether the entanglement exists when both qubits are pumped incoherently. As shown in Fig. 36, the entanglement is optimum when the less dissipative system is pumped (at a rate w_1) and gradually decreases as the pump rate (w_2) approaches w_1. It is however important to mention here that for equal pumping rates, the entanglement only exists at high degree of squeezing.

E. Conclusion

In conclusion, we have shown effective entanglement transfer from squeezed light to two spatially separated and initially uncoupled qubits via a two photon coherence in a cavity. An incoherent pump then assist in attaining a substantial steady state value for the transferred entanglement. Furthermore, we find that strongest entanglement is achieved for asymmetric qubits when the less dissipative one is incoherently pumped. This is encouraging in particular for quantum dot qubits, where such asymmetry is quite natural. Given the advancement in cavity QED [111] and effective coupling of atoms with squeezed light in a cavity [112], experimental realization of our proposal is quite feasible.

CHAPTER VI

PHASE-CONTROLLED ENTANGLEMENT IN A QUANTUM-BEAT LASER: APPLICATION TO QUANTUM LITHOGRAPHY *

A. Introduction

Quantum coherence induced by an external laser field is responsible for many fascinating optical phenomena in atomic and molecular systems [20]. In this Chapter, we exploit quantum coherence induced my external field to generate entangled radiation in continuous variables.

Continuous-variable (CV) entanglement based on the amplitude or phase of the quadrature of the electromagnetic field has received great attention in connection with its accessibility to experiment. In this regard, there have been large number of proposals for generating CV entanglement in general and bipartite entanglement in particular. In a seminal work, Zubairy and co-workers [9] proposed a source for an entanglement amplifier based on correlated spontaneous emission laser. Subsequent studies [10, 113, 114] showed variety of schemes for generation of CV entanglement in the steady state regime and in the presence of losses.

From application standpoint, entanglement between optical photons has been widely used for fundamental tests of quantum mechanics [115]. Numerous experiments demonstrated quantum entanglement of optical photons in trapped ions [116], atoms [117, 118], and atomic ensembles [119, 120]. Beyond fundamental applications, entanglement has been used for secure communication [121] and quantum informa-

---

* Reprinted with permission from "Phase-controlled entanglement in a quantum-beat laser: Application to quantum lithography" by Eyob A. Sete, K. E. Dorfman, and J. P. Dowling, 2011. *J. Phys. B.: At. Mol. Opt. Phys.*, 44, 225504, Copyright [2011] by Institute of Physics.

tion processing [122]. In recent times, several proposals [123, 124, 125] have been suggested to improve the spatial resolution of interferometric lithography beyond the diffraction limit utilizing entangled photons.

Quantum-beat laser concept was originally used as a means of quenching of spontaneous emission noise [126, 127, 128, 129, 130] and later for demonstration of lasing without population inversion [6]. Moreover, quantum-beat lasers are well-studied in context of quantum-statistical description of radiation [131]. More recently, schemes based on three-and four-level quantum-beat lasers have been proposed as a source for continuous-variable entanglement with the coherence induced by external lasers [132, 133]. However, in most of the previous studies involving quantum-beat lasers the generated entanglement is short-lived and exists only in the transient regime. For certain quantum information processing protocols entanglement that survives for long time is desirable.

In this Chapter, we propose a scheme that can generate controllable steady-state entanglement in continuous variables. In particular, we study a two-photon quantum-beat laser coupled to a two-mode squeezed vacuum reservoir that was shown to enhance entanglement between two cavity modes [113]. Our scheme consists of an ensemble of three-level atoms in a V configuration injected into a cavity at a constant rate and interacts with quantized cavity modes. A microwave field induces coherence by coupling the two upper levels of each atom. We treat the amplitude of the microwave driving field to all orders keeping its phase as an external control parameter. We explore how the entanglement can be controlled using the phase of the driving field and other system parameters. We also consider the effect of decoherence in our analysis. We show that the steady-state entanglement survives in the presence of decoherence due to interaction with the environment, making our scheme a robust entanglement source. A possible application of our scheme to quantum lithography

with externally controlled resolution is also suggested.

B. Hamiltonian and equations of motion

We consider a two-photon quantum-beat laser coupled to a squeezed light through the partially transmitting mirror of the cavity. Atoms, in a so-called V configuration, are injected into the cavity at rate r_a and are removed after time τ longer than the spontaneous emission time. During this time interval each atom interacts with the cavity modes of frequency ν_1 and ν_2. Our scheme is depicted in Fig. 37. The upper two levels are coupled by a microwave field of frequency ν_μ. In addition, the atomic transition $|a_1\rangle \rightarrow |b\rangle$ and $|a_2\rangle \rightarrow |b\rangle$ are off-resonant with the cavity modes.

The interaction picture Hamiltonian for the system plus the reservoir is given by

$$\hat{H} = \hat{H}_1 + \hat{H}_2 + \hat{H}_3, \tag{6.1}$$

$$\hat{H}_1 = -\hbar\Omega(e^{i\phi}|a_1\rangle\langle a_2| + e^{-i\phi}|a_2\rangle\langle a_1|), \tag{6.2}$$

$$\hat{H}_2 = -\hbar g(|a_1\rangle\langle b|\hat{a}\ e^{i\Delta t} + |a_2\rangle\langle b|\hat{b}\ e^{i\Delta t}) + \text{H.c.}, \tag{6.3}$$

$$\hat{H}_3 = \hat{a}\hat{\Gamma}_a^\dagger + \hat{\Gamma}_a\hat{a}^\dagger + \hat{b}\hat{\Gamma}_b^\dagger + \hat{\Gamma}_b\hat{b}^\dagger, \tag{6.4}$$

where Ω and ϕ are the Rabi frequency and the phase of the microwave field, respectively; $\hat{a}$ and $\hat{b}$ are the annihilation operators for cavity modes, g is the atom-cavity mode coupling constant assumed to be the same for the two cavity modes, $\Delta = \omega_1 - \nu_1 = \omega_2 - \nu_2$, ω_1 and ω_2 are the atomic transition frequencies for $|a_1\rangle \rightarrow |b\rangle$ and $|a_2\rangle \rightarrow |b\rangle$ transitions, respectively. $\hat{\Gamma}_a$ and $\hat{\Gamma}_b$ are the reservoir operators responsible for the damping of the cavity modes by the squeezed vacuum reservoir.

We next transform the microwave field away to obtain a new interaction Hamiltonian which treats Ω to all orders. The new Hamiltonian can be derived using the

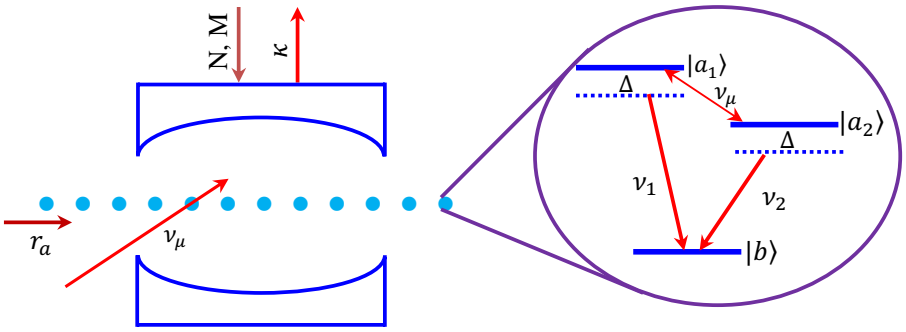

Fig. 37. Schematic of a quantum-beat laser coupled to a squeezed reservoir (N,M) in which atoms are injected into the cavity at a rate r_a. The energy level diagram for a three-level atom is shown on the right. The upper two levels are coupled by a microwave field of frequency ν_μ. The transition between levels $|a_1\rangle$ and $|b\rangle$, and $|a_2\rangle$ and $|b\rangle$ at frequencies ω_1 and ω_2 are detuned by the same amount Δ from the cavity modes.

transformation

$$\hat{H}_I = e^{i\hat{H}_1 t/\hbar}\hat{H}_2 e^{-i\hat{H}_1 t/\hbar} \tag{6.5}$$

which gives

$$\begin{aligned}\hat{H}_I = -\hbar g\Big\{ &\left(\cos\Omega t - ie^{i\phi}\sin\Omega t\right) e^{i\Delta t}|a_1\rangle\langle b|\hat{a} \\ &+ \left(\cos\Omega t - ie^{-i\phi}\sin\Omega t\right) e^{i\Delta t}|a_2\rangle\langle b|\hat{b}\Big\} + \text{H.c.}\end{aligned} \tag{6.6}$$

Under secular approximation [6], neglecting highly oscillating terms $e^{\pm i(\Delta+\Omega)t}$ compared to $e^{\pm i(\Delta-\Omega)t}$ and at resonance, $\Omega = \Delta$, the Hamiltonian takes the form

$$\hat{H}_I = -\frac{\hbar g}{2}\Big\{(|a_1\rangle\langle b| + e^{-i\phi}|a_2\rangle\langle b|)\hat{a} + (|a_2\rangle\langle b| + |a_1\rangle\langle b|e^{i\phi})\hat{b}\Big\} + \text{H.c.} \tag{6.7}$$

We note that the Hamiltonian only depends on the coupling constant g and the phase of the microwave field ϕ. The strength of the microwave field is determined by the amount of detuning. Thus, through out this paper, we treat the amplitude of the

driving field as a constant and vary the phase. This allows us to coherently control the entanglement in the system.

We further assume that atoms are injected into the laser cavity in a coherent superposition of the two upper levels. Thus the initial state of a single atom can be written as

$$|\psi(0)\rangle = a_1|a_1\rangle + a_2|a_2\rangle, \tag{6.8}$$

where a_1 and a_2 are probability amplitudes. Therefore, the density operator for the atom at the initial time may be written as $\rho_A(0) = \rho_{11}^{(0)}|a_1\rangle\langle a_1| + \rho_{22}^{(0)}|a_2\rangle\langle a_2| + \rho_{12}^{(0)}|a_1\rangle\langle a_2| + \rho_{21}^{(0)}|a_2\rangle\langle a_1|$, in which $\rho_{11}^{(0)} = |a_1|^2, \rho_{22}^{(0)} = |a_2|^2$, and $\rho_{12}^{(0)} = \rho_{21}^{(0)*} = a_1^* a_2$. We study the properties of the entanglement between the cavity modes as a function of initial population and atomic coherence.

Following the standard laser theory methods [20, 134], we obtain the master equation for the cavity radiation to be

$$\begin{aligned}\frac{d}{dt}\hat{\rho} &= \frac{1}{2}[A\xi + \kappa N](2\hat{a}^\dagger\hat{\rho}\hat{a} - \hat{a}\hat{a}^\dagger\hat{\rho} - \hat{\rho}a\hat{a}^\dagger) + \frac{1}{2}[A\xi + \kappa N](2\hat{b}^\dagger\hat{\rho}\hat{b} - \hat{b}\hat{b}^\dagger\hat{\rho} - \hat{\rho}\hat{b}\hat{b}^\dagger) \\ &+ \frac{A\xi}{2}e^{-i\phi}(2\hat{b}^\dagger\hat{\rho}\hat{a} - \hat{a}\hat{b}^\dagger\hat{\rho} - \hat{\rho}\hat{a}\hat{b}^\dagger) + \frac{A\xi}{2}e^{i\phi}(2\hat{a}^\dagger\hat{\rho}\hat{b} - \hat{b}\hat{a}^\dagger\hat{\rho} - \hat{\rho}\hat{b}\hat{a}^\dagger) \\ &+ \frac{\kappa}{2}(N+1)(2\hat{a}\hat{\rho}\hat{a}^\dagger - \hat{a}^\dagger\hat{a}\hat{\rho} - \hat{\rho}\hat{a}^\dagger\hat{a} + 2\hat{b}\hat{\rho}\hat{b}^\dagger - \hat{b}^\dagger\hat{b}\hat{\rho} - \hat{\rho}\hat{b}^\dagger\hat{b}) \\ &+ \kappa M(\hat{\rho}\hat{a}\hat{b} + \hat{a}\hat{b}\hat{\rho} - \hat{b}\hat{\rho}\hat{a} - \hat{a}\hat{\rho}\hat{b}) + \kappa M^*(\hat{\rho}\hat{a}^\dagger\hat{b}^\dagger + \hat{a}^\dagger\hat{b}^\dagger\hat{\rho} - \hat{a}^\dagger\hat{\rho}\hat{b}^\dagger - \hat{b}^\dagger\hat{\rho}\hat{a}^\dagger),\end{aligned} \tag{6.9}$$

where

$$A = 2\mathrm{g}^2 r_a/\gamma^2$$

is the linear gain coefficient and

$$\xi = \frac{\gamma}{4\Gamma}\left[1 + \frac{\gamma}{\Gamma}\sqrt{1-\eta^2}\cos(\alpha - \phi)\right].$$

We introduce new variable η related to initial condition as $\rho_{11}^{(0)} = (1-\eta)/2$, $\rho_{22}^{(0)} =$

$(1+\eta)/2$ and $\rho_{12}^{(0)} = e^{i\alpha}\sqrt{1-\eta^2}/2$, where α is the phase of the initial atomic coherence. We assume that the cavity mode decay rate κ is the same for both modes. Parameters N present the mean number of photons in the squeezed field and $M = |M|e^{i\theta} = \sqrt{N(N+1)}$ with θ being the phase of the squeezed vacuum, characterize the two-mode squeezed vacuum reservoir. Here we have included spontaneous emission rate γ, assumed to be the same for all the three levels, and dephasing rate Γ. Note that the effect of the microwave field is manifested in the master equation via its phase ϕ which can be used to control the entanglement properties (see Sec. C).

The master equation is used to derive the evolution equations for the moments of the cavity mode operators. The steady-state solutions of these equations are used, in the following sections, to analyze the entanglement and correlation properties of the cavity radiation.

C. Phase-controlled entanglement

Numerous entanglement measures have been proposed for Gaussian states [135, 136], which are only sufficient for non-Gaussian states. We employ the entanglement measure proposed by Duan-Giedke-Cirac-Zoller (DGCZ) [136], which is sufficient and necessary condition for gaussian states and necessary condition for non-Gaussian states. According to DGCZ a state of a system is said to be entangled if the quantum fluctuations of the two Einstein-Podolsky-Rosen-like operator $\hat{u}$ and $\hat{v}$ of the two modes satisfy the inequality

$$\Delta u^2 + \Delta v^2 < 2, \tag{6.10}$$

where

$$\hat{u} = \hat{x}_a - \hat{x}_b, \qquad \hat{v} = \hat{p}_a + \hat{p}_b \tag{6.11}$$

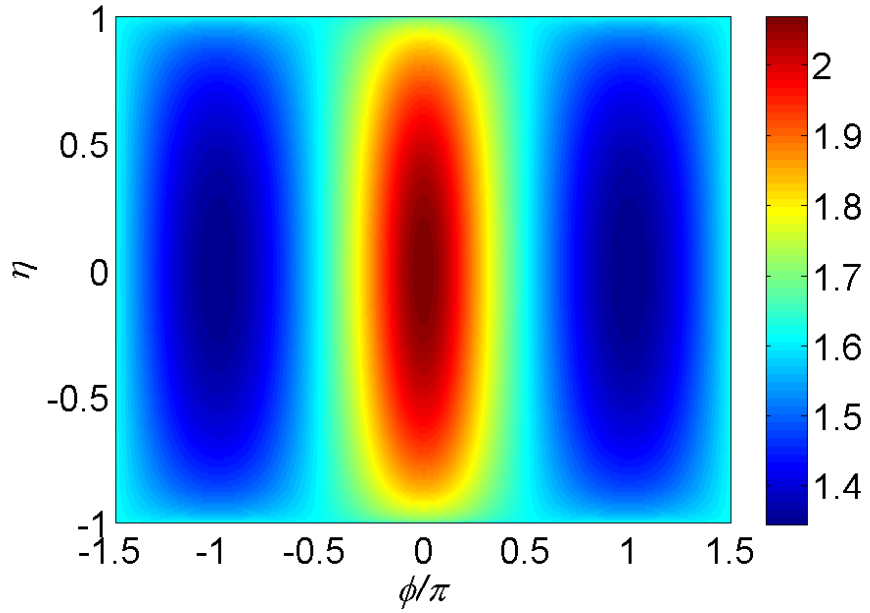

Fig. 38. Density plot of $\Delta u^2 + \Delta v^2$ vs ϕ and η for a linear gain coefficient $A/\Gamma = 0.25$, $\kappa/\Gamma = 0.8$, $\gamma/\Gamma = 1$, $N = 0.04$, $\alpha = 0$, $\theta = 0$.

in which $\hat{x}_j = (\hat{j}^\dagger + \hat{j})/\sqrt{2}$, $\hat{p}_j = i(\hat{j}^\dagger - \hat{j})/\sqrt{2}$ (with $j = a, b$) are the quadrature operators of the two modes of the cavity field. These operators can be measured by the method of homodyne detection [137]. Taking into account (6.11), Eq. (6.10) yields

$$\Delta u^2 + \Delta v^2 = 2(1 + \langle \hat{a}^\dagger \hat{a} \rangle + \langle \hat{b}^\dagger \hat{b} \rangle - \langle \hat{a} \hat{b} \rangle - \langle \hat{a}^\dagger \hat{b}^\dagger \rangle). \tag{6.12}$$

Using the steady state expression for the average quantities that appear in Eq. (6.12), we readily obtain

$$\begin{aligned} \Delta u^2 + \Delta v^2 = & -2 - 4\kappa(\kappa - A\xi)\Big[\frac{M\cos\theta}{(\kappa - A\xi)^2 - 2A^2\xi^2} \\ & - \frac{2(1+N)}{2(\kappa - A\xi)^2 - A^2\xi^2(1+\cos 2\phi)}\Big]. \end{aligned} \tag{6.13}$$

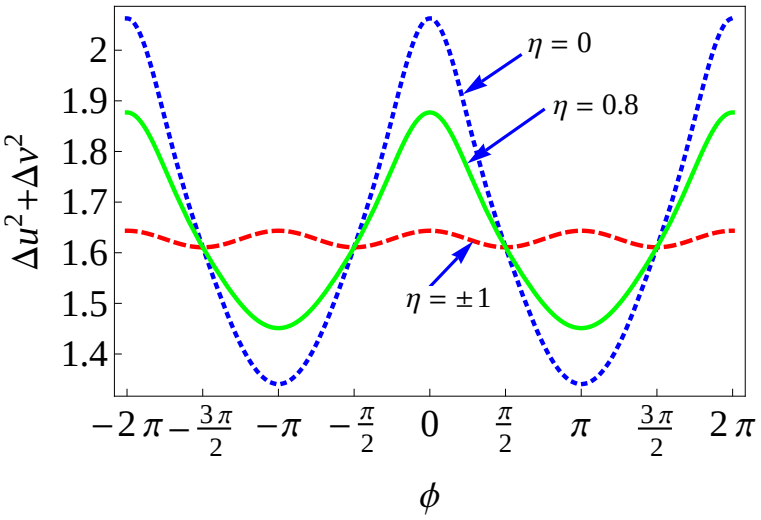

Fig. 39. Plots of $\Delta u^2 + \Delta v^2$ vs ϕ for the linear gain coefficient $A/\Gamma = 0.25$, $\kappa/\Gamma = 0.8$, $\Gamma/\gamma = 1$, $N = 0.04$, $\alpha = 0$, $\theta = 0$ and for various initial conditions.

We note that the entanglement measure depends on the relative phase shift between the phase of injected atomic coherence and that of the microwave field. In the following we discuss possible cases in which one can control the entanglement between the cavity modes by manipulating these phases and other system parameters.

We begin by examining the entanglement between the cavity modes as a function of the phase of the microwave field ϕ and the initial coherence. In Fig. 38 we plot the function (6.13) versus the microwave phase and initial population distribution η for a fixed phases of the atomic coherence and input squeezed field ($\alpha = \theta = 0$). Figure 38 illustrates that the entanglement condition (6.10) is satisfied for certain values of η and ϕ in the absence of decoherence ($\Gamma = \gamma$), indicating entanglement of the two cavity modes. Moreover, the degree of entanglement depends on the phase ϕ. For instance, stronger entanglement is observed when the microwave phase is an odd multiple of π, while the entanglement gradually disappears when the phase changes from $\phi = (2n + 1)\pi$ to $\phi = 2\pi n$, where n is an integer. The parameters in Fig. 38

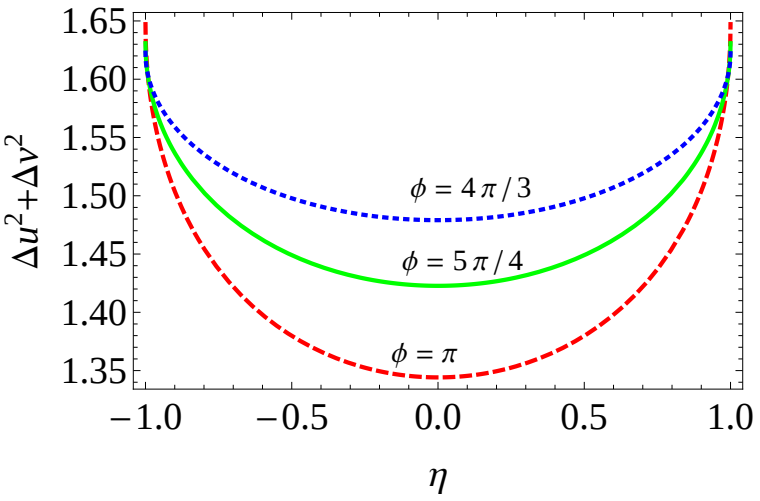

Fig. 40. Plots of $\Delta u^2 + \Delta v^2$ vs η for various values of the microwave phase ϕ. All parameters are the same as in Fig. 39.

are chosen to satisfy condition $\kappa - A\xi > 0$, a condition for a well-defined steady-state solutions for the equations of the moments of the cavity mode operators. One might interpret $\kappa = A\xi$ as the threshold condition for the system.

To clearly see to what extent the initial atomic coherence influences the degree of entanglement, we plot the function (6.13) versus ϕ by considering various initial conditions (see Fig. 39). For maximum initial atomic coherence ($\eta = 0$), which corresponds to equal populations distribution between the two upper levels, the sum of the variances shows oscillatory behavior with a period of 2π and with a maximum value a little over 2. The optimum entanglement is obtained when $\phi = \pm\pi$. This optimum value decreases as one decreases the coherence, that is, when one increases $|\eta|$. It is interesting to note that despite a decrease on the optimum value, the cavity modes remain entangled for all values of the microwave field phase at higher values of $|\eta|$. Furthermore, a simple observation of the plots reveals that for $\eta = \pm 1$ (no initial coherence), the system exhibits fairly constant entanglement. Therefore, the system

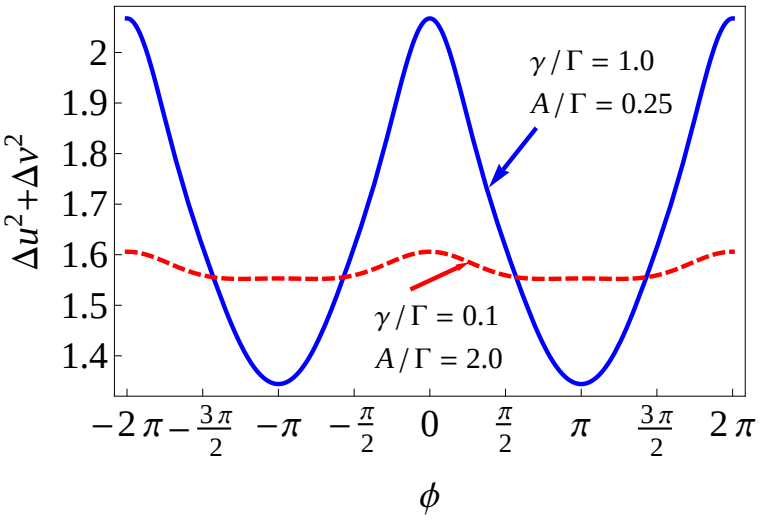

Fig. 41. Plots of the $\Delta u^2 + \Delta v^2$ vs ϕ for $\eta = 0$ in the absence ($A/\Gamma = 0.25$, $\gamma/\Gamma = 1$ blue solid curve) and in the presence ($A/\Gamma = 2$ and $\gamma/\Gamma = 0.1$ red dashed curve) of decoherence. The rest of the parameters are the same as in Fig. 39.

can exhibit steady-state entanglement even without initial atomic coherence.

Figure 40 shows the entanglement measure versus η for different values of ϕ. For fixed η the amount of entanglement decreases when the phase increases from $\phi = \pi$ to $\phi = 3\pi/2$ with its maximum being at $\phi = \pi$. Moreover, the entanglement exists for all values of η.

So far, we have considered two types of losses in our system: the spontaneous emission γ and the cavity decay κ. Given that our system involves coherence it is imperative to include decoherence into the analysis. To this end, we assume that the decoherence rate Γ is greater than the spontaneous emission rate γ. In the following we show that the entanglement can still survive in the presence of decoherence at the expense of high pumping rate of atoms into the cavity. In Fig. 41, we plot $\Delta u^2 + \Delta v^2$ versus the phase of the microwave field in the presence and absence of decoherence. This figure shows that for a decoherence rate 10 times stronger that the

spontaneous emission rate the system still exhibits entanglement. However, it comes at the expense of higher pump rate, A due to the steady state condition $\kappa - A\xi > 0$, which is necessary for steady state solution to exist. That is for a given κ one has to increase A accordingly for larger ξ to keep the inequality satisfied. We thus conclude here that–for our parameters–it is possible to overcome the effect of decoherence by pumping atoms into the cavity at higher rates.

The cavity mode entanglement properties analyzed above allows us to study the output mode which is accessible to experiment. In this regard, we use the standard input-output relation:

$$\hat{a}_{out} = \sqrt{\kappa}\hat{a} - \hat{a}_{in}, \tag{6.14}$$

$$\hat{b}_{out} = \sqrt{\kappa}\hat{b} - \hat{b}_{in}, \tag{6.15}$$

where $\hat{a}_{in}$ and $\hat{b}_{in}$ represent the input two-mode squeezed field. Up on using these equations, we obtain the relation between the input and output mode entanglement condition to be

$$(\Delta u^2 + \Delta v^2)_{\rm out} = \Delta u^2 + \Delta v^2 + 2(1-\kappa)(N - |M|). \tag{6.16}$$

For ideal squeezed vacuum $|M| = \sqrt{N(N+1)}$. We note that the last term in Eq. (6.16) is always negative for nonzero mean photon numbers N. Thus the output mode entanglement is stronger than the cavity modes.

Next we consider the total mean photon number in the cavity $\bar{n} = \langle a^\dagger a\rangle + \langle b^\dagger b\rangle$ given by

$$\bar{n} = -2 + \frac{4(1+N)\kappa(\kappa - A\xi)}{2(\kappa - A\xi)^2 - A^2\xi^2(1+\cos 2\phi)}. \tag{6.17}$$

Equation (6.17) shows that the total mean photon number of the two cavity modes is maximum for $\phi = \pi$. On the other hand, for $\phi = \pi/2$ the denominator of the second

term in (6.17) becomes relatively large and hence the total mean photon number gets smaller. Therefore, a better entanglement is achieved at the expense of weaker signal.

D. Application to quantum lithography

A possible application of the proposed scheme is quantum interferometric optical lithography. Proposed by Dowling and co-workers [123] and later demonstrated experimentally [125], this lithographic method allows one to obtain sub-diffraction limit resolution (see Fig. 42). Depending on the order N or the NOON state [138], it allows one to print features of minimum size $\lambda/2N$, where λ is the wavelength of light. This method is based on the properties of the multiphoton absorption probability. For the simple case of two-photon processes, where the atomic lifetime is much shorter than the decoherence time, the probability is given by [139]

$$W_2 = 2|g|^2 G^{(2)}(0) \frac{\gamma/2}{(\gamma/2)^2 + (2\omega - \omega_0)^2}. \tag{6.18}$$

For the two-mode squeezed vacuum field generated by spontaneous parametric down conversion (SPDC), the second-order correlation as a function of mean photon number $\bar{n} = \bar{n}_a + \bar{n}_b$ is given by

$$G^{(2)}_{ab}(0) = \langle n_a n_b \rangle = \frac{1}{2}\left(\bar{n}^2 + \bar{n}\right) \tag{6.19}$$

which gives for $\bar{n} \ll 1$ a linear intensity dependence versus quadratic for coherent light. In the present model, for $\bar{n} \ll 1$ and $|\kappa - \xi A| \ll \kappa$ the leading term in two-photon correlation function reads

$$G^{(2)}_{ab}(0) = \left[\frac{1 + \cos 2\phi}{\kappa - \xi A}\left(\frac{\kappa^2}{2(\kappa - \xi A)} + 1\right) + \frac{1}{16}\left(\cos 4\phi + 24\cos 2\phi - 1\right)\right]\bar{n}. \tag{6.20}$$

Thus, for $\phi = 0, \pi$ Eq. (6.20) yields super-poissonian statistics

$$G^{(2)}_{ab}(0) \approx \frac{\kappa^2 \bar{n}}{(\kappa - \xi A)^2} \gg \frac{\bar{n}}{2}, \tag{6.21}$$

which has much more rapid rate compare to the SPDC result. However, by tuning ϕ to $\pi/2$, we obtain sub-poissonian result

$$G^{(2)}_{ab}(0) \approx -\frac{3\bar{n}}{2}. \tag{6.22}$$

Therefore, intensity of the laser field used for quantum lithography printing can be controlled by the external phase.

Furthermore, in order to determine the resolution of printing we can calculate the two-photon exposure dosage $\Delta_{2\gamma} = \frac{1}{2}\langle \hat{e}^{\dagger 2}\hat{e}^2 \rangle$ [123], where the average is taken over the initial states at the arms A and B. For the interference experiment at the substrate, the two photons should have the same frequency. This, in principle, can be realized by introducing an optical frequency modulator in one of the arms of the interferometer just before the beam splitter. The exposure dosage is proportional to the two-photon absorption at the imaging surface. The operator $\hat{e}$ is the combination of modes resulting from the beam splitter (see Fig. 42). The phase shift induced by a phase plate (PS) is represented by single parameter $2\varphi = 2kx$, where $k = 2\pi/\lambda$ with λ and x being the optical wavelength and the lateral dimension on the substrate, respectively. The mode that emerges from the arm that has a phase shifter (PS) experience a phase shift of $2kx$ while other mode emerges without phase shift. The output field operators $\hat{c}, \hat{d}$ are related to input field operators $\hat{a}, \hat{b}$ through beam splitter and phase plate by $\hat{c} = (\hat{a} - i\hat{b})e^{2ikx}/\sqrt{2}$, $\hat{d} = (-i\hat{a} + \hat{b})/\sqrt{2}$. Two-photon correlation function at the output is $G^{(2)}(0) = \langle \hat{e}^{\dagger 2}\hat{e}^2 \rangle$, where $\hat{e} = \hat{c} + \hat{d}$. The resulting expression for two-photon exposure dosage is given by

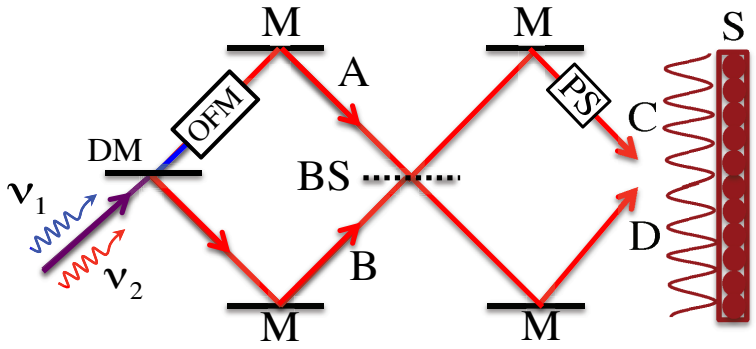

Fig. 42. Interferometric lithography setup utilizing input photons entering ports A and B. Here DM is a dichroic mirror, OFM is optical frequency modulator, BS is symmetric lossless beam splitter, and M represents the mirrors. Upper arm of the interferometer experiences a phase shift 2φ at the phase shifter (PS) before both branches interfere on the substrate S.

$$\begin{aligned} 2\Delta_{2\gamma} =& [1-\sin(2kx)]^2\langle\hat{a}^{\dagger 2}\hat{a}^2\rangle_{\rm o} + [1+\sin(2kx)]^2\langle\hat{b}^{\dagger 2}\hat{b}^2\rangle_{\rm o} \\ &+ 2\cos(2kx)[1-\sin(2kx)][\langle\hat{a}^{\dagger 2}\hat{a}\hat{b}\rangle_{\rm o} + \langle\hat{a}^\dagger\hat{a}^2\hat{b}^\dagger\rangle_{\rm o}] \\ &+ 2\cos(2kx)[1+\sin(2kx)][\langle\hat{a}\hat{b}^{\dagger 2}\hat{b}\rangle_{\rm o} + \langle\hat{a}^\dagger\hat{b}^\dagger\hat{b}^2\rangle_{\rm o}] \\ &+ \cos^2(2kx)[4\langle\hat{a}^\dagger\hat{a}\hat{b}^\dagger\hat{b}\rangle_{\rm o} + \langle\hat{a}^{\dagger 2}\hat{b}^2\rangle_{\rm o} + \langle\hat{a}^2\hat{b}^{\dagger 2}\rangle_{\rm o}], \end{aligned} \tag{6.23}$$

where $\langle\hat{O}\rangle_{\rm o} \equiv \langle\hat{O}_{out}\rangle$. Inspection of Eq. (6.23) shows that depending on the expectation values of output mode operators the period of the imprinted structure can be either determined by the classical Rayleigh limit $\lambda/2$ or quantum limit $\lambda/4$.In this regard, we calculate the steady state solutions of equations of the cavity mode

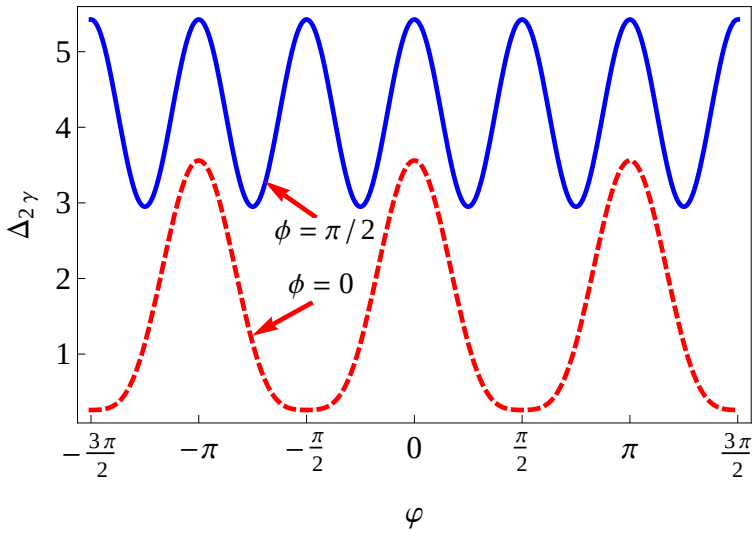

Fig. 43. Plots of the exposure dosage versus path-difference phase shift for $\gamma/\Gamma = 1$, $\kappa/\Gamma = 0.8$, $A/\gamma = 2$, $\alpha = 0$, $N = 0.1$, $\eta = 0$, and for $\phi = 0$ (red dotted curve) and $\phi = \pi/2$ (blue solid curve $5\Delta_{2\gamma}$). Note here that dotted curve corresponds to a classical Rayleigh limit of resolution $\lambda/2$ and the solid curve shows the quantum limit with a resolution improvement of 100%.

moments. For instance, for $\xi A \ll 1$, Eq. (6.23) reads

$$\begin{aligned}\Delta_{2\gamma} \approx & N[5N + 1 + 10(N + 1)q] + N(N + 1) \\ & \times [12q \cos\phi \cos(2kx) + (2q + 1)\cos(4kx)],\end{aligned} \tag{6.24}$$

where $q = \xi A$. Equation (6.24) yields $\lambda/4$ resolution for $\phi = \pi/2$ and classical result $\lambda/2$ for $\phi = 0$ (see Fig. 43). Therefore, as shown in Fig. 43 the resolution of imprinted profile can be controlled by varying the single parameter–phase of the microwave field ϕ. While quantum lithography as originally proposed remains challenging due to the lack of suitable N-photon absorbing resists, quantum light sources can still be used successfully in a non-lithographic setting where number-resolving detector arrays and centroid measurements are deployed [140, 141].

E. Conclusion

In conclusion, we have shown steady state entanglement induced by quantum coherence via a driving microwave field in a two-photon quantum beat laser coupled to a squeezed field. The entanglement can be controlled by adjusting the phases of the microwave and the squeezed input fields. Our results show that the entanglement is robust against cavity losses and decoherence and thus can be used for various applications. For instance, the output mode of the generated light can be used to enhance resolution beyond the Rayleigh limit. More importantly one can switch from classical resolution $\lambda/2$ to quantum limit $\lambda/4$ by adjusting the phase of the driving field. Experimentally, our system can be realized along the lines of similar previously successful microwave experiments [142, 143, 144].

CHAPTER VII

EFFECT OF DEPHASING ON TRANSIENT AND STEADY-STATE ENTANGLEMENT IN A QUANTUM-BEAT LASER *

A. Introduction

Quantum properties of cavity radiation strongly relies on the dissipation processes that the system is subjected to. Among all dissipation processes, dephasing–the decay of atomic coherence due to its interaction with the surrounding environment–might lead to adverse effects on the quantum features of the cavity field. In particular, quantum entanglement is one which is fragile in the face of decoherence. Recently, entanglement generation using two-photon lasers such as correlated emission lasers [9, 10, 113] and quantum-beat lasers (QBL) [133, 145, 146, 147] has received a renewed interest. In these types of lasers, the entanglement is dependent on quantum coherence and is susceptible to dephasing processes. Here we address the role of dephasing on entanglement generated by quantum-beat lasers.

As mentioned in the previous Chapter, QBLs are shown to be a source for entangled radiation [133, 145, 146, 147]. In such lasers, the generated entanglement is attributed to atomic coherence induced via coupling the upper two levels of a V-type three-level atoms by strong laser field or *driven coherence*. This coherence translates into correlations between two modes of the cavity field due to interference between two pathways that lead to the lower level. Note that since the generated coherence crucially depends on the amplitude of the laser field [133, 145, 146], the time for which the cavity exhibits entanglement strongly relies on the strength of the driving field.

---

* Reprinted with permission from "Effect of dephasing on transient and steady-state entanglement in a quantum-beat laser" by Eyob A. Sete, 2011. *Phys. Rev. A*, 84, 063808, Copyright [2011] by American Physical Society.

It has also been shown that the entanglement created via driven coherence only exist in the transient regime and hence depends on the initial condition of the cavity field. Besides, almost all previous studies in QBLs neglected dephasing processes which otherwise lead to fast decay of coherence and hence entanglement. For a practical application of quantum information processing, it is desirable to have entanglement which can survive for longer times and robust against decoherence.

This Chapter is thus devoted to the formulation and analysis of the role of dephasing on entanglement properties of the cavity modes of a QBL. We present a detailed derivation of the pertinent master equation in the good-cavity limit by taking into account all dissipation processes namely, spontaneous emission, cavity losses, and dephasing. Unlike earlier studies, where driven coherence is used as a primary way of inducing coherence in the system, our scheme includes coherence induced via initial coherent superposition of the two upper levels of a V-type atoms or *injected coherence*. We investigate to what extent the dephasing rate modifies the entanglement between the cavity modes for the cases of injected coherence as well as driven coherence using Hillery-Zubairy entanglement criterion [148]. We also discuss the interplay between the cavity mode detunings and pumping rates in optimizing the entanglement. Our results show that when the coherence is induced by initial coherent superposition of atomic levels, the resulting entanglement exists both in transient and steady state regimes and is more sensitive to dephasing processes. In particular, the steady-state entanglement is achieved when only cavity mode detunings are different. We also show that it is possible to reduce the effect of dephasing on entanglement by injecting atoms at higher rates and tuning the cavity modes at far-off resonances (large detunings). In contrast, when coherence is induced by coupling the upper two levels by strong laser field, we obtain only transient entanglement which is relatively robust against decoherence.

B. Hamiltonian and master equation

We consider a two-photon QBL coupled to a vacuum reservoir through the partially transmitting mirror of the cavity. Atoms, in a V configuration, are injected into the laser cavity at rate r_a and are removed after time τ longer than the spontaneous emission time. During this time interval each atom nonresonantly interacts with the cavity mode of frequencies ν_1 and ν_2. Moreover, to externally induce coherence, a strong laser field of Rabi frequency Ω and phase ϕ is resonantly coupled to the $|a_1\rangle \leftrightarrow |a_2\rangle$ transition. The energy level diagram for the atom is shown in Fig. 44. The interaction picture Hamiltonian for the system, in the rotating wave and dipole approximations, is given by ($\hbar = 1$)

$$\hat{H}_I = \sum_{j=1}^{2} \Delta_j |a_j\rangle\langle a_j| + g_j(\hat{a}_j|a_j\rangle\langle b| + |b\rangle\langle a_j|\hat{a}_j^\dagger) - \frac{\Omega}{2}(e^{-i\phi}|a_1\rangle\langle a_2| + e^{i\phi}|a_2\rangle\langle a_1|). \quad (7.1)$$

Here $\hat{a}_1(\hat{a}_1^\dagger)$ and $\hat{a}_2(\hat{a}_2^\dagger)$ are the annihilation (creation) operators for the cavity modes 1 and 2, respectively. g_i are atom-cavity mode coupling constants. The modes of the cavity are detuned from the transitions $|a_1\rangle \leftrightarrow |b\rangle$ and $|a_2\rangle \leftrightarrow |b\rangle$ by $\Delta_1 = \omega_{1b} - \nu_1$ and $\Delta_2 = \omega_{2b} - \nu_2$, respectively.

We next derive the master equation for the cavity radiation by applying the Hamiltonian (7.1). While there are several approaches for obtaining the master equation, we here employ the procedure outlined in [20, 134]. Suppose that $\hat{\rho}_{AR}(t, t_j)$ represent the density operator for the radiation plus an atom in the cavity at time t that is injected at earlier time t_j. Since the atom stays in the cavity for time τ, it easy to see that $t - \tau \leq t_j \leq t$. Then the density operator for all atoms in the cavity plus the two-mode radiation at time t can be written as

$$\hat{\rho}_{AR}(t) = r_a \sum_j \hat{\rho}_{AR}(t, t_j)\Delta t'_j, \quad (7.2)$$

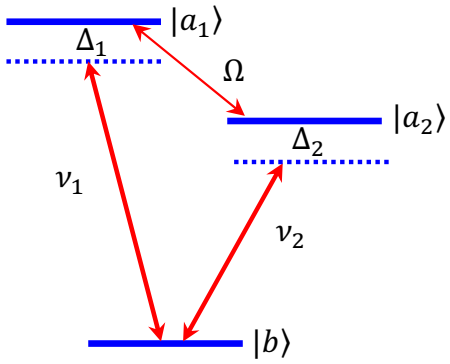

Fig. 44. Energy level diagram for a three-level atom in a V configuration with the cavity modes interacting with the atoms nonresonantly.

where $r_a \Delta t'_j$ is the total number of atoms injected into the cavity in a small time interval $\Delta t'_j$. Assuming that large number of atoms are injected in a time interval $\Delta t'_j$, we change the summation by integration. Thus, differentiating both sides of the resulting equation, we arrive at

$$\frac{d}{dt}\hat{\rho}_{AR}(t) = r_a \frac{d}{dt}\int_{t-\tau}^{t} \hat{\rho}_{AR}(t,t')dt'. \tag{7.3}$$

In order to incorporate the initial preparation of the atoms into the dynamics, we transform the above equation into

$$\frac{d}{dt}\hat{\rho}_{AR}(t) = r_a\Big\{[\hat{\rho}_{AR}(t,t) - \hat{\rho}_{AR}(t,t-\tau)] + \int_{t-\tau}^{t} \frac{\partial}{\partial t}\hat{\rho}_{AR}(t,t')dt'\Big\}. \tag{7.4}$$

Here $\hat{\rho}_{AR}(t,t)$ represents the density operator for atom plus radiation at time t for an atom injected at an earlier time t. Since the atomic and radiation variables are uncorrelated at the instant the atom is injected into the cavity, one can write

$$\hat{\rho}_{AR}(t,t) \equiv \hat{\rho}(t)\hat{\rho}_A(0), \tag{7.5}$$

where $\hat{\rho}(t)$ is the filed density operator and $\hat{\rho}_A(0)$ is the initial density operator for an

atom. For simplicity, we further assume that the atomic and radiation variables are uncorrelated just after the atom is removed from the cavity, which allows as to write

$$\hat{\rho}_{AR}(t, t-\tau) \equiv \hat{\rho}(t)\hat{\rho}_A(t-\tau), \tag{7.6}$$

where $\hat{\rho}_A(t-\tau)$ is the density operator for an atom injected at $t-\tau$. In this work we assume that atoms are initially injected into the cavity in coherent superposition of the upper two levels. The corresponding initial density operator then reads

$$\hat{\rho}_A(0) = \rho_{11}^{(0)}|a_1\rangle\langle a_1| + \rho_{22}^{(0)}|a_2\rangle\langle a_2| + \rho_{12}^{(0)}|a_1\rangle\langle a_2| + \rho_{21}^{(0)}|a_2\rangle\langle a_1|, \tag{7.7}$$

where $\rho_{ii}^{(0)}$ and $\rho_{ij}^{(0)}$ are initial population and coherence, respectively. Using Eqs. (7.5) and (7.6), Eq. (7.4) becomes

$$\frac{d}{dt}\hat{\rho}_{AR}(t) = r_a\Big\{[\hat{\rho}_A(0) - \hat{\rho}_A(t-\tau)]\hat{\rho} + \int_{t-\tau}^{t}\frac{\partial}{\partial t}\hat{\rho}_{AR}(t,t')dt'\Big\}. \tag{7.8}$$

Furthermore, it is obvious that the time evolution of the density operator $\hat{\rho}_{AR}(t,t')$ has a form $\partial\hat{\rho}_{AR}(t,t')/\partial t = -i[H_I, \hat{\rho}_{AR}(t,t')]$ which together with

$$\frac{\partial}{\partial t}\hat{\rho}_{AR}(t) = r_a\int_{t-\tau}^{t}\frac{\partial}{\partial t}\hat{\rho}_{AR}(t,t')dt'$$

gives

$$\frac{d}{dt}\hat{\rho}_{AR}(t) = r_a[\hat{\rho}_A(0) - \hat{\rho}_A(t-\tau)]\hat{\rho} - i[H_I, \hat{\rho}_{AR}(t)]. \tag{7.9}$$

We are interested in the dynamics of the cavity radiation. In this regard, we trance the atom-plus-radiation density operator over atomic variables. This yields

$$\frac{d}{dt}\hat{\rho}(t) = -i\mathrm{Tr}_A[H_I, \hat{\rho}_{AR}(t)], \tag{7.10}$$

where we have used the fact that $\mathrm{Tr}_A[\hat{\rho}_A(0)] = \mathrm{Tr}_A[\hat{\rho}_A(t-\tau)] = 1$. Substituting the

Hamiltonian in Eq. (7.10), we obtain

$$\frac{d}{dt}\hat{\rho}(t) = -ig_1(a_1\hat{\rho}_{b1} - \hat{\rho}_{b1}a_1 + a_1^\dagger\hat{\rho}_{1b} - \hat{\rho}_{1b}a_1^\dagger) \\ -ig_2(\hat{a}_2\hat{\rho}_{b2} - \hat{\rho}_{b2}\hat{a}_2 + \hat{a}_2^\dagger\hat{\rho}_{2b} - \hat{\rho}_{2b}\hat{a}_2^\dagger). \quad (7.11)$$

Here for typographical convenience we set $\hat{\rho}_{ba_1} \equiv \hat{\rho}_{b1}$ and $\hat{\rho}_{ba_2} \equiv \hat{\rho}_{b2}$. The next task is to obtain $\hat{\rho}_{b1}$, $\hat{\rho}_{b2}$ and their complex conjugates. To this end, multiplying Eq. (7.9) on the left by $\langle\alpha|$ and on the right by $|\beta\rangle$, one gets

$$\frac{d}{dt}\hat{\rho}_{\alpha\beta}(t) = r_a\langle\alpha|[\hat{\rho}_A(0) - \hat{\rho}_A(t, t-\tau)]|\beta\rangle\hat{\rho} - i\langle\alpha|[H_I, \hat{\rho}_{AR}(t)]|\beta\rangle - \gamma_{\alpha\beta}\hat{\rho}_{\alpha\beta}, \quad (7.12)$$

where $\alpha, \beta = a_1, a_2, b$. We phenomenologically included the last term to account for spontaneous emission and dephasing processes. $\gamma_{\alpha\alpha}$ is the spontaneous emission rate and $\gamma_{\alpha\beta}(\alpha \neq \beta)$ is the dephasing rate. The equations of motion for the elements of the density operator that appear in Eq. (7.11) read

$$\dot{\hat{\rho}}_{1b} = -(\Gamma_1 + i\Delta_1)\hat{\rho}_{1b} + ig_1(\hat{\rho}_{11}\hat{a}_1 - \hat{a}_1\hat{\rho}_{bb}) + ig_2\hat{\rho}_{12}\hat{a}_2 + \frac{i\Omega}{2}e^{-i\phi}\hat{\rho}_{2b}, \quad (7.13)$$

$$\dot{\hat{\rho}}_{2b} = -(\Gamma_2 + i\Delta_2)\hat{\rho}_{2b} + ig_2(\hat{\rho}_{22}\hat{a}_2 - \hat{a}_2\hat{\rho}_{bb}) + ig_1\hat{\rho}_{21}\hat{a}_1 + \frac{i\Omega}{2}e^{i\phi}\hat{\rho}_{2b}, \quad (7.14)$$

where $\hat{\rho}_{11} \equiv \hat{\rho}_{a_1a_1}$, $\hat{\rho}_{22} \equiv \hat{\rho}_{a_2a_2}$, and Γ_1 and Γ_2 are the dephasing rate for single-photon coherence terms $\hat{\rho}_{1b}$ and $\hat{\rho}_{2b}$, respectively.

To proceed further we adopt certain approximation schemes. The first is the good cavity limit where the cavity damping rate is much smaller than the dephasing and spontaneous emission rates. In this limit, the cavity mode variables slowly varies than the atomic variables, and thus the atomic variables reach steady state in short time. The time derivatives of such variables can be set to zero keeping the cavity mode variables at time t, which is also called *adiabatic approximation*. Moreover, we apply linearization scheme which amounts to keeping terms up to second order in the

cavity-atom coupling constant, g in the master equation. To do so, we first write the equations of motion for $\hat{\rho}_{11}, \hat{\rho}_{22}, \hat{\rho}_{12}$, and $\hat{\rho}_{bb}$ in the zero order in the coupling constant:

$$\dot{\hat{\rho}}_{11} = r_a \rho_{11}^{(0)} \hat{\rho} + \frac{i\Omega}{2}(\exp^{-i\phi} \hat{\rho}_{21} - e^{i\phi}\hat{\rho}_{12}) - \gamma_1 \hat{\rho}_{11}, \tag{7.15}$$

$$\dot{\hat{\rho}}_{22} = r_a \rho_{22}^{(0)} \hat{\rho} + \frac{i\Omega}{2}(\exp^{i\phi} \hat{\rho}_{12} - e^{-i\phi}\hat{\rho}_{21}) - \gamma_2 \hat{\rho}_{22}, \tag{7.16}$$

$$\dot{\hat{\rho}}_{12} = r_a \rho_{12}^{(0)} \hat{\rho} + \frac{i\Omega}{2} \exp^{-i\phi}(\hat{\rho}_{22} - \hat{\rho}_{11}) - \Gamma_{12} \hat{\rho}_{12}, \tag{7.17}$$

$$\dot{\hat{\rho}}_{bb} = 0, \tag{7.18}$$

where γ_1 and γ_2 are spontaneous emission decay rates of levels $|a_1\rangle$ and $|a_2\rangle$ to lower level $|b\rangle$, respectively; Γ_{12} is the two-photon dephasing rate. Now we apply the adiabatic approximation, that is, we set the time derivatives in Eqs. (7.15)-(7.17) to zero to obtain

$$\hat{\rho}_{11} = \frac{r_a \hat{\rho}}{\chi}[\gamma_2(1-\eta)\Gamma_{12} + \Omega^2 + \gamma_2 \Omega \sqrt{1-\eta^2} \sin\phi], \tag{7.19}$$

$$\hat{\rho}_{22} = \frac{r_a \hat{\rho}}{\chi}[\gamma_1(1+\eta)\Gamma_{12} + \Omega^2 - \gamma_1 \Omega \sqrt{1-\eta^2} \sin\phi], \tag{7.20}$$

$$\begin{aligned} \hat{\rho}_{12} &= \frac{r_a \hat{\rho}}{2\Gamma_{12}\chi}\Big[\sqrt{1-\eta^2}(\chi \cos\phi - 2i\Gamma_{12}\gamma_1\gamma_2 \sin\phi) \\ &+ i\Gamma_{12}[\gamma_1 - \gamma_2 + (\gamma_1+\gamma_2)\eta]\Omega\Big] e^{-i\phi}, \end{aligned} \tag{7.21}$$

where

$$\chi = 2\gamma_1\gamma_2\Gamma_{12} + (\gamma_1+\gamma_2)\Omega^2. \tag{7.22}$$

We have introduced a useful notation to describe the initial condition with a single variable η such that $\rho_{11}^{(0)} = (1-\eta)/2$, $\rho_{22}^{(0)} = (1+\eta)/2$ and $|\rho_{12}^{(0)}| = \frac{1}{2}\sqrt{1-\eta^2}$. It is easy to see that $\rho_{12}^{(0)} = [0, 1/2]$ with 0 being no coherence and 1/2 corresponds to maximum coherence. In section 1, we will show that this coherence is responsible for entanglement between the cavity modes. Applying adiabatic approximation in Eqs.

(7.13) and (7.14) and using the solutions for $\hat{\rho}_{11}, \hat{\rho}_{22}, \hat{\rho}_{12}$, we obtain

$$-ig_1\hat{\rho}_{1b} = \zeta_{11}\hat{\rho}\hat{a}_1 + \zeta_{12}\hat{\rho}\hat{a}_2, \tag{7.23}$$

$$-ig_2\hat{\rho}_{2b} = \zeta_{22}\hat{\rho}\hat{a}_2 + \zeta_{21}\hat{\rho}\hat{a}_1, \tag{7.24}$$

where

$$\zeta_{11} = \frac{g_1^2 r_a}{\mathcal{D}}\Big\{\Gamma_{12}\Big[4\gamma_2\Gamma_{12}(\Gamma_2 + i\Delta_2)(1-\eta) + [\gamma_1 - \gamma_2 + 4\Gamma_2 + 4i\Delta_2 + (\gamma_1+\gamma_2)\eta]\Omega^2\Big] + \Omega\sqrt{1-\eta^2}\Big[i\chi\cos\phi + 2\gamma_2\Gamma_{12}(\gamma_1 + 2\Gamma_2 + 2i\Delta_2)\sin\phi\Big]\Big\}, \tag{7.25}$$

$$\zeta_{12} = \frac{2g_1g_2r_a}{\mathcal{D}}\Big\{i\Gamma_{12}\Omega\Big[-\gamma_2(\Gamma_2 + i\Delta_2)(1-\eta) + \gamma_1(\Gamma_2 + \Gamma_{12} + i\Delta_2)(1+\eta) + \Omega^2\Big] + \sqrt{1-\eta^2}\Big[(\Gamma_2 + i\Delta_2)\chi\cos\phi + i\gamma_1\Gamma_{12}(2\gamma_2\Gamma_2 + 2i\gamma_2\Delta_2 - \Omega^2)\sin\phi\Big]\Big\}, \tag{7.26}$$

$$\zeta_{21} = \frac{2g_1g_2r_a}{\mathcal{D}}\Big\{i\Gamma_{12}\Omega\Big[-\gamma_1(\Gamma_1 + i\Delta_1)(1+\eta) + \gamma_2(\Gamma_1 + \Gamma_{12} + i\Delta_1)(1-\eta) + \Omega^2\Big] + \sqrt{1-\eta^2}\Big[(\Gamma_1 + i\Delta_1)\chi\cos\phi - i\gamma_2\Gamma_{12}(2\gamma_1\Gamma_1 + 2i\gamma_1\Delta_1 - \Omega^2)\sin\phi\Big]\Big\}, \tag{7.27}$$

$$\zeta_{22} = \frac{g_2^2 r_a}{\mathcal{D}}\Big\{\Gamma_{12}\Big[4\gamma_1\Gamma_{12}(\Gamma_1 + i\Delta_1)(1+\eta) + [\gamma_2 - \gamma_1 + 4\Gamma_1 + 4i\Delta_1 - (\gamma_1+\gamma_2)\eta]\Omega^2\Big] + \Omega\sqrt{1-\eta^2}\Big[i\chi\cos\phi - 2\gamma_1\Gamma_{12}(\gamma_2 + 2\Gamma_1 + 2i\Delta_1)\sin\phi\Big]\Big\}, \tag{7.28}$$

where

$$\mathcal{D} = \Gamma_{12}\chi[4(\Gamma_1 + i\Delta_1)(\Gamma_2 + i\Delta_2) + \Omega^2], \tag{7.29}$$

$$\chi = 2\gamma_1\gamma_2\Gamma_{12} + (\gamma_1 + \gamma_2)\Omega^2. \tag{7.30}$$

Therefore, using Eqs. (7.23), (7.24), and (7.11), the master equation for the cavity radiation, taking into account the damping of cavity modes by vacuum reservoir,

becomes

$$\begin{aligned}\dot{\hat{\rho}} &= \zeta_{11}^{*}(\hat{a}_1^{\dagger}\hat{\rho}\hat{a}_1 - \hat{a}_1\hat{a}_1^{\dagger}\hat{\rho}) + \zeta_{11}(\hat{a}_1^{\dagger}\hat{\rho}\hat{a}_1 - \hat{\rho}\hat{a}_1\hat{a}_1^{\dagger}) \\ &+ \zeta_{22}^{*}(\hat{a}_2^{\dagger}\hat{\rho}\hat{a}_2 - \hat{a}_2\hat{a}_2^{\dagger}\hat{\rho}) + \zeta_{22}(\hat{a}_2^{\dagger}\hat{\rho}\hat{a}_2 - \hat{\rho}\hat{a}_2\hat{a}_2^{\dagger}) \\ &+ [\zeta_{21}^{*}(\hat{a}_1^{\dagger}\hat{\rho}\hat{a}_2 - \hat{a}_1^{\dagger}\hat{a}_2\hat{\rho}) + \zeta_{12}(\hat{a}_1^{\dagger}\hat{\rho}\hat{a}_2 - \hat{\rho}\hat{a}_1^{\dagger}\hat{a}_2)]e^{-i\phi} \\ &+ [\zeta_{12}^{*}(\hat{a}_2^{\dagger}\hat{\rho}\hat{a}_1 - \hat{a}_1\hat{a}_2^{\dagger}\hat{\rho}) + \zeta_{21}(\hat{a}_2^{\dagger}\hat{\rho}\hat{a}_1 - \hat{\rho}\hat{a}_1\hat{a}_2^{\dagger})]e^{i\phi} \\ &+ \sum_{j=1}^{2}\frac{\kappa_j}{2}(2\hat{a}_j\hat{\rho}\hat{a}_j^{\dagger} - \hat{a}_j^{\dagger}\hat{a}_j\hat{\rho} - \hat{\rho}\hat{a}_j^{\dagger}\hat{a}_j), \end{aligned} \tag{7.31}$$

where k_j is the damping rate of the jth cavity mode. The terms proportional to ζ_{11} and ζ_{22} represent gain for cavity mode 1 and mode 2, respectively whereas terms proportional to ζ_{12} and ζ_{21}^{*} are phase sensitive and are due to atomic coherence.

C. Entanglement of cavity modes

We analyze the entanglement properties of the cavity field when the coherence is induced by initial coherent superposition of atoms. In general, criteria proposed to detect bipartite entanglement rely on the nature of the field, whether field exhibit Gaussian statistics or not, and the form of the entanglement created. For instance, in three-level QBL, since there are two possible pathways for an atom in coherent superposition of the upper two levels to decay to the lower level $|b\rangle$ the entanglement created in our system is of the form: $\alpha|0_1 1_2\rangle + \beta|1_1 0_2\rangle$. Such type of entanglement can only be detected by certain class of inseparability criteria [148, 149, 150]. In order to detect entanglement between the cavity modes, we employ Hillery-Zubairy (HZ) entanglement criterion [148], which is sufficient test for two mode non-Gaussian states. This criterion relies on a combination of second-and fourth-order correlations among the cavity mode variables. According to this criterion, the two modes are

entangled if the following inequality is satisfied

$$E_{\rm HZ} \equiv \langle \hat{n}_1 \hat{n}_2 \rangle - |\langle \hat{a}_1^\dagger \hat{a}_2 \rangle|^2 < 0. \tag{7.32}$$

where $\hat{n}_1 = \hat{a}_1^\dagger \hat{a}_1$ and $\hat{n}_2 = \hat{a}_2^\dagger \hat{a}_2$ are photon number operators for the cavity modes.

1. Entanglement via injected coherence

In order to clearly see the contribution of the injected coherence in creating entanglement between the cavity modes, we switch off the driving field ($\Omega = 0$). The master equation corresponding to the injected coherence obtained by setting $\Omega = 0$ in the coefficients ζ_{ij} in Eq. (7.31) reads

$$\begin{aligned}
\dot{\hat{\rho}} &= \alpha_{11}^*(\hat{a}_1^\dagger \hat{\rho} \hat{a}_1 - \hat{a}_1 \hat{a}_1^\dagger \hat{\rho}) + \alpha_{11}(\hat{a}_1^\dagger \hat{\rho} \hat{a}_1 - \hat{\rho} \hat{a}_1 \hat{a}_1^\dagger) \\
&+ \alpha_{22}^*(\hat{a}_2^\dagger \hat{\rho} \hat{a}_2 - \hat{a}_2 \hat{a}_2^\dagger \hat{\rho}) + \alpha_{22}(\hat{a}_2^\dagger \hat{\rho} \hat{a}_2 - \hat{\rho} \hat{a}_2 \hat{a}_2^\dagger) \\
&+ [\alpha_{21}^*(\hat{a}_1^\dagger \hat{\rho} \hat{a}_2 - \hat{a}_1^\dagger \hat{a}_2 \hat{\rho}) + \alpha_{12}(\hat{a}_1^\dagger \hat{\rho} \hat{a}_2 - \hat{\rho} \hat{a}_1^\dagger \hat{a}_2)] e^{-i\phi} \\
&+ [\alpha_{12}^*(\hat{a}_2^\dagger \hat{\rho} \hat{a}_1 - \hat{a}_1 \hat{a}_2^\dagger \hat{\rho}) + \beta_{21}(\hat{a}_2^\dagger \hat{\rho} \hat{a}_1 - \hat{\rho} \hat{a}_1 \hat{a}_2^\dagger)] e^{i\phi} \\
&+ \sum_{j=1}^{2} \frac{\kappa_j}{2}(2\hat{a}_j \hat{\rho} \hat{a}_j^\dagger - \hat{a}_j^\dagger \hat{a}_j \hat{\rho} - \hat{\rho} \hat{a}_j^\dagger \hat{a}_j),
\end{aligned} \tag{7.33}$$

where

$$\alpha_{11} = \frac{g_1^2 r_a \Gamma_{12} \gamma_2 (1+\eta)}{(\Gamma_1 + i\Delta_1)\chi}, \tag{7.34}$$

$$\alpha_{12} = \frac{g_1 g_2 r_a \sqrt{1-\eta^2}(\chi \cos\phi + 2i\gamma_1 \Gamma_{12} \gamma_2 \sin\phi)}{2\Gamma_{12}(\Gamma_1 + i\Delta_1)\chi}, \tag{7.35}$$

$$\alpha_{21} = \frac{g_1 g_2 r_a \sqrt{1-\eta^2}(\chi \cos\phi - 2i\gamma_2 \Gamma_{12} \gamma_1 \sin\phi)}{2\Gamma_{12}(\Gamma_2 + i\Delta_2)\chi}, \tag{7.36}$$

$$\alpha_{22} = \frac{g_2^2 r_a \Gamma_{12} \gamma_1 (1-\eta)}{(\Gamma_2 + i\Delta_2)\chi}. \tag{7.37}$$

It is worth to note that when atoms are pumped into the cavity in state $|a_1\rangle$ or $|a_2\rangle$, i.e., when $\eta = \pm 1$ the off diagonal terms α_{12} and α_{21} vanishes. This implies that the

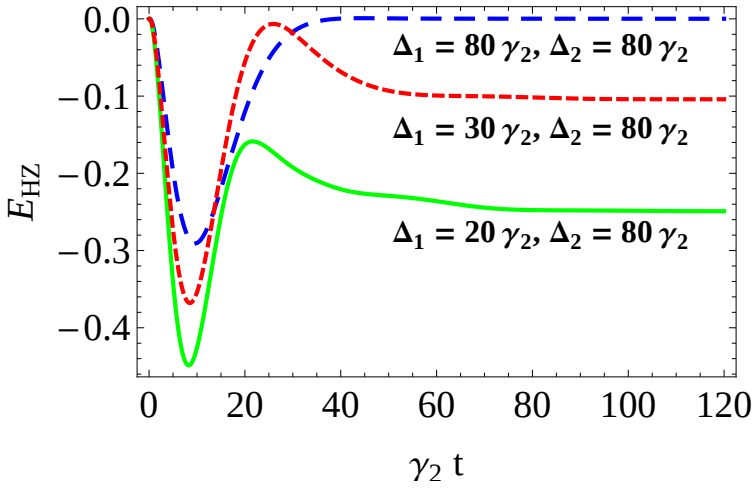

Fig. 45. Plots of E_{HZ} versus $\gamma_2 t$ for $g_1 = 50$kHz, $g_2 = 43$kHz, $r_a = 22$kHz, $\gamma_1 = 25$kHz, $\gamma_2 = 20$kHz, $\kappa_1 = 1.5$kHz, $\kappa_2 = 2$kHz, $\Gamma_{12} = \Gamma_1 = \Gamma_2 = \gamma_1$ (no dephasing condition), $\phi = \pi/2$ in the absence of the driving field ($\Omega = 0$) and when cavity mode 1 is initially in number state with 5 photons and mode 2 in vacuum state and for $\eta = 0$ (maximum injected coherence) and for various values of detunings.

cross correlation terms in the master equation disappear and results in disentanglement of the cavity modes.

a. Transient regime

Since the HZ criterion involves forth-order correlation and many coupled differential equations, obtaining analytical solutions is rather an involved problem. We thus present the results of our numerical simulations. We begin by investigating the dependence of the entanglement on the detuning. Figure 45 illustrates the HZ criterion as a function of dimensionless time $\gamma_2 t$ for various values of detunings Δ_1 and Δ_2. Here other parameters are chosen so as to comply with the micromaser experiments [143, 144]. We assume that the cavity modes are initially in a prod-

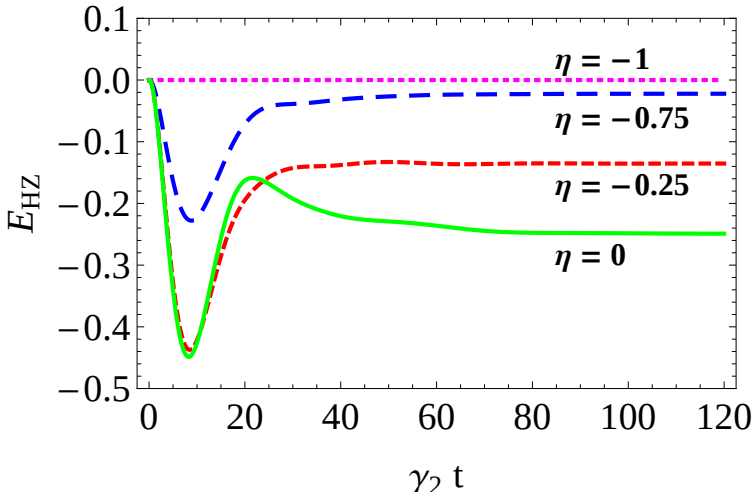

Fig. 46. Plots of E_{HZ} versus $\gamma_2 t$ for $\Delta_1 = 20\gamma_2, \Delta_2 = 80\gamma_2$ and for various initial conditions for the atoms (various values of η). All other parameters are the same as in Fig. 45.

uct state: cavity mode 1 in number state with 5 photons and mode 2 in a vacuum state, i.e., $|\Psi(0)\rangle_F = |5_1 0_2\rangle$ and atoms are injected into the cavity in a state $|\Psi(0)\rangle_A = \frac{1}{2}(|a_1\rangle + |a_2\rangle)$ or $\eta = 0$. As can be seen from Fig. 45, the quantity E_{HZ} is negative for short time for all cases indicating creation of entanglement between the cavity modes in the transient regime. We also observe that the transient entanglement vanishes at longer time scale for identical detunings $\Delta_1 = \Delta_2 = 80\gamma_2$. However, steady-state entanglement is obtained when the cavity detunings are different. This is quite interesting and markedly different from the result reported when one induces the coherence via strong laser field [133, 145, 146]. We thus note that in order to create a steady-state entanglement, which is more attractive and robust for quantum information processing protocols, one should induce coherence by initially preparing atoms in a coherent superpositions states.

Next, we explore how the initial populations and coherences influence the entan-

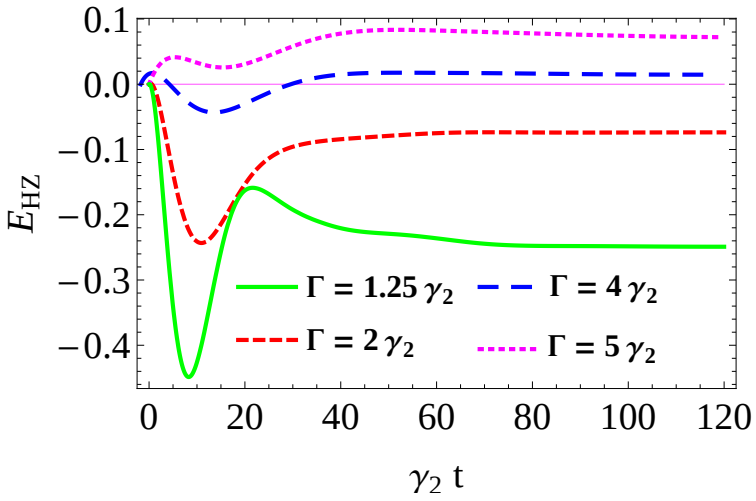

Fig. 47. Plots of E_{HZ} versus $\gamma_2 t$ for $\Delta_1 = 20\gamma_2, \Delta_2 = 80\gamma_2, \eta = 0$ and for various values of dephasing rates $\Gamma \equiv \Gamma_1 = \Gamma_2 = \Gamma_{12}$. All other parameters are the same as in Fig. 45.

glement dynamics. Figure 46 shows the plot of E_{HZ} versus $\gamma_2 t$ for fixed detunings: $\Delta_1 = 20\gamma_2$ and $\Delta_2 = 80\gamma_2$ and for various values of η. Recall that $\eta = \pm 1$ corresponds to no coherence whereas other values of η gives non zero coherence. Figure 46 reveals that whenever there is coherence, the system exhibit transient as well as steady state entanglement. Moreover, as the coherence decreases from maximum value $\eta = 0$ to no coherence $\eta = -1$ the quantity E_{HZ} approaches to zero faster. That means for weak coherence the generated entanglement is more susceptible to dephasing processes.

So far we have assumed no dephasing in the system, that is, the dephasing rate is the same as the spontaneous emission rate $\Gamma = \gamma_2$. However, the dephasing rates are in general higher than the spontaneous emission and cavity decay rates and may alter the entanglement behavior substantially. The dephasing rates Γ_1 and Γ_2 corresponding to the single-photon lasing transitions $|a_1\rangle \leftrightarrow |b\rangle$ and $|a_2\rangle \leftrightarrow |b\rangle$ are, in general, smaller than the two-photon dephasing rate Γ_{12}. We, however, assume,

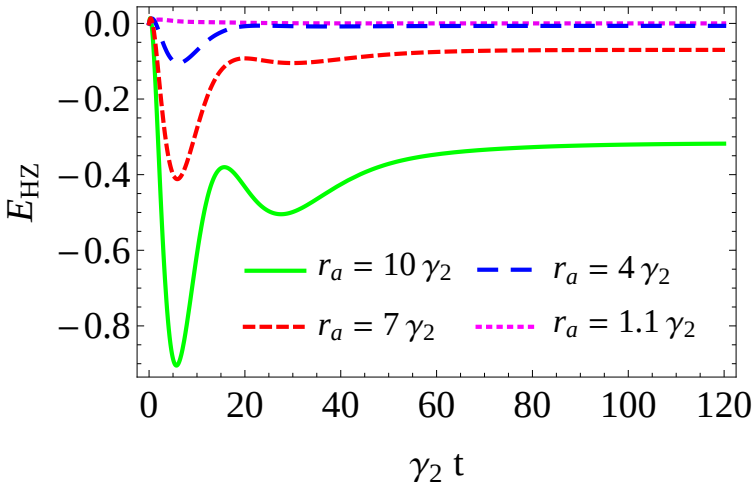

Fig. 48. Plots of E_{HZ} for $g_1 = 5\gamma_2, g_2 = 2.15\gamma_2, \gamma_1 = 1.25\gamma_2, \Gamma_{12} = \Gamma_1 = \Gamma_2 = 5\gamma_2$, $\Delta_1 = 500\gamma_2, \Delta_2 = 100\gamma_2, \kappa_1 = 0.2\gamma_2, \kappa_2 = 0.075\gamma_2, \eta = 0, \phi = \pi/2$, $\gamma_2 = 20$kHz, in the absence of the driving field ($\Omega = 0$) and for various values of the pumping rate r_a. The initial condition for the cavity field is the same as in Fig. 45.

for the sake of simplicity, all dephasing rates to be the same, $\Gamma = \Gamma_{12} = \Gamma_1 = \Gamma_2$. Now keeping the initial atomic coherence at maximum value ($\eta = 0$), we explore the effect of dephasing on the dynamics of the entanglement in the system. Figure 47 shows the plots of E_{HZ} versus $\gamma_2 t$ for $\Delta_1 = 20\gamma_2, \Delta_2 = 80\gamma_2$, and for various values of dephasing rate. This figure indicates that the entanglement is sensitive to dephasing. For instance, when the dephasing rate is increased to $\Gamma = 4\gamma_2$, only the transient entanglement survives. When one further increases the dephasing rate to $\Gamma = 5\gamma_2$ the entanglement condition is no longer satisfied. To keep the entanglement intact even in the presence of dephasing one can, in principle, tune other system parameters. To produce a robust steady state entanglement one has to choose a parameter range for which the system operates in large detuning condition. In Fig. 48, we plot E_{HZ} versus $\gamma_2 t$ for $g_1 = 5\gamma_2, g_2 = 2.15\gamma_2, \Gamma = \Gamma_{12} = \Gamma_1 = \Gamma_2 = 5\Gamma_2$,

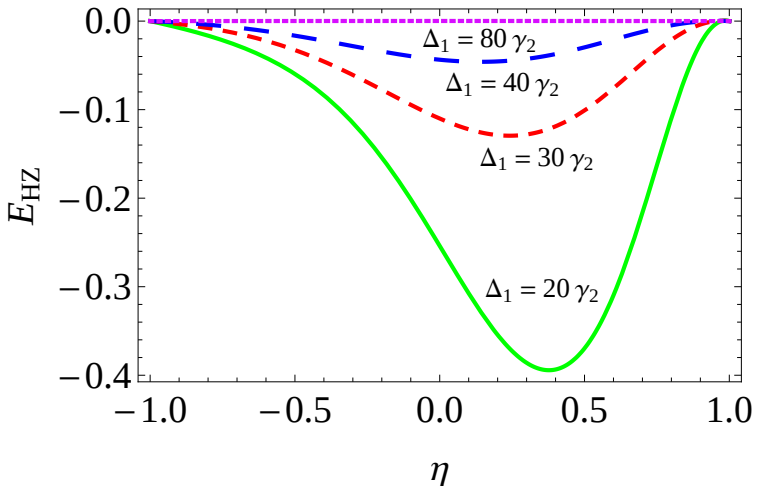

Fig. 49. Plots of E_{HZ} in the steady state versus η for $\Delta_2 = 80\gamma_2$ and for various values of Δ_1. All other parameters as the same as in Fig. 45.

$\gamma_1 = 1.25\gamma_2, \Delta_1 = 500\gamma_2, \Delta_2 = 100\gamma_2$, $\eta = 0$, and for various values of pumping rate r_a. As can be seen from this figure, for $r_a = 1.1\gamma_2$ the quantity E_{HZ} is always positive. However, if one gradually increases the pumping rate, the system starts to exhibit transient entanglement for short times. Steady-state entanglement can also be obtained by further increasing the pumping rate of the atoms into the cavity. It is noteworthy to mention here that since the pumping rate is externally controllable, it is experimentally feasible to control the effect of dephasing on the entanglement at least for dephasing rates as high as $\Gamma = 5\gamma_2$. In essence, the adverse effect of dephasing can be counterbalanced by tuning the pumping rate accordingly.

b. Steady state regime

As pointed out in the previous section, the cavity radiation exhibits steady-state entanglement. We here explore the entanglement as a function of system parameters and effect of dephasing. Analytical solution for this case is also non-trivial; we thus

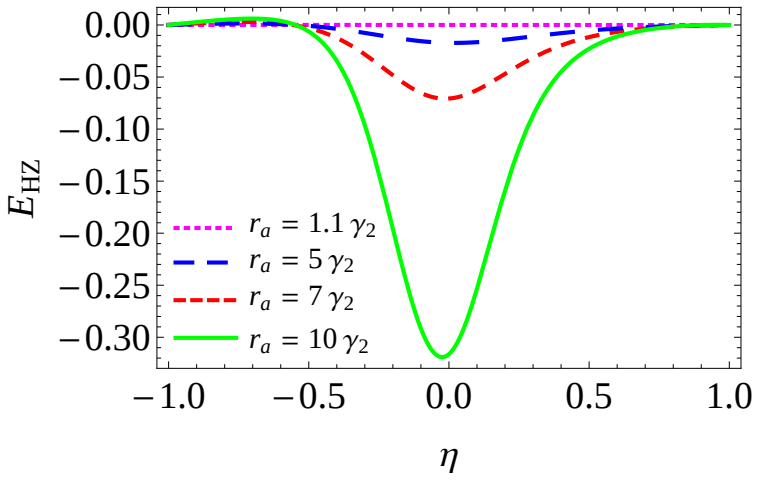

Fig. 50. Plots of E_{HZ} in the steady state versus η for dephasing rate $\Gamma = 5\gamma_2$ and for various values of pumping rates . All other parameters as the same as in Fig. 48.

solve the coupled equation and evaluate the function E_{HZ} numerically. In order to see the entanglement behavior as a function of the initial coherence, we then plot E_{HZ} as a function of η (see Fig. 49). This figure reveals that the cavity radiation exhibits steady-state entanglement for all values of η but, $\eta = \pm 1$, which confirms our previous assertion. We also observe that the entanglement exists only when the two cavity detunings are different. For example, for $\Delta_1 = \Delta_2 = 80\gamma_2$, no entanglement observed. Besides, it is counterintuitive to see that the minima for the E_{HZ} function does not occur at maximum initial coherence, $\eta = 0$. They rather appear for values of η between 0 and 0.5, depending on the value of the detuning Δ_1. It appears that, for this range of detunings, robust steady-state entanglement can be obtained by initially injecting more atoms in the level $|a_2\rangle$ than $|a_1\rangle$.

To clearly see the effect of dephasing on steady state entanglement, we plot in Fig. 50, the HZ criterion as a function of η for dephasing rate $\Gamma = 5\gamma_2$, $\Delta_1 = 500\gamma_2, \Delta_2 = 100\gamma_2$ and other parameters the same as in Fig. 48. As can be seen from this figure,

by increasing the pumping rates, one can counterbalance the dephasing effect. This however only works for strong coherence condition, that is when $\eta \approx [-0.5, 0.5]$. We also note that the entanglement is relatively robust at maximum coherence $\eta = 0$. We thus note that when the system is far detuned and at higher pumping rates only strong initial coherence can create entanglement that is robust against decoherence.

2. Entanglement via driven coherence

In this section the role of dephasing on entanglement dynamics when the atomic coherence is induced by coupling of the upper two levels by external laser is investigated. We assume that atoms are injected in their excited state $|a_1\rangle$, i.e., no coherence at the initial time. The evolution of entanglement in quantum-beat laser when coherence is induced by strong laser field has been previously considered without taking into account the dephasing process [133, 145, 146]. Here we focus on how the generated entanglement is modified by the dephasing rate.

The master equation corresponding to driven coherence and when atoms injected into the cavity at level $|a_1\rangle$ can be obtained by setting $\eta = -1$ in Eqs. (7.31). This yields

$$\begin{aligned}
\dot{\hat{\rho}} &= \beta_{11}^{*}(\hat{a}_1^{\dagger}\hat{\rho}\hat{a}_1 - \hat{a}_1\hat{a}_1^{\dagger}\hat{\rho}) + \beta_{11}(\hat{a}_1^{\dagger}\hat{\rho}\hat{a}_1 - \hat{\rho}\hat{a}_1\hat{a}_1^{\dagger}) \\
&+ \beta_{22}^{*}(\hat{a}_2^{\dagger}\hat{\rho}\hat{a}_2 - \hat{a}_2\hat{a}_2^{\dagger}\hat{\rho}) + \beta_{22}(\hat{a}_2^{\dagger}\hat{\rho}\hat{a}_2 - \hat{\rho}\hat{a}_2\hat{a}_2^{\dagger}) \\
&+ [\beta_{21}^{*}(\hat{a}_1^{\dagger}\hat{\rho}\hat{a}_2 - \hat{a}_1^{\dagger}\hat{a}_2\hat{\rho}) + \beta_{12}(\hat{a}_1^{\dagger}\hat{\rho}\hat{a}_2 - \hat{\rho}\hat{a}_1^{\dagger}\hat{a}_2)]e^{-i\phi} \\
&+ [\beta_{12}^{*}(\hat{a}_2^{\dagger}\hat{\rho}\hat{a}_1 - \hat{a}_1\hat{a}_2^{\dagger}\hat{\rho}) + \beta_{21}(\hat{a}_2^{\dagger}\hat{\rho}\hat{a}_1 - \hat{\rho}\hat{a}_1\hat{a}_2^{\dagger})]e^{i\phi} \\
&+ \sum_{j=1}^{2}\frac{\kappa_j}{2}(2\hat{a}_j\hat{\rho}\hat{a}_j^{\dagger} - \hat{a}_j^{\dagger}\hat{a}_j\hat{\rho} - \hat{\rho}\hat{a}_j^{\dagger}\hat{a}_j),
\end{aligned} \tag{7.38}$$

where

$$\beta_{11} = \frac{2g_1^2 r_a}{\Upsilon}[4\gamma_2\Gamma_{12}(\Gamma_2 + i\Delta_2) + (-\gamma_2 + 4\Gamma_2 + 4i\Delta_2)\Omega^2], \tag{7.39}$$

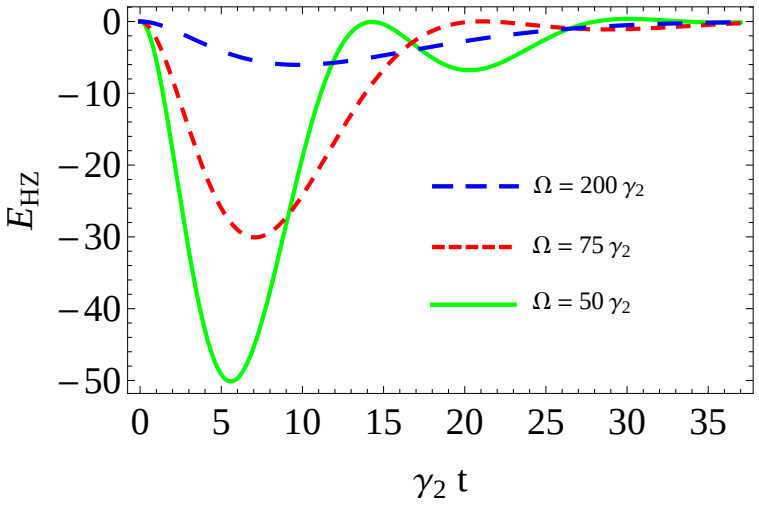

Fig. 51. Temporal behavior of E_{HZ} when the cavity modes are initially in a product state $|\Psi(0)\rangle = |25_1 0_2\rangle$ and when atoms are injected in their excited state $|a_1\rangle$ and for $\Delta_1 = \Delta_2 = 0$, $\Gamma = \gamma_2$. The curves correspond to various values of Rabi frequencies. All other parameters are the same as in Fig. 45.

$$\beta_{12} = \frac{2ig_1g_2r_a}{\Upsilon}[\Omega^2 - 2\gamma_2(\Gamma_2 + i\Delta_2)], \tag{7.40}$$

$$\beta_{21} = \frac{2ig_1g_2r_a}{\Upsilon}[\Omega^2 + 2\gamma_2(\Gamma_1 + \Gamma_{12} + i\Delta_1)], \tag{7.41}$$

$$\beta_{22} = \frac{2g_2^2r_a}{\Upsilon}[2\Gamma_1 + \gamma_2 + 2i\Delta_1]\Omega^2, \tag{7.42}$$

where

$$\Upsilon \equiv \chi[4(\Gamma_1 + i\Delta_1)(\Gamma_2 + i\Delta_2) + \Omega^2].$$

We note that this master equation has the same form as that of the injected coherence but, with different interpretation. When the driving laser field is switched off ($\Omega = 0$), the cross terms does not vanish. However, a close inspection of Eq. (7.42) shows that when we turn off the driving laser field, the gain for mode a_2 vanishes. This implies that population transfer from the initially populated level $|a_1\rangle$ to level $|a_2\rangle$ will not occur and hence no build up of coherence between these two levels. As analytical

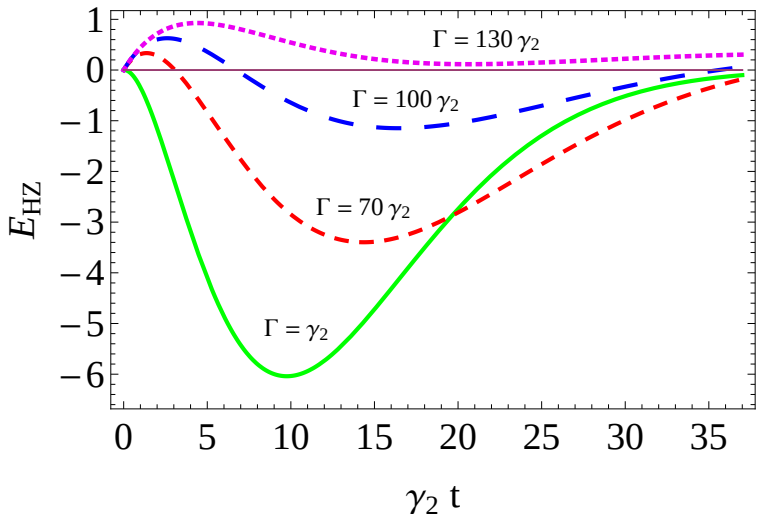

Fig. 52. Temporal behavior of E_{HZ} for laser field of Rabi frequency $\Omega = 200\gamma_2$. The curves correspond to various values of dephasing rates. All other parameters are the same as in Fig. 51.

solutions are rather nontrivial, we only present numerical results.

We consider an initial condition for the cavity field to be $|25_1 0_2\rangle$. In Fig. 51, we plot the E_{HZ} versus dimensionless time $\gamma_2 t$ when the cavity modes are tuned with their respective atomic transitions and for various values of the Rabi frequency of the laser field. This figure shows that an initially product state evolves to an entangled state even in the presence of cavity losses [145]. However, the time of entanglement is limited by the strength of the applied driving laser. This can be understood by recalling that the coherence, which is responsible for the creation of entanglement in this model, strongly relies on the strength of laser field. For this reason, the existence of entanglement crucially depends of the field strength.

Furthermore, a natural question that follows is how this transient entanglement behaves in the presence of dephasing. In Fig. 52, we present the effect of dephasing on dynamical behavior of entanglement for $\Omega = 200\gamma_2$, $\Delta_1 = \Delta_2 = 0$, and for various

values of the dephasing rate Γ. It is worth to note that the requirement of non zero detuning for having well-behaved solution is now relaxed due to the presence of a strong laser field. As illustrated in Fig. 52, in the presence of dephasing, the initial product state gets entangled after short time. However, when the dephasing rate increases, the two cavity modes remain disentangled for sometime and get entangled for a window of time before they become disentangled again. In addition, the time for which the modes remain entangled gets shorter with increasing dephasing rate. For parameters given in Fig. 52, the transient entanglement eventually vanishes when the dephasing rate becomes more than two order of magnitude stronger than the spontaneous emission rate. Furthermore, comparison of Figs. 48 and 52 shows that the entanglement generated via driven coherence is more robust against dephasing than that created via injected coherence. This might be explained in terms of the nature of the coherence induced by the two methods. It is clear that the coherence induced by the driving laser field is strong and controllable while the injected coherence is rather weak and fixed once the atoms are pumped into the cavity.

D. Conclusion

We have studied the effect of dephasing on the entanglement generated in a quantum-beat laser via quantum coherence induced either by initially preparing injected atoms in a coherent superposition of atomic levels or coupling the same levels by strong laser field. It turns out that the injected coherence give rise to transient as well as steady state entanglement for realistic parameters. The steady state entanglement only exists when the cavity detunings are different and relies strongly on the amount of detunings and pumping rates. Moreover, the entanglement is more sensitive to dephasing processes. We also show that the adverse effect of dephasing on the entan-

glement can be circumvented by injecting atoms into the cavity at higher pumping rates. On the other hand, the entanglement created through coherence induced by coupling of atomic levels by strong laser field is relatively robust against dephasing. The formulation outlined in this work will help better understand the inevitable effect of dephasing processes on quantum features exhibited by two-photon lasers.

CHAPTER VIII

SUMMARY

In summary we have studied quantum coherence effects and their applications in many quantum optical systems. In particular, we have considered lasing without inversion, cooperative spontaneous emission, and generation of quantum entanglement in discrete as well as continuous variable settings. Using the concept of cancelation of absorption via quantum interference we proposed lasing without inversion in the x-ray regime which otherwise is difficult to achieve under traditional lasing condition. We demonstrated transient Raman lasing at 58.4 nm in Helium gas and transient lasing without inversion at 6.1 nm in Helium-like Boron (triply ionized). As another application of quantum coherence, we considered cooperative spontaneous emission from large number of atoms initially prepared in a collective state and showed that even though one atom is excited from out of the N atoms, the emission rate of such a system is enhanced by a factor N. The virtual processes that involves rapid emission and absorption of virtual photon appears to influence the dynamics of the one-atom excited state and lead to large infinite-free collective Lamb (frequency) shift as opposed to single-atom Lamb shift which otherwise involves cut-off to avoid infinities.

Furthermore, we have studied the effect of quantum interference induced by position-dependent excitation phase in protecting a rapid decay of entanglement in a two-qubit system. We showed that the coherence created between the symmetric and antisymmetric state protects the entanglement from decaying with an enhanced rate. We also propose a scheme to create entanglement between two spatially separated and initially uncoupled qubits via interaction with correlated photons in a cavity QED setup. In continuous-variable setting, we put forward a scheme based of microwave driven three-level quantum beat laser to generate robust bipartite entanglement be-

tween two modes of a cavity field and proposed application to phase-controlled quantum lithography. We also addressed the inevitable effect of decoherence in the same model and discussed the possibility of generating steady-state entanglement.

REFERENCES

[1] G. Alzetta, A. Gozzini, L. Moi, and G. Orriols, Nuovo Cimento B **36**, 5 (1976).

[2] R. M. Whitley and C. R. Stroud, Jr., Phys. Rev. A **14**, 1498 (1976).

[3] E. Arimondo and G. Orriols, Lett. Nuovo Cimento **17**, 333 (1976).

[4] O. Kocharovskaya and Ya. I. Khanin, JETP Lett. **48**, 581 (1988).

[5] S. E. Harris, Phys. Rev. Lett. **62**, 1033 (1989).

[6] M. O. Scully, S. -Y. Zhu, and A. Gavrielides, Phys. Rev. Lett. **62**, 2813 (1989).

[7] R. Dicke, Phys. Rev. **93**, 99 (1954).

[8] R. Horodecki, P. Horodecki, M. Horodecki, and K.Horodecki, Rev. Mod. Phys. **81**, 865 (2009).

[9] H. Xiong, M. O. Scully, and M. S. Zubairy, Phys. Rev. Lett. **94**, 023601 (2005).

[10] E. Alebachew, Phys. Rev. A **76**, 023808 (2007).

[11] M. O. Scully, E. S. Fry, C. H. Raymond Ooi, and K. Wodkiewicz, Phys. Rev. Lett. **96**, 010501 (2006).

[12] M. O. Scully, Laser Phys. **17**, 635 (2007).

[13] M. O. Scully, Phys. Rev. Lett. **102**, 143601 (2009).

[14] A. A. Svidzinsky and M. O. Scully, Opt. Commun. **282**, 2894 (2009).

[15] E. A. Sete, A. A. Svidzinsky, H. Eleuch, Z. Yang, R. D. Nevels, and M. O. Scully, J. Mod. Opt. **57**, 1311 (2010).

[16] Z. Ficek and S. Swain, J. Mod. Opt. **49**, 3 (2002).

[17] E. A. Sete and S. Das, Phys. Rev. A **83**, 042301 (2011).

[18] T. Jennewein, C. Simon, G. Weihs, H. Weinfurter, and A. Zeilinger, Phys. Rev. Lett. **84**, 4729 (2000).

[19] T. S. -Manderbach, H. Weier, M. Fürst, R. Ursin, F. Tiefenbacher, Th. Scheidl, J. Perdigues, Z. Sodnik, J. G. Rarity, A. Zeilinger, and H. Weinfurter, Phys. Rev. Lett. **98**, 010504 (2007).

[20] M. O. Scully and M. S. Zubairy, *Quantum Optics* (Cambriage University Press, Cambridge, 1997).

[21] F. A. Hopf, P. Meystre, M. O. Scully, and J. F. Seely, Phys. Rev. Lett. **35**, 511 (1975).

[22] R. Bonifacio, F. A. Hopf, P. Meystre, and M. O. Scully, Phys. Rev. A. **12**, 2568 (1975).

[23] F. A. Hopf and M.O. Scully, Phys. Rev. **179**, 399 (1969).

[24] V. Kocharovsky, S. Cameron, K. Lehmann, R. Lucht, R. Miles, Y. Rostovtsev, W. Warren, G. R. Welch, and M. O. Scully, Proc. Natl. Acad. Sci. U.S.A. **102**, 7806 (2005).

[25] A. S. Zibrov, M. D. Lukin, D. E. Nikonov, L. Hollberg, M. O. Scully, V. L. Velichansky, and H. G. Robinson, Phys. Rev. Lett. **75**, 1499 (1995).

[26] G. Padmabandu, G. R. Welch, Ivan N. Shubin, E. S. Fry, D. E. Nikonov, M. D. Lukin, and M. O. Scully, Phys. Rev. Lett. **76**, 2053 (1996).

[27] S. -Y. Zhu, D. E. Nikonov, and M. O. Scully, Found. of Phys. **28**, 611 (1998).

[28] D. Braunstein and R. Shuker, Phys. Rev. A **68**, 013812 (2003).

[29] S. E. Harris and J. J. Macklin, Phys. Rev. A **40**, 4135 (1989).

[30] M. O. Scully, in *Advances in multi-photon processes and spectroscopy*, proceedings of the US-Japan Workshop, Honolulu, USA, edited by R. J. Gordon and Y. Fujimura (Wolrd Scientific, Singapore, 1999), vol. 14, p. 126.

[31] S. Ya. Kilin, K. T. Kapale, and M. O. Scully, Phys. Rev. Lett. **100**, 173601 (2008).

[32] E. A. Sete, A. A. Svidzinsky, Y. V. Rostovtsev, H. Eleuch, P. K. Jha, S. Suckewer, and M. O. Scully, IEEE J. Sel. Top. Quantum Electron. **18**, 541 (2012).

[33] G. W. F. Drake and D. C. Morton, ApJSS **170**, 251 (2007).

[34] L. V. Keldysh, Soviet Phys. JETP **20**, 1307 (1965).

[35] N. H. Burnett and P. B. Corkum, J. Opt. Soc. Am. B **6**, 1195 (1989).

[36] Y. Avitzour, S. Suckewer, and E. Valeo, Phys. Rev. E **69**, 046409 (2004).

[37] Y. Avitzour and S. Suckewer, JOSA B **24**, 819 (2007).

[38] K. Bergmann, H. Theuer, and B. W. Shore, Rev. Mod. Phys. **70**, 1003 (1998).

[39] S. -Y. Zhu, D. E. Nikonov, and M. O. Scully, Found. of Phys. **28**, 611 (1998).

[40] G. W. F. Drake, Phys. Rev. A **19**, 1387 (1979).

[41] W. R. Johnson, I. M. Savukov, U. I. Safronova, A. Dalgarno, and Argon, ApSS **141**, 543 (2002).

[42] J. J. Rocca, V. Shlyaptsev, F. G. Tomasel, O. D. Cortázar, D. Hartshorn, and J. L. A. Chilla, Phys. Rev. Lett. **73**, 2192 (1994).

[43] S. V. Milton *et al.*, Science **292**, 2037 (2001).

[44] B. E. Lemoff, G. Y. Yin, C. L. Gordon, C. P. J. Barty, and S. E. Harris, Phys. Rev. Lett. **74**, 1574 (1995).

[45] S. Suckewer, C. H. Skinner, H. Milchberg, C. Keane, and D. Voorhees, Phys. Rev. Lett. **55**, 1753 (1985).

[46] D. V. Korobkin, C. H. Nam, S. Suckewer, and A. Goltsov, Phys. Rev. Lett. **77**, 5206 (1996).

[47] Y. Nagata, K. Midorikawa, S. Kubodera, M. Obara, H. Tashiro, and K. Toyoda, Phys. Rev. Lett. **71**, 3774 (1993).

[48] K. M. Krushelnick, W. Tighe, and S. Suckewer, J. Opt. Soc. Am. B **13**, 306 (1996).

[49] R. H. Dicke, in *Proceeding of the Third International Congresss in Quantum Electronics, Paris, France, 1964*, edited by P. Grivet and N. Bloembergen (Columbia University Press, 1964), p. 35.

[50] N. E. Rehler and J. H. Eberly, Phys. Rev. A **3**, 1735 (1971).

[51] T. Chanelire, D. N. Matsukevich, S. D. Jenkins, S. -Y. Lan, T. A. B. Kennedy, and A. Kuzmich, Nature **438**, 833 (2005).

[52] A. Kuzmich, W. P. Bowen, A. D. Boozer, A. Boca, C. W. Chou, L. M. Duan, and H. J. Kimble, Nature **423**, 731 (2003).

[53] A. T. Black, J. K. Thompson, and V. Vuletic, Phys. Rev. Lett. **95**, 133601 (2005).

[54] A. A. Svidzinsky, J. T. Chang, and M. O. Scully, Phys. Rev. Lett. **100**, 160504 (2008).

[55] F. W. Cummings and A. Dorri, Phys. Rev. A **28**, 2282 (1983).

[56] F. W. Cummings, Phys. Rev. Lett. **54**, 2329 (1985).

[57] F. W. Cummings, Phys. Rev. A **33**, 1683 (1986).

[58] G. Benivegna and A. Messina, Phys. Lett. A **126**, 249 (1988).

[59] V. Buzek, G. Drobny, M. G. Kim, M. Havukainen, and P. L. Knight, Phys. Rev. A **60**, 582 (1999).

[60] V. Buzek, Phys. Rev. A **39**, 2232 (1989).

[61] A. A. Svidzinsky and J. -T. Chang, Phys. Rev. A **77**, 043833 (2008).

[62] R. Friedberg and J. Manassah, Phys. Lett. A **372**, 6833 (2008).

[63] R. H. Lehmberg, Phys. Rev. A **2**, 883 (1970).

[64] R. Friedberg, S. R. Hartmann, and J. T. Manassah, Phys. Lett. A **35**, 161 (1971).

[65] J. T. Manassah, Laser Phys. **19**, 2102 (2009).

[66] G. S. Agarwal, *Quantum Statistical Theories of Spontaneous Emission, Springer Tracts in Modern Physics* (Springer Verlag, Berlin, 1974), Vol. 70.

[67] U. Fano, Phys. Rev. **124**, 1866 (1961).

[68] W. E. Lamb, Jr. and R. C. Retherford, Phys. Rev. **72**, 241 (1947).

[69] S. E. Harris, J. E. Field, and A. Imamoglu, Phys. Rev. Lett. **64**, 1107 (1990).

[70] S. Longhi, Phys. Rev. Lett. **101**, 193902 (2008).

[71] A. Politi, M. J. Cryan, J. G. Rarity, S. Yu, and J. L. O'Brien, Science **320**, 646 (2008).

[72] J. C. F. Matthews, A. Politi, A. Stefanov, and J. L. O'Brien, Nat. Photon. **3**, 346 (2009).

[73] D. W. Berry and H. M. Wiseman, Nat. Photon. **3**, 317 (2009).

[74] E. A. Sete, Opt. Commun. **281**, 6124 (2008).

[75] M. Nielsen and I. Chuang, *Quantum Computation and Quantum Information* (Cambridge University Press, Cambridge, 2004).

[76] C. H. Bennett, G. Brassard, C. Crépeau, R. Jozsa, A. Peres, and W. K. Wootters, Phys. Rev. Lett. **70**, 1895 (1993).

[77] D. Bouwmeester, J. -W. Pan, K. Mattle, M. Eibl, H. Weinfurter, and A. Zeilinger, Nature **390**, 375 (1997).

[78] M. Riebe, H. Häffner, C. F. Roos, W. Hänsel, J. Benhelm, G. P. T. Lancaster, T. W. Körber, C. Becher, F. Schmidt-Kaler, D. F. V. James, and R. Blatt, Nature **429**, 734 (2004).

[79] M. D. Barrett, J. Chiaverini, T. Schaetz, J. Britton, W. M. Itano, J. D. Jost, E. Knill, C. Langer, D. Leibfried, R. Ozeri, and D. J. Wineland, Nature **429**, 737 (2004).

[80] S. Olmschenk, D. N. Matsukevich, P. Maunz, D. Hayes, L. -M. Duan and C. Monroe, Science **323**, 486 (2009).

[81] W. H. Zurek, Rev. Mod. Phys. **75**, 715 (2003).

[82] L. Diosi, *Irreversible Quantum Dynamics*, edited by F. Benatti and R. Floreanini (Springer, New York, 2003).

[83] S. Daffer, K. Wodkiewicz, and J. K. McIver, Phys. Rev. A **67**, 062312 (2003).

[84] R. Tanas and Z. Ficek, J. Opt. B **6**, S90 (2004).

[85] P. J. Dodd and J. J. Halliwell, Phys. Rev. A **69**, 052105 (2004).

[86] F. Mintert, A. R. R. Carvalho, M. Kus, and A. Buchleitner, Phys. Rep. **415**, 207 (2005).

[87] T. Yu and J. H. Eberly, Phys. Rev. Lett. **93**, 140404 (2004).

[88] Z. Ficek and R. Tanas, Phys. Rev. A **74**, 024304 (2006).

[89] S. Das and G. S. Agarwal, J. Phys. B. **42**, 205502 (2009).

[90] G. Schedelbeck, W. Wegscheider, M. Bichler and G. Abstreiter, Science **278**, 1792 (1997).

[91] J. R. Petta, A. C. Johnson, J. M. Taylor, E. A. Laird, A. Yacoby, M. D. Lukin, C. M. Marcus, M. P. Hanson, and A. C. Gossard, Science **309**, 2180 (2005).

[92] A. Barenco, D. Deutsch, A. Ekert, and R. Jozsa, Phys. Rev. Lett. **74**, 4083 (1995).

[93] C. H. Raymond Ooi, B. -G. Kim, and H. -W. Lee, Phys. Rev. A. **75**, 063801 (2007).

[94] S. Das, G. S. Agarwal, and M. O. Scully, Phys. Rev. Lett. **101**, 153601 (2008).

[95] S. -Y. Zhu and M. O. Scully, Phys. Rev. Lett. **76**, 388 (1996).

[96] P. Zhou and S. Swain, Phys. Rev. Lett. **77**, 3995 (1996).

[97] C. H. Keitel, Phys. Rev. Lett. **83**, 1307 (1999).

[98] R. Röhlsberger, K. Schlage, B. Sahoo, S. Couet, and R. Rüffer, Science **328**, 1248 (2010).

[99] W. K. Wootters, Phys. Rev. Lett. **80**, 2245 (1998).

[100] C. Thiel, J. von Zanthier, T. Bastin, E. Solano, and G. S. Agarwal, Phys. Rev. Lett. **99**, 193602 (2007).

[101] E. A. Stinaff, M. Scheibner, A. S. Bracker, I. V. Ponomarev, V. L. Korenev, M. E. Ware, M. F. Doty, T. L. Reinecke, and D. Gammon, Science **311**, 636 (2006).

[102] D. Loss and D. P. DiVincenzo, Phys. Rev. A **57**, 120 (1998).

[103] J. Clarke and F. K. Wilhelm, Nature **453**, 1031 (2008).

[104] B. Kraus and J. I. Cirac, Phys. Rev. Lett. **92**, 013602 (2004).

[105] C. Cabrillo, J. I. Cirac, P. García-Fernández, and P. Zoller, Phys. Rev. A **59**, 1025 (1999).

[106] A. Imamoglu, D. D. Awschalom, G. Burkard, D.P. DiVincenzo, D. Loss, M. Sherwin, and A. Small, Phys. Rev. Lett. **83**, 4204 (1999).

[107] M. Paternostro, G. Falci, M. Kim, and G. M. Palma, Phys. Rev. B **69**, 214502 (2004).

[108] A. Serani, M. Paternostro, M. S. Kim, and S. Bose, Phys. Rev. A**73**, 022312 (2006).

[109] E. del Valle, JOSA B **28**, 228 (2011).

[110] J. I. Cirac, Phys. Rev. A **46**, 4354 (1992).

[111] J. McKeever, J. R. Buck, A. D. Boozer, A. Kuzmich, H. -C. Nägerl, D. M. Stamper-Kurn, and H. J. Kimble, Phys. Rev. Lett. **90**, 133602 (2003).

[112] N. Ph. Georgiades, E. S. Polzik, K. Edamatsu, and H. J. Kimble, Phys. Rev. Lett. **75**, 3426 (1995).

[113] E. Alebachew, Opt. Commun. **280**, 133 (2007).

[114] H. -T. Tan, S. -Y. Zhu, and M. S. Zubairy, Phys. Rev. A **72**, 022305 (2005).

[115] A. Aspect, P. Grangier and G. Roger, Phys. Rev. Lett. **49**, 91 (1982).

[116] B. B. Blinov, D. L. Moehring, L. M. Duan, C. Monroe, Nature **428**, 153 (2004).

[117] J. Volz, M. Weber, D. Schlenk, W. Rosenfeld, J. Vrana, K. Saucke, C. Kurtsiefer, and H. Weinfurter, Phys. Rev. Lett. **96**, 030404 (2006).

[118] T. Wilk, S. C. Webster, A. Kuhn, G. Rempe, Science **317**, 488 (2008).

[119] Z. -S. Yuan, Y. -A. Chen, B. Zhao, S. Chen, J. Schmiedmayer, and J. -W. Pan, Nature **454**, 1098 (2008).

[120] D. Matsukevich, T. Chaneliere, M. Bhattacharya, S. -Y. Lan, S. D. Jenkins, T. A. B. Kennedy, and A. Kuzmich , Phys. Rev. Lett. **95**, 040405 (2005).

[121] T. Jennewein, C. Simon, G. Weihs, H. Weinfurter, and A. Zeilinger, Phys. Rev. Lett. **84**, 4729 (2000).

[122] S. L. Braunstein and H. J. Kimble, Phys. Rev. A **61**, 042302 (2000).

[123] A. N. Boto, P. Kok, D. S. Abrams, S. L. Braunstein, C. P. Williams, and J. P. Dowling, Phys. Rev. Lett. **85**, 2733 (2000).

[124] G. S. Agarwal, R. W. Boyd, E. M. Nagasako, and S. J. Bentley, Phys. Rev. Lett. **86**, 1389 (2001).

[125] M. D'Angelo, M. V. Chekhova, and Y. Shih, Phys. Rev. Lett. **87**, 013602 (2001).

[126] W. Bickel and S. Bashkin, Phys. Rev. **162**, 12 (1967).

[127] W. Chow, M. O. Scully, and J. Stoner, Phys. Rev. A **11**, 1380 (1975).

[128] R. M. Herman, H. Grotch, R. Kornblith, and J. H. Eberly, Phys. Rev. A **11**, 1389 (1975).

[129] M. O. Scully, Phys. Rev. Lett. **55**, 2802 (1985).

[130] M. O. Scully and M. S. Zubairy, Phys. Rev. A **35**, 752 (1987).

[131] U. W. Rathe and M. O. Scully, Phys. Rev. A **52**, 3193 (1995).

[132] S. Qamar, M. Al-Amri, S. Qamar, and M. S. Zubairy, Phys. Rev. A **80**, 033818 (2009).

[133] R. Tahira, M. Ikram, H. Nha, and M. S. Zubairy, Phys. Rev. A **83**, 054304 (2011).

[134] W. H. Louisell, *Quantum Statistical Properties of Radiation* (Wiley, New York, 1973).

[135] R. Simon, Phys. Rev. Lett. **84**, 2726 (2000).

[136] L. M. Duan, G. Giedke, J. I. Cirac, and P. Zoller, Phys. Rev. Lett. **84**, 2722 (2000).

[137] H. P. Yuen and H. H. Shapiro, IEEE Trans. Inf. Theor. **26**, 78 (1980).

[138] P. Kok, H. Lee, and J. P. Dowling Phys. Rev. A **65**, 052104 (2002).

[139] B. R. Mollow, Phys. Rev. **175**, 1555 (1968).

[140] M. Tsang, Phys. Rev. Lett. **102**, 253601 (2009).

[141] H. Shin, K. W. C. Chan, H. J. Chang, and R. W. Boyd, Phys. Rev. Lett. **107**, 083603 (2011).

[142] G. Raqithel, C. Wagner, H. Walther, L. M. Narducci, and M. O. Scully, in *Advances in Atomic Molecular and Optical Physics*, edited by P. Berman (Academic, New York, 1994), Supp. 2, p. 57.

[143] D. Meschede, H. Walther, and G. Muller, Phys. Rev. Lett. **54**, 551 (1985).

[144] J. M. Raimond, M. Brune, and S. Haroche, Rev. Mod. Phys.**73**, 565 (2001).

[145] S. Qamar, F. Ghafoor, M. Hillery, and M. S. Zubairy, Phys. Rev. A **77**, 062308 (2008).

[146] A. P. Fang, Y. L. Chen, F. L. Li, H. R. Li, and P. Zhang, Phys. Rev. A **81**, 012323 (2010).

[147] E. A. Sete, K. E. Dorfman, and J. P. Dowling, J. Phys. B: At. Mol. Opt. Phys. **44**, 225504 (2011).

[148] M. Hillery and M. S. Zubairy, Phys. Rev. A **74**, 032333 (2006).

[149] G. S. Agarwal and A. Biswas, New J. Phys. **7**, 211 (2005).

[150] H. Nha and J. Kim, Phys. Rev. A **74**, 012317 (2006).

[151] A. P. Throne, *Spectrophysics* (Chapman and Hall, London, 1988), p. 169.

[152] H. R. Griem, *Plasma Spectroscopy* (McGraw-Hill Book Co., NY, 1964), p.97.

[153] W. Lochte-Holtgreven, *Plasma Diagnostics* (North-Holland Publishing Co., Amsterdam, 1968), p. 144, 160, 124.

APPENDIX A

TOPICS RELATED TO CHAPTER II

LWI in Λ scheme for optically thin sample

For an optically thin sample the density of the medium may approximately be written as

$$\eta \simeq \alpha\delta(z), \tag{A.1}$$

where α is proportional to the absorption coefficient. Assuming that the off diagonal terms ρ_{ca} and ρ_{cb} are slowly varying function of retarded time $\mu = t - z/c$, we set $\frac{\partial}{\partial\mu}\rho_{ca} = 0$ and $\frac{\partial}{\partial\mu}\rho_{cb} = 0$. By doing so we obtain the corresponding steady state expressions:

$$\rho_{ca} = i\frac{\Omega\gamma_{bc}}{\gamma_{ac}\gamma_{bc} + |\Omega_l|^2}(\rho_{aa} - \rho_{bb}) + \frac{\Omega\Omega_l\rho_{ab}}{\gamma_{ac}\gamma_{bc} + |\Omega_l|^2}, \tag{A.2}$$

$$\rho_{cb} = i\frac{\Omega\gamma_{ac}}{\gamma_{ac}\gamma_{bc} + |\Omega_l|^2}\rho_{ab} + \frac{\Omega\Omega_l(\rho_{aa} - \rho_{bb})}{\gamma_{ac}\gamma_{bc} + |\Omega_l|^2}, \tag{A.3}$$

where $\gamma_{ac} = \gamma_{ab} = (\gamma + \Gamma)/2$. If we assume the fields to be real, then ρ_{ca} and ρ_{ab} will be pure imaginary numbers and ρ_{cb} real number. Thus on account of this and using the steady state expressions for ρ_{ca} and ρ_{cb}, we obtain

$$\frac{\partial}{\partial\mu}\rho_{cc} = \Gamma\rho_{cc} + \frac{2\Omega^2}{\gamma_{ac}}(\rho_{aa} - \rho_{cc}) + \frac{2\Omega^2\Omega_l}{\gamma_{ac}}\mathrm{Im}(\rho_{ab}), \tag{A.4a}$$

$$\frac{\partial}{\partial\mu}\rho_{aa} = -(\gamma + \Gamma)\rho_{aa} - \frac{2\Omega^2}{\gamma_{ac}}(\rho_{aa} - \rho_{cc}) + 2\Omega_l\frac{1 - \Omega^2}{\gamma_{ac}\gamma_{cb}}\mathrm{Im}(\rho_{ab}), \tag{A.4b}$$

$$\frac{\partial}{\partial\mu}\rho_{aa} = \gamma\rho_{bb} - 2\Omega_l\mathrm{Im}(\rho_{ab}), \tag{A.4c}$$

$$\frac{\partial}{\partial\mu}\mathrm{Im}(\rho_{ab}) = -\left(\gamma_{ab} + \frac{2\Omega^2}{\gamma_{cb}}\right)\mathrm{Im}(\rho_{ab}) + \Omega_l\left[\rho_{bb} - \rho_{aa} + \frac{\Omega^2(\rho_{aa} - \rho_{cc})}{\gamma_{ac}\gamma_{cb}}\right], \tag{A.4d}$$

where we have dropped higher order terms in Ω_l assuming the input field is very weak.

Further, we treat the driving field as a constant assuming it is strong and doesn't change appreciably during the time of interaction with the medium. To this end, we have only the wave equation for the lasing field:

$$\frac{\partial}{\partial z}\Omega_l = -\alpha\delta(z)\mathrm{Im}(\rho_{ab}). \tag{A.5}$$

The formal solution of Eq. (A.4d) has the form

$$\mathrm{Im}(\rho_{ab}) = \int_0^\mu d\mu' e^{-\Gamma_{ab}(\mu-\mu')}\Omega_l(z',\mu')\left(\rho_{bb} - \rho_{aa} + \frac{\Omega^2(\rho_{aa} - \rho_{cc})}{\gamma_{ac}\gamma_{cb}}\right), \tag{A.6}$$

where $\Gamma_{ab} = (\gamma_{ab} + \frac{2\Omega^2}{\gamma_{cb}})$. Substituting (A.6) into Eq. (A.5) and making use of (A.1), we get

$$\begin{aligned}\Omega_l(z,\mu) =& \Omega_l(0,\mu) - \alpha\int_0^\mu d\mu' \\ &\times \int_0^z dz'\delta(z')e^{-\Gamma_{ab}(\mu-\mu')}\Omega_l(z',\mu')\left(\tilde{\rho_{aa}}(z',\mu') - \tilde{\rho_{bb}}(z',\mu')\right),\end{aligned} \tag{A.7}$$

where

$$\begin{aligned}\tilde{\rho}_{aa} &= \rho_{aa} + \frac{\Omega^2}{\gamma_{ac}\gamma_{cb}}\rho_{cc}, \\ \tilde{\rho}_{bb} &= \rho_{bb} + \frac{\Omega^2}{\gamma_{ac}\gamma_{cb}}\rho_{aa}.\end{aligned}$$

Now performing the integration over z', we easily get

$$\Omega_l(z,\mu) = \Omega_l(0,\mu) - \alpha\int_0^\mu d\mu' e^{-\Gamma_{ab}(\mu-\mu')}\Omega_l(0,\mu')\left(\tilde{\rho}_{aa}(0,\mu') - \tilde{\rho}_{bb}(0,\mu')\right). \tag{A.8}$$

Taking a delta function input pulse say $\Omega_l(0,\mu) = \Omega_0\delta(\mu)$, one finds

$$\Omega_l(z,\mu) = \Omega_l(0,\mu) - \alpha\Omega_0 e^{-\Gamma_{ab}\mu}\left(\tilde{\rho}_{aa}(0,0) - \tilde{\rho}_{bb}(0,0)\right). \tag{A.9}$$

We immediately notice from Eq. (A.9) that amplification of the lasing field is possible when $\tilde{\rho}_{aa}(0,0) < \tilde{\rho}_{bb}(0,0)$. If the population is initially distributed between levels $|c\rangle$ and $|b\rangle$ then the condition for the amplification of the lasing field reads $\Omega^2\rho_{cc}(0)/\gamma_{ac}\gamma_{bc} < \rho_{bb}(0)$. Thus lasing in the $|a\rangle \rightarrow |b\rangle$ transition is possible in the absence of population inversion as well as Raman inversion.

Spectral line broadening in plasma

It is well known that broadening of spectral lines occurs mainly due to the interaction of the radiating atoms or ions with the surrounding particles and depends notably on pressure and temperature. There are various line-broadening mechanisms. In what follows we discuss the two major broadening mechanisms.

Doppler broadening

The motion of a radiating particle away or from an observer leads to a wavelength shift of the emitted line–also called the Doppler shift. At low density, besides natural broadening, Doppler broadening is always present and dominates the shapes near the line center. For example, in the case of thermal Doppler broadening where the velocity distribution is Maxwellian $P(v)dv = \sqrt{m/2\pi k_B T}\exp[-mv^2/2k_B T]dv$ the full width at half maximum (FWHM) is given by

$$\Delta\lambda_{\text{Doppler}} = \lambda\sqrt{\frac{(8\ln 2)k_B T}{mc^2}} \tag{A.10}$$

where λ is the wavelength of center of the absorption line (m), T is the temperature, k_B is the Boltzmann constant, m is mass of the atoms or ion, and c is the speed of light. Inspection of Eq. (A.10) shows that the thermal Doppler broadening is most pronounced for the lines of light elements at high temperature.

Pressure broadening

In dense plasma, however, natural and Doppler line broadenings are usually negligible. The line profiles emitted by atoms or ions, predominately depends on the interactions between the emitters and the surrounding particles. These interaction brings in frequency disturbance and phase shifts. This type of line broadening is generally called pressure broadening.

Pressure broadening theory was developed from two different point of views, which essentially are based on two extreme approximations–impact and quasi-static approximations. In impact approximation, the light emitted from an ion or an atom is momentarily perturbed by fast impacts, which disrupts completely the emission process. This effect depends on both the density and temperature of the gas. On other hand, in quasi-static approximation, the emitters are continuously under the influence of the perturbers during the whole emission process. Furthermore, the perturbing particles are assumed to move slowly during the time of emission that the perturbing field may be thought of as quasi-static. This effect is insensitive to temperature but depends on the density of the gas.

Pressure broadening of spectral lines emitted from a plasma can be subdivided based on range of interaction. In general the phase shift obeys the inverse power law $\Delta\omega = C/r^p$, where C is a constant and r is the distance of the perturber from the emitter.

- Linear Stark broadening, $p = 2$, occurs through the linear Stark effect which is a result of interaction of the emitter with an electric field. The change in frequency is linear in the electric field, i.e. $\Delta\omega \sim 1/r^2$. This types of shift occurs only in hydrogen due to degeneracy in l [151].

- Resonance broadening results due to the interaction between identical emitters

and has the form of dipole-dipole interaction, which introduces the possibility of an energy exchange, $\Delta\omega \sim 1/r^3$. Here the lines are symmetrically broadened but unshifted.

- Quadratic stark broadening, $p = 4$ occurs via quadratic Stark effect which results from interaction of an emitter with an electric field. The change in frequency is quadratic in electric field, that is, $\Delta\omega \sim 1/r^4$. All atoms or ions experience quadratic Stark effect except hydrogen. The formula given by Griem [152] were obtained in the impact approximation and also incorporated quasistatic line broadening due to ions. They can be used together with calculated parameters for several spectral lines to estimate the FWHM ($\Delta\lambda_{\text{Stark width}}$) and the line shift ($\Delta\lambda_{\text{Stark shift}}$) using the following formula [153]:

$$\Delta\lambda_{\text{Stark width}} = 2[1 + 5.53 \times 10^{-6} n_e^{1/4} \alpha (1 - 0.0068 n_e^{1/6} T^{-1/2})] 10^{-22} \text{w} n_e \quad \text{(A.11)}$$

$$\Delta\lambda_{\text{Stark shift}} = [d/\text{w} + 6.32 \times 10^{-6} n_e^{1/4} \alpha (1 - 0.0068 n_e^{1/6} T^{-1/2})] 10^{-22} \text{w} n_e, \quad \text{(A.12)}$$

where n_e is the electron number density in m^{-3}, w is the electron impact half width in m, d/w is the ratio of shift to width (dimensionless), T is the absolute temperature in K, and α is the ion broadening parameter. These empirical formulae are valid only for neutral or singely ionized atoms. All the parameters are given in Ref. [152] for different elements.

In plasmas with ions and electrons present in sufficiently high concentration–say at least one percent of the total density–the long range Coulomb forces are dominant and we are concerned with the quadratic Stark broadening.

For example, for electron density $n_e = 10^{16}\text{cm}^{-3}$, plasma temperature, $k_B T_e = 1eV$ the parameters that appears in Eqs. (A.13) and (A.14) for 1S to 2P transition in neutral Helium atom is given in Ref. [152] as: the electron broadening parameter $\alpha = 0.01$, electron impact width $w = 1.58 \times 10^{-14}\text{m}$, and shift $d = -5.67 \times 10^{-16}\text{m}$. Therefore, using these values the Stark width becomes $\Delta\lambda_{\text{Stark width}} = 3.2 \times 10^{-14}\text{m}$ which gives a width in frequency domain $\Delta\nu_{\text{Stark}} = c\Delta\lambda_{\text{Stark width}}/\lambda^2 = 2.9 \times 10^{9}\text{s}^{-1}$. The corresponding Stark shift is $\Delta\lambda_{\text{Stark shift}} = -3.8 \times 10^{-16}\text{m}$.

For multiply ionized atoms such as in our case, B^{3+} and C^{4+}, the collision rate can be calculated using the formula derived below.

Consider an electron moving with velocity v_e and an ion containing Z number of electrons. If b is the impact parameter, the collision time (the order of time that electron feels the Coulomb force) is given by

$$\Delta t \approx \frac{2b}{v_e}. \tag{A.13}$$

The Coulomb force that the electron experience is

$$F = m_e \frac{\Delta v_e}{\Delta t} = \frac{Ze^2}{4\pi\varepsilon_0 b^2} \tag{A.14}$$

and hence

$$\Delta v_e \approx \frac{Ze^2}{2\pi\varepsilon_0 b v_e m_e}. \tag{A.15}$$

In order to calculate the collision time we determine how fast Δv_e^2 changes in time. Note that the rate at which the electron encounters ions is $n_i \sigma v_e$ where n_i is the ion density, $d\sigma = 2\pi b db$ is the cross section. Thus the rate at which Δv_e^2 changes is given by

$$\frac{d}{dt}\langle \Delta v_e^2 \rangle = \int_{r_s}^{b_{max}} 2\pi n_i b v_e \Delta v_e^2 db$$
$$= \frac{n_i Z^2 e^4}{2\pi \varepsilon_0^2 m_e^2 v_e} \int_{r_s}^{b_{max}} \frac{db}{b}. \tag{A.16}$$

Obviously the size of the impact parameter is finite. The electron feels the action of the ions up to certain range due to the Debye shielding. Thus we take the upper limit for the integral to be the Debye length: $b_{max} = r_D = \sqrt{\varepsilon k_B T_e / n_e e^2}$. Care should also be taken when one takes the minimum value of the impact parameter. This simple way gives infinite change in velocity for the head-on collision ($b = 0$)–which is not the case. We rather expect the change in velocity to be $\sim v_e$. Equating the centripetal force with the Coulomb force one can find the lower limit of the integral to be $r_s = Ze^2/2\pi\varepsilon_0 m v_e^2$, which is the distance of closest approach.

Note that during the collision time, τ the change in velocity is of the order of the velocity, thus from (A.16) we have

$$\nu_{ei} = 1/\tau = \frac{n_i Z^2 e^4}{2\pi \varepsilon_0^2 m_e^2 v_e^3} \ln \Lambda, \tag{A.17}$$

where

$$\Lambda = r_D / r_s = \sqrt{\frac{\varepsilon_0 k_B T}{n_e e^2}} \frac{2\pi \varepsilon_0 m v_e^2}{Ze^2}. \tag{A.18}$$

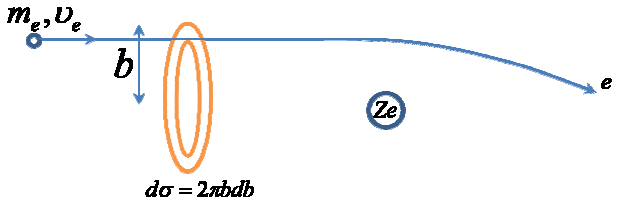

Fig. 53. Schematic of scattering of an electron by an ion containing Ze charge.

Table III. Spontaneous decay rates, and collision rates without external field and radiation wavelengths for B^{3+} and C^{4+}.

Ion	Z	$\Gamma(s^{-1})$	$\gamma(s^{-1})$	$\nu_{ei}(s^{-1})$	λ_{ac} (nm)	λ_{ab}(nm)
B^{3+}	3	4.5×10^7	4.2×10^6	2.0×10^{11}	282	6.1
C^{4+}	4	5.7×10^7	2.7×10^7	3.3×10^{11}	227	4.1

In the following table we summarize the collision frequency for a plasma temperature $k_B T_e = 1eV$ ($v_e = 3 \times 10^5 \mathrm{m/s}$) and electron density $n_e = n_i = 10^{20} \mathrm{m}^{-3}$ for Helium-like ions.

We note from Table III that the collision rate between ions and electrons is larger than the spontaneous decay rates. Thus one has to cleverly reduce the collision rates.

APPENDIX B

DERIVATION OF SOME OF THE RESULTS IN CHAPTER III

Derivation of $R_{00}(t,t')$ and $R_{0l}(t,t')$ in Eq. (3.43)

Setting $l=0$ in Eq. (3.42) we get

$$\dot{\beta}_0(t) = -\sum_{\mathbf{k}} g_{\mathbf{k}}^2 \int_0^t dt' \Big[R_{0,0}(t,t')\beta_0(t') + \sum_{l=1}^{N-1} \mathcal{R}_{0,l}(t,t')\beta_l(t') \Big], \tag{B.1}$$

in which

$$\begin{aligned} R_{00}(t,t') = &\sum_{i,j} \langle B_0|\sigma_j^+|C_0\rangle\langle C_0|\sigma_i|B_0\rangle e^{i\mathbf{k}\cdot(\mathbf{r}_j-\mathbf{r}_i)} e^{-ic(k-k_0)(t-t')} \\ &+ \sum_{i,j} \langle B_0|\sigma_j\sigma_i^\dagger|B_0\rangle e^{i\mathbf{k}\cdot(\mathbf{r}_j-\mathbf{r}_i)} e^{-ic(k+k_0)(t-t')}, \end{aligned} \tag{B.2}$$

$$\begin{aligned} R_{0l}(t,t') = &\sum_{i,j} \langle B_0|\sigma_j^+|C_0\rangle\langle C_0|\sigma_i|B_l\rangle e^{i\mathbf{k}\cdot(\mathbf{r}_j-\mathbf{r}_i)} e^{-ic(k-k_0)(t-t')} \\ &+ \sum_{i,j} \langle B_0|\sigma_j\sigma_i^\dagger|B_l\rangle e^{i\mathbf{k}\cdot(\mathbf{r}_j-\mathbf{r}_i)} e^{-ic(k+k_0)(t-t')} \end{aligned} \tag{B.3}$$

with

$$|C_0\rangle = |\downarrow\downarrow ... \downarrow_N\rangle, \qquad |B_0\rangle = \frac{1}{\sqrt{N}} \sum_{m=1}^{N} e^{i\mathbf{k}_0\cdot\mathbf{r}_m} |\downarrow\downarrow ... \uparrow_m ... \downarrow_N\rangle, \tag{B.4}$$

$$|B_l\rangle = \frac{1}{\sqrt{l(l+1)}} \Big[\sum_{m=1}^{l} e^{i\mathbf{k}_0\cdot\mathbf{r}_m} |\downarrow\downarrow ... \uparrow_m ... \downarrow_{l+1}\rangle - l e^{i\mathbf{k}_0\cdot\mathbf{r}_{l+1}} |\downarrow\downarrow ... \uparrow_{l+1}\rangle \Big], \; 1 \le l \le N-1. \tag{B.5}$$

Now using Eq. (B.4) one can easily verify that

$$\sum_i e^{-i\mathbf{k}\cdot\mathbf{r}_j} \langle C_0|\sigma_i|B_0\rangle = \frac{1}{\sqrt{N}} \sum_i e^{-i(\mathbf{k}-\mathbf{k}_0)\cdot\mathbf{r}_i} \tag{B.6}$$

and hence

$$\sum_{i,j}\langle B_0|\sigma_j^+|C_0\rangle\langle C_0|\sigma_i|B_0\rangle e^{i\mathbf{k}\cdot(\mathbf{r}_j-\mathbf{r}_i)} = \frac{1}{N}\sum_{i,j} e^{i(\mathbf{k}-\mathbf{k}_0)\cdot(\mathbf{r}_j-\mathbf{r}_i)}$$
$$= 1 + \frac{1}{N}\sum_{i\neq j} e^{i(\mathbf{k}-\mathbf{k}_0)\cdot(\mathbf{r}_j-\mathbf{r}_i)}. \tag{B.7}$$

Applying Eq. (B.4) one can similarly find that

$$\sum_{i,j}\langle B_0|\sigma_j\sigma_i^\dagger|B_0\rangle e^{i\mathbf{k}\cdot(\mathbf{r}_j-\mathbf{r}_i)} = N - 1 + \frac{1}{N}\sum_{i\neq j} e^{i(\mathbf{k}+\mathbf{k}_0)\cdot(\mathbf{r}_j-\mathbf{r}_i)}. \tag{B.8}$$

Therefore in view of Eqs. (B.7) and (B.8), Eq. (B.2) takes the form

$$R_{00}(t,t') = \Big(1 + \frac{1}{N}\sum_{i\neq j} e^{i(\mathbf{k}-\mathbf{k}_0)\cdot(\mathbf{r}_j-\mathbf{r}_i)}\Big)e^{-ic(k-k_0)(t-t')}$$
$$+ \Big(N - 1 + \frac{1}{N}\sum_{i\neq j} e^{i(\mathbf{k}+\mathbf{k}_0)\cdot(\mathbf{r}_j-\mathbf{r}_i)}\Big)e^{-ic(k+k_0)(t-t')}. \tag{B.9}$$

Further, making use of Eq. (B.4) and (B.5), we obtain

$$\sum_i \langle C_0|\sigma_i|B_l\rangle e^{-i\mathbf{k}\cdot\mathbf{r}_i} = \frac{1}{\sqrt{l(l+1)}}\Big[\sum_{i=1}^{l} e^{-i(\mathbf{k}-\mathbf{k}_0)\cdot\mathbf{r}_i} - l e^{-i(\mathbf{k}-\mathbf{k}_0)\cdot\mathbf{r}_{l+1}}\Big]. \tag{B.10}$$

Replacing i by j in Eq. (B.6) and taking the complex adjoint and multiplying the resulting expression by Eq. (B.10) yields

$$\sum_{i,j}\langle B_0|\sigma_j^+|C_0\rangle\langle C_0|\sigma_i|B_l\rangle e^{i\mathbf{k}\cdot(\mathbf{r}_j-\mathbf{r}_i)} = \frac{1}{\sqrt{Nl(l+1)}}\sum_j e^{i(\mathbf{k}-\mathbf{k}_0)\cdot\mathbf{r}_j}$$
$$\times\Big[\sum_{i=1}^{l} e^{-i(\mathbf{k}-\mathbf{k}_0)\cdot\mathbf{r}_i} - l e^{-i(\mathbf{k}-\mathbf{k}_0)\cdot\mathbf{r}_{l+1}}\Big]. \tag{B.11}$$

In a similar fashion, we obtain

$$\sum_{i,j}\langle B_0|\sigma_j\sigma_i^+|B_l\rangle e^{i\mathbf{k}\cdot(\mathbf{r}_j-\mathbf{r}_i)} = \frac{1}{\sqrt{Nl(l+1)}}\sum_j e^{-i(\mathbf{k}+\mathbf{k}_0)\cdot\mathbf{r}_j}\Big[\sum_{i=1}^{l} e^{i(\mathbf{k}+\mathbf{k}_0)\cdot\mathbf{r}_i} - l e^{i(\mathbf{k}+\mathbf{k}_0)\cdot\mathbf{r}_{l+1}}\Big]. \tag{B.12}$$

With the help of Eqs. (B.11) and (B.12), one can put Eq. (B.3) in the form

$$\begin{aligned} R_{0l}(t,t') = & \frac{1}{\sqrt{Nl(l+1)}} \sum_j e^{i(\mathbf{k}-\mathbf{k}_0)\cdot\mathbf{r}_j} \Big[\sum_{i=1}^{l} e^{-i(\mathbf{k}-\mathbf{k}_0)\cdot\mathbf{r}_i} \\ & - l e^{-i(\mathbf{k}-\mathbf{k}_0)\cdot\mathbf{r}_{l+1}} \Big] e^{-ic(k-k_0)(t-t')} \\ & + \frac{1}{\sqrt{Nl(l+1)}} \sum_j e^{-i(\mathbf{k}+\mathbf{k}_0)\cdot\mathbf{r}_j} \Big[\sum_{i=1}^{l} e^{i(\mathbf{k}+\mathbf{k}_0)\cdot\mathbf{r}_i} \\ & - l e^{i(\mathbf{k}+\mathbf{k}_0)\cdot\mathbf{r}_{l+1}} \Big] e^{-ic(k+k_0)(t-t')}. \end{aligned} \tag{B.13}$$

Discussion of Γ_{0l} terms under certain approximations

Here we calculate Γ_{0l} given by

$$\begin{aligned} \Gamma_{0l} = & \sum_{\mathbf{k}} g_{\mathbf{k}}^2 \int_0^t dt' R_{0l}(t,t') \\ = & \frac{1}{\sqrt{Nl(l+1)}} \sum_{\mathbf{k}} g_{\mathbf{k}}^2 \int_0^t dt' \Big\{ \sum_j e^{i(\mathbf{k}-\mathbf{k}_0)\cdot\mathbf{r}_j} \\ & \times \Big[\sum_{i=1}^{l} e^{-i(\mathbf{k}-\mathbf{k}_0)\cdot\mathbf{r}_i} - l e^{-i(\mathbf{k}-\mathbf{k}_0)\cdot\mathbf{r}_{l+1}} \Big] e^{-ic(k-k_0)(t-t')} \\ & + \sum_j e^{-i(\mathbf{k}+\mathbf{k}_0)\cdot\mathbf{r}_j} \Big[\sum_{i=1}^{l} e^{i(\mathbf{k}+\mathbf{k}_0)\cdot\mathbf{r}_i} - l e^{i(\mathbf{k}+\mathbf{k}_0)\cdot\mathbf{r}_{l+1}} \Big] e^{-ic(k+k_0)(t-t')} \Big\}. \end{aligned} \tag{B.14}$$

Using the transformation

$$\sum_{\mathbf{k}} \to \frac{V_{ph}}{(2\pi)^3} \int k^2 dk d\hat{\Omega}_{\mathbf{k}}, \tag{B.15}$$

where $\hat{\Omega}_{\mathbf{k}}$ is the angular unit vector and noting that for large enough N,

$$\sum_j e^{i(\mathbf{k}_0 \pm \mathbf{k})\cdot\mathbf{r}_j} \to \delta(\mathbf{k} \pm \mathbf{k}_0),$$

should be a good approximation for some problems. One should note, however, that replacement of the summation over atoms by delta function is not rigorous for the

finite size of atomic cloud. The results thus obtained will be only approximate even for large atomic sample.

Now rewriting the δ function as

$$\delta(\mathbf{k} \pm \mathbf{k}_0) = \frac{1}{2\pi k^2} \int_{-R}^{R} dr \; e^{i(k-k_0)r} \delta\left(\hat{\Omega}_{\mathbf{k}} - \hat{\Omega}_{\pm\mathbf{k}_0}\right). \tag{B.16}$$

equation (B.14) becomes

$$\begin{aligned}
\Gamma_{0,l} = & \frac{\omega^2 \wp^2}{2\pi^2 \hbar \varepsilon_0 c \sqrt{Nl(l+1)}} \int \frac{dk}{k} \delta(k - k_0) \\
& \times \Big\{ \Big[\sum_{j=1}^{l} e^{i(k_0-k)x_j} - l e^{i(k_0-k)x_{l+1}} \Big] \frac{1 - e^{ic(k_0-k)}}{ic(k-k_0)} \\
& + \Big[\sum_{j=1}^{l} e^{i(k_0+k)x_j} - l e^{i(k_0+k)x_{l+1}} \Big] \frac{1 - e^{-ic(k_0+k)}}{ic(k+k_0)} \Big\},
\end{aligned} \tag{B.17}$$

where $x_j = \mathbf{k}_0 \cdot \mathbf{r}_j$. The Sokhotsky's formula allows us to write

$$\begin{aligned}
\frac{1 - e^{-ic(k \pm k_0)t}}{ic(k \pm k_0)} &= \frac{1 - \cos(c(k \pm k_0)t)}{ic(k \pm k_0)} + \frac{\sin(c(k \pm k_0)t)}{c(k \pm k_0)} \\
&\equiv \frac{-i}{c} P \frac{1}{k \pm k_0} + \frac{\pi}{c} \delta(k \pm k_0),
\end{aligned} \tag{B.18}$$

where P represents the Cauchy principal part. The expression for Γ_{0l} then becomes

$$\begin{aligned}
\Gamma_{0l} = & \frac{\omega^2 \wp^2}{2\pi^2 \hbar \varepsilon_0 c \sqrt{Nl(l+1)}} \int \frac{dk}{k} \delta(k - k_0) \\
& \times \Big\{ \Big[\sum_{j=1}^{l} e^{i(k_0-k)x_j} - l e^{i(k_0-k)x_{l+1}} \Big] [\frac{-i}{c} P \frac{1}{k-k_0} + \frac{\pi}{c} \delta(k-k_0)] \\
& + \Big[\sum_{j=1}^{l} (e^{i(k_0+k)x_j} - l e^{i(k_0+k)x_{l+1}} \Big] \Big[\frac{-i}{c} P \frac{1}{k+k_0} + \frac{\pi}{c} \delta(k+k_0) \Big] \Big\}.
\end{aligned} \tag{B.19}$$

Performing the integration over k and keeping the principal part term in the first

integral, we obtain

$$\Gamma_{0l} = \frac{\omega^2 \wp^2}{2\pi^2 \hbar \varepsilon_0 c \sqrt{Nl(l+1)}} \int \frac{dk}{k} \delta(k-k_0) \times \Big[\sum_{j=1}^{l} e^{i(k_0-k)x_j} - l e^{i(k_0-k)x_{l+1}}\Big] \Big[\frac{-i}{c} P \frac{1}{k-k_0}\Big]. \tag{B.20}$$

Some care is required in dealing with the factor $P[1/(k-k_0)]$. It is convenient to use the original form

$$\frac{1-\cos(c(k-k_0)t)}{ic(k-k_0)} = \frac{-i}{c} P \frac{1}{k-k_0} \tag{B.21}$$

so that Eq. (B.20) yields

$$\begin{aligned} \Gamma_{0l} &= \frac{\omega^2 \wp^2}{2\pi^2 \hbar \varepsilon_0 c \sqrt{Nl(l+1)}} \int \frac{dk}{k} \delta(k-k_0) \Big[\sum_{j=1}^{l} e^{i(k_0-k)x_j} - l e^{i(k_0-k)x_{l+1}}\Big] \\ &\times \Big[\frac{1-\cos(c(k-k_0)t)}{ic(k-k_0)}\Big] \\ &= \lim_{k\to k_0} \frac{\omega^2 \wp^2/(2\pi^2 \hbar \varepsilon_0 c)}{\sqrt{Nl(l+1)}} \Big[\sum_{j=1}^{l} e^{i(k_0-k)x_j} - l e^{i(k_0-k)x_{l+1}}\Big] \frac{\Big(1-\cos[c(k-k_0)t]\Big)}{ic(k-k_0)k} \end{aligned} \tag{B.22}$$

which goes to zero for a very large number of atoms.

Calculation of the integral in Eq. (3.47)

Consider the integral

$$I_3 = P \int_0^{\infty} \frac{dk}{k} \int_{-R}^{r} dr e^{i(k-k_0)r} \Big[\frac{1}{k-k_0} + \frac{1}{k-k_0}\Big]. \tag{B.23}$$

Performing the radial integration, we obtain

$$I_3 = 2P \int_0^{\infty} \frac{dk}{k} \Big[\frac{1}{k-k_0} + \frac{1}{k+k_0}\Big] \frac{\sin\Big[(k-k_0)R\Big]}{(k-k_0)}. \tag{B.24}$$

This integral can be rewritten using the partial fraction decomposition as

$$I_3 = \frac{1}{k_0^2}\left\{\int_{k_0R}^{\infty} dy \frac{\sin(y-2k_0R)}{y} - \int_{-k_0R}^{\infty} \frac{\sin(y)}{y} dy + 2k_0 P \int_{-k_0R}^{\infty} \frac{\sin(y)}{y^2}\right\} \tag{B.25}$$

and can be transformed to

$$\begin{aligned} I_3 &= \frac{1}{k_0^2}\Big[\int_{k_0R}^{\infty} dy \frac{\sin(y)}{y}(\cos(2k_0R)-1) - P\int_{k_0R}^{\infty} dy \frac{\cos(y)}{y}(\sin(2k_0R))\Big] \\ &+ \frac{2}{k_0}\Big[\frac{\sin(k_0R)}{k_0} + RP\int_{-k_0R}^{\infty} dy \frac{\cos(y)}{y}\Big]. \end{aligned} \tag{B.26}$$

Let us now determine the principal value of $\int_{-k_0R}^{\infty} dy \frac{\cos(y)}{y}$

$$\begin{aligned} P\int_{-k_0R}^{\infty} dy \frac{\cos(y)}{y} &= \lim_{\varepsilon\to 0}\Big[\int_{-k_0R}^{-\varepsilon} dy \frac{\cos(y)}{y} + \int_{\varepsilon}^{\infty} dy \frac{\cos(y)}{y}\Big] \\ &= \lim_{\varepsilon\to 0}\Big[\int_{k_0R}^{\varepsilon} dy \frac{\cos(y)}{y} + \int_{\varepsilon}^{\infty} dy \frac{\cos(y)}{y}\Big] \\ &= -Ci(k_0R). \end{aligned}$$

I_3 has then the exact result

$$\begin{aligned} I_3 = \frac{1}{k_0^2}&\left[-\mathrm{Si}(k_0R)(1+\cos(2k_0R)) + \mathrm{Ci}(k_0R)(\sin(2k_0R)-2k_0R)\right] \\ &+\frac{1}{k_0^2}\left[\frac{\pi}{2}\cos(2k_0R) - \frac{\pi}{2} + 2\sin(k_0R)\right], \end{aligned} \tag{B.27}$$

where

$$\int_0^{\infty} dy \frac{\sin(y)}{y} = \frac{\pi}{2}, \tag{B.28}$$

and

$$\mathrm{Si}(x) = \int_0^x \frac{\sin(t)}{t} dt, \tag{B.29}$$

$$\mathrm{Ci}(x) = -\int_x^{\infty} \frac{\cos(t)}{t} dt \tag{B.30}$$

are the sine and cosine integrals, respectively. For $k_0R \gg 1$ the asymptotic of the

sine and cosine integrals are

$$\mathrm{Si}(x) \approx \frac{\pi}{2} - \frac{\cos(x)}{x}, \tag{B.31}$$

$$\mathrm{Ci}(x) \approx \frac{\sin(x)}{x}, \tag{B.32}$$

and we finally obtain

$$I_3 \approx -\frac{\pi}{k_0^2}\left[1 - \frac{2}{\pi k_0 R}\cos(k_0 R)\right]. \tag{B.33}$$

VITA

Name: Eyob Alebachew Sete

Address: Department of Physics and Astronomy

Texas A&M University, College Station, TX 77843-4242

Email Address: eyobas@physics.tamu.edu

Education: B.S., Addis Ababa University, 2000

M.S., Addis Ababa University, 2003

Ph.D., Texas A&M University, 2012

Selected Publications:

1. Eyob A. Sete, A. A. Svidzinsky, Y. Rostovtsev, H. Elecuh, P. K. Jha, S. Suckewer, and M. O. Scully, IEEE J. Sel. Top. Quantum Electron. **18**, 541 (2012).

2. Eyob A. Sete and H. Eleuch, Phys. Rev. A **85**, 043824 (2012).

3. Eyob A. Sete and S. Das, Opt. Lett., in press (2012).

4. Eyob A. Sete, Phys. Rev. A **84**, 063808 (2011).

5. Eyob A. Sete, K. E. Dorfman, and J. P. Dowling, J. Phys. B: At. Mol. Opt. Phys. **44**, 225504 (2011).

6. Eyob A. Sete and S. Das, Phys. Rev. A **83**, 042301 (2011).

7. Eyob A. Sete, S. Das, and H. Eleuch, Phys. Rev. A **83**, 023822 (2011).

8. Eyob A. Sete and H. Eleuch, Phys. Rev. A **82**, 043810 (2010).

9. Eyob A. Sete, A. A. Svidzinsky, H. Eleuch, Z. Yang, R. D. Nevels, and M. O. Scully, J. Mod. Opt . **57**, 1311 (2010).

The typist for this thesis was Eyob A. Sete.